bioRxiv preprint doi: https://doi.org/10.1101/2021.07.06.451358; this version posted November 28, 2022. The copyright holder for this preprint (which was not certified by peer review) is the author/funder, who has granted bioRxiv a license to display the preprint in perpetuity. It is made available under aCC-BY-NC-ND 4.0 International license.

Cacna2d2 is an hnRNP H target of the striatal mRNA targetome and regulates methamphetamine behavior

Qiu T. Ruan[1,2,3], William B. Lynch[2,3,4], Rebecca H. Cole[2], Michael A. Rieger[5], Jacob A. Beierle[1,2,3], Emily J. Yao[2], Jiayi W. Cox[3,6], Amarpreet Kandola[2], Kayla T. Richardson[2], Melanie M. Chen[2], Julia C. Kelliher[2], Richard K. Babbs[2], Peter E. A. Ash[7], Benjamin Wolozin[7], Karen K. Szumlinski[8], W. Evan Johnson[9], Joseph D. Dougherty[5], and Camron D. Bryant[1,2,3]*

1. Biomolecular Pharmacology T32 Training Program, Department of Pharmacology and Experimental Therapeutics, Boston University Chobanian and Avedisian School of Medicine; Boston, MA USA
2. Laboratory of Addiction Genetics, Department of Pharmacology and Experimental Therapeutics and Psychiatry, Boston University Chobanian and Avedisian School of Medicine; Boston, MA USA
3. Transformative Training Program in Addiction Science, Boston University Chobanian and Avedisian School of Medicine, Graduate Program for Neuroscience, Boston University; Boston, MA USA
4. Graduate Program for Neuroscience, Boston University, Boston, MA USA
5. Department of Genetics, Department of Psychiatry, Washington University School of Medicine in St. Louis; St. Louis, MO USA
6. Ph.D. Program in Biomedical Sciences, Graduate Program in Genetics and Genomics, Boston University Chobanian and Avedisian School of Medicine; Boston, MA USA
7. Laboratory of Neurodegeneration, Department of Pharmacology and Experimental Therapeutics and Neurology, Boston University Chobanian and Avedisian School of Medicine; Boston, MA USA
8. Department of Psychological and Brain Sciences, University of California, Santa Barbara, CA USA
9. Division of Infectious Disease, Department of Medicine and Center for Data Science, Rutgers University - New Jersey Medical School, Newark, NJ USA

***Corresponding Author**
Camron D. Bryant, Ph.D.
Department of Pharmacology and Experimental Therapeutics and Department of Psychiatry
Boston University Chobanian and Avedisian School of Medicine
72 E. Concord St. L-606B
Boston, MA 02118 USA
E: camron@bu.edu
P: (617) 358-9575

Number of pages: 45
Number of figures, tables, multimedia, and 3D models (separately): 17 figures and 9 tables
Number of words for Abstract: 250
Number of words for Introduction: 649
Number of words for Discussion: 1497
Conflict of interest statement: The authors declare no competing financial interests.
Acknowledgments: R01DA039168 (C.D.B.), U01DA050243 (C.D.B.), Burroughs Wellcome Fund (#1011479)

bioRxiv preprint doi: https://doi.org/10.1101/2021.07.06.451358; this version posted November 28, 2022. The copyright holder for this preprint (which was not certified by peer review) is the author/funder, who has granted bioRxiv a license to display the preprint in perpetuity. It is made available under aCC-BY-NC-ND 4.0 International license.

ABSTRACT

Methamphetamine addiction remains a major public health concern in the United States that has paralleled the opioid epidemic. Psychostimulant use disorders have a heritable genetic component that remains unexplained. Methamphetamine targets membrane and vesicular transporters to increase synaptic dopamine, norepinephrine, and serotonin. We previously identified *Hnrnph1* (heterogeneous nuclear ribonucleoprotein H1) as a quantitative trait gene underlying methamphetamine behavioral sensitivity. *Hnrnph1* encodes the RNA-binding protein hnRNP H1 that is ubiquitously expressed in neurons throughout the brain. Gene-edited mice with a heterozygous frameshift deletion in the first coding exon of *Hnrnph1* showed reduced methamphetamine-induced dopamine release and behaviors. To inform the mechanism linking hnRNP H dysfunction with reduced methamphetamine neurobehavioral effects, we surveyed the mRNA targetome of hnRNP H via cross-linking immunoprecipitation coupled with RNA-sequencing in striatal tissue at baseline and at 30 min post-methamphetamine. Methamphetamine induced opposite changes in RNA-binding targets of hnRNP H in *Hnrnph1* mutants versus wild-types, including 3'UTR targets in mRNAs enriched for synaptic proteins involved in dopamine release and excitatory synaptic plasticity. Targetome, transcriptome, and spliceome analyses triangulated on a methamphetamine-induced upregulation of the calcium channel subunit transcript *Cacna2d2* and decreased its 3'UTR usage in hyposensitive *Hnrnph1* mutants. Pretreatment with pregabalin, an inhibitor of α2δ2 and α2δ1 voltage-gated calcium channel subunits attenuated methamphetamine-induced locomotor activity in wild-type females but not in *Hnrnph1* mutants, supporting Cacna2d2 as a hnRNP H target. Our study identifies a dynamic hnRNP H RNA targetome that can rapidly and adaptively respond to methamphetamine to regulate gene expression and likely synaptic plasticity and behavior.

bioRxiv preprint doi: https://doi.org/10.1101/2021.07.06.451358; this version posted November 28, 2022. The copyright holder for this preprint (which was not certified by peer review) is the author/funder, who has granted bioRxiv a license to display the preprint in perpetuity. It is made available under aCC-BY-NC-ND 4.0 International license.

SIGNIFICANCE STATEMENT

The genetic risks mediating psychostimulant addiction are unknown and there are no FDA-approved treatments. We identified *Hnrnph1* in modulating methamphetamine behavioral sensitivity in mice. *Hnrnph1* codes for hnRNP H1, an RNA-binding protein. Here, we asked whether an *Hnrnph1* mutation and methamphetamine treatment would change the hnRNP H RNA targets and whether these targets could tell us how *Hnrnph1* is linked to behavior. We identified a calcium channel subunit that is a primary target of the FDA-approved drug pregabalin (a.k.a. Lyrica®). Like the *Hnrnph1* mutation, pregabalin reduced methamphetamine behaviors in wild-type mice. We propose hnRNP H regulates calcium channels in response to methamphetamine-induced perturbations in neurotransmitter release. Accordingly, pregabalin could represent a novel treatment to restore synaptic function following methamphetamine administration.

bioRxiv preprint doi: https://doi.org/10.1101/2021.07.06.451358; this version posted November 28, 2022. The copyright holder for this preprint (which was not certified by peer review) is the author/funder, who has granted bioRxiv a license to display the preprint in perpetuity. It is made available under aCC-BY-NC-ND 4.0 International license.

INTRODUCTION

Methamphetamine is addictive and neurotoxic (Kish, 2008; Galbraith, 2015). In the U.S., drug overdose deaths involving psychostimulants increased ~5-fold from 2012-2018 and continue rising (Hedegaard et al., 2020). There are no FDA-approved treatments for methamphetamine addiction. Methamphetamine is a substrate for membrane dopamine transporters (and norepinephrine and serotonin) and vesicular monoamine transporters and causes reverse transport of dopamine from the presynaptic terminal and increased dopamine release (Fleckenstein et al., 2009; Siciliano et al., 2014). Increased dopamine release is a major contributor to methamphetamine's addiction liability (Baumann et al., 2002). The rapid cell biological adaptations following methamphetamine action are not fully understood but could inform treatments for restoring cellular/synaptic function.

RNA binding proteins (**RBPs**) such as hnRNP H1 (coded by *Hnrnph1*; heterogeneous nuclear ribonucleoprotein H1; codes for hnRNP H1) regulate all aspects of RNA metabolism (Darnell, 2013; Hentze et al., 2018). Mutations in RBP-coding genes are implicated in substance use disorders (Bryant and Yazdani, 2016). For example, deletion of fragile X mental retardation protein (**FMRP**) disrupts dopaminergic neuron development and alters psychostimulant-induced neuroplasticity and behavior (Fulks et al., 2010; Fish et al., 2013; Smith et al., 2014; Huebschman et al., 2021). Furthermore, alternative splicing of exon 2 and transcriptional regulation of *Oprm1* (codes for mu opioid receptor) are mediated through binding of hnRNP H1 and recruitment of other hnRNPs to its intronic AGGG sequence (Xu et al., 2014), suggesting hnRNPs also target transcripts related to substance abuse. Interestingly, coding mutations in *HNRNPH1* and *HNRNPH2* lead to severe neurodevelopmental disorders (Pilch et al., 2018; Reichert et al., 2020).

We identified *Hnrnph1* as a quantitative trait gene for methamphetamine stimulant sensitivity in mice (Yazdani et al., 2015) and 5'UTR variants associated with decreased hnRNP H protein and methamphetamine-induced behavior (Ruan et al., 2020b). We also generated mice heterozygous for a 16 bp indel within the first coding exon of *Hnrnph1* ("*Hnrnph1* mutants") that also showed reduced methamphetamine-induced locomotion, reward, reinforcement, and ventral striatal dopamine release (Ruan et al., 2020a). Striatal, synaptosomal proteomics identified opposite methamphetamine-induced changes in mitochondrial protein expression between genotypes, suggesting mitochondrial perturbations could contribute to reduced methamphetamine-induced dopamine release and behavior (Ruan et al., 2020a).

bioRxiv preprint doi: https://doi.org/10.1101/2021.07.06.451358; this version posted November 28, 2022. The copyright holder for this preprint (which was not certified by peer review) is the author/funder, who has granted bioRxiv a license to display the preprint in perpetuity. It is made available under aCC-BY-NC-ND 4.0 International license.

Hnrnph1 codes for an RBP expressed throughout the brain that belongs to the hnRNP H/F subfamily of hnRNP RBPs that engage in all aspects of RNA processing (Honoré et al., 1995; Arhin et al., 2002; Han et al., 2010; Geuens et al., 2016; Uren et al., 2016). During cellular stress, RBPs (Markmiller et al., 2018) including hnRNP H (Wall et al., 2020), hnRNP A1 (Guil et al., 2006), and hnRNP K (Fukuda et al., 2009) localize to cytoplasmic stress granules and sequester mRNAs from translation. These hnRNP H-associated stress granules suggest hnRNP H interactions with its target mRNAs can change rapidly following perturbations in the cellular environment.

Methamphetamine-induced dopamine release within the nucleus accumbens contributes to its stimulant and addictive properties (Wise, 2004). Because we observed reduced methamphetamine-induced ventral striatal dopamine release and behaviors in *Hnrnph1* mutants (Yazdani et al., 2015; Ruan et al., 2020a), here, we sought to identify striatal RNA-binding targets of hnRNP H. We examined RNA-binding, mRNA expression, and splicing in *Hnrnph1* at baseline and following methamphetamine. We hypothesized that the *Hnrnph1* mutation would disrupt basal and methamphetamine-induced RNA-binding, splicing, and expression. hnRNP H is primarily localized to the nucleus but is also detected in cytoplasm (Wall et al., 2020). We predicted we would identify presynaptic (e.g., dopaminergic terminals originating from midbrain cell bodies) and post-synaptic (striatal neurons) RNA targets relevant to dopaminergic transmission and signaling that could link hnRNP H dysfunction to decreased methamphetamine-induced dopamine release and behavior. Our results triangulated on Cacna2d2 (voltage-dependent calcium channel subunit, alpha2/delta2), a methamphetamine-induced hnRNP H target exhibiting changes in 3'UTR splicing and transcript levels of Cacna2d2 resulting from *Hnrnph1* mutation and methamphetamine. Pharmacological inhibition of CACNA2D2 with FDA-approved drug pregabalin (a.k.a. Lyrica®) reduced methamphetamine-induced locomotion in wild-type females, thus recapitulating the mutant phenotype.

bioRxiv preprint doi: https://doi.org/10.1101/2021.07.06.451358; this version posted November 28, 2022. The copyright holder for this preprint (which was not certified by peer review) is the author/funder, who has granted bioRxiv a license to display the preprint in perpetuity. It is made available under aCC-BY-NC-ND 4.0 International license.

MATERIALS AND METHODS

Mice

Hnrnph1 mutants were generated via TALENs-mediated induction of a small, 16 bp deletion in the first coding exon as described (Yazdani et al., 2015) and have been deposited to The Jackson Laboratory repository (JAX, Bar Harbor, ME; Cat#JAX033968). A two-fold increase in hnRNP H protein expression was detected in the striatal synaptosome of *Hnrnph1* mutants compared to wild-types with no change in total tissue level (Ruan et al., 2020a). Mice were generated by mating heterozygous *Hnrnph1* mutant males with C57BL/6J females purchased from The Jackson Laboratory (JAX, Bar Harbor, ME; Cat#JAX000664), yielding offspring that were approximately 50% heterozygotes for the *Hnrnph1* mutation and 50% wild-types. Both female and male offspring (ranging from 50 – 100 days old at the start of the experiment) from this breeding scheme were used in the study and were genotyped as described (Yazdani et al., 2015). Mice were housed in same-sex groups of 2-5 in standard mouse cages in ventilated racks under standard housing conditions on a 12 h:12 h light:dark schedule with food and water supplied ad libitum. All protocols involving mice were written in accordance with the Guideline for the Care and Use of Laboratory Animals and were approved by Boston University's IACUC committee.

Methamphetamine-induced locomotor activity followed by dissection of whole striatum and cross-linking immunoprecipitation (CLIP)

As described (Yazdani et al., 2015), on Days 1 and 2, all mice received a saline injection (10 ml/kg, i.p.) and were recorded for locomotor activity in Plexiglas chambers (40 cm length x 20 cm width x 45 cm height) for 1 h. On Day 3, mice received either saline (i.p.) again or methamphetamine (2 mg/kg, i.p.; Sigma Aldrich, St. Louis, MO; Cat#1399001) and were recorded for locomotor activity for 30 min and the whole striata (left and right sides) were dissected from each mouse at 30 min post-injection (Ruan et al., 2020a). Dissected whole striata were stored in RNAlater (ThermoFisher Scientific, Waltham, MA; Cat#AM7020) following manufacturer's instructions to stabilize the RNA and protein, followed by CLIP.

Striata from four mice were pooled per replicate (3 replicates per Genotype per Treatment) to provide a sufficient amount of RNA for CLIP. Each replicate used for CLIP-seq and RNA-seq was generated by pooling striata from 4 *Hnrnph1* mutants or 4 wild-types across multiple litters. Each pool consisted of samples from 2 females and 2 males. The striatum was chosen because of its involvement in the methamphetamine locomotor stimulant response, reinforcement and reward (Keleta and Martinez, 2012; Lominac et al., 2014). Given the large

bioRxiv preprint doi: https://doi.org/10.1101/2021.07.06.451358; this version posted November 28, 2022. The copyright holder for this preprint (which was not certified by peer review) is the author/funder, who has granted bioRxiv a license to display the preprint in perpetuity. It is made available under aCC-BY-NC-ND 4.0 International license.

amount of striatal tissue needed for generating the CLIP-seq libraries in this study, we did not examine the ventral tegmental area (**VTA**, where the nuclei of the dopaminergic neurons reside) because the number of mice required to obtain a sufficient amount of tissue from the VTA per replicate was not feasible. The striatum punches contained primarily post-synaptic cells, but they also contained presynaptic dopaminergic terminals originating from VTA as well as other presynaptic terminals (e.g., glutamatergic terminals from prefrontal cortex). Thus, any low levels of cytosolic hnRNP H (Wall et al., 2020) and its bound RNAs at the presynaptic terminals were expected to be captured within our samples and thus, potentially relevant to rapid, dynamic regulation of in the cellular response to methamphetamine. The experimental design is outlined in **Table 1**. Tissue was flash frozen in mortar-filled liquid nitrogen and crushed into powder with the pestle and kept on dry ice in a 100 mm Petri dish until use. Prior to crosslinking, a portion of the pooled tissue from each replicate was removed and stored in -80°C for later RNA extraction and bulk RNA-seq library preparation. The tissue was kept on dry ice in the dish while crosslinking was performed for three rounds using a 400 mJ/cm^2 dosage of 254 nm ultraviolet radiation. The crosslinked tissue was then homogenized in 1 ml of lysis buffer (50 mM Tris-HCl pH7.4, 100 mM NaCl, 1% NP-40, 0.1% SDS, 0.5% sodium deoxycholate (protect from light), protease and phosphatase inhibitor cocktail (1:100; ThermoFisher Scientific, Waltham, MA; Cat#78444) and recombinant RNasin ribonuclease inhibitor (1 ul/ml; Promega, Madison, WI; Cat#N2511) with a mechanical homogenizer followed by addition of TURBO DNase (2 μl; ThermoFisher Scientific, Waltham, MA; Cat#AM2239). The lysate was kept on ice for 30 min followed by the addition of RNAse I_f (125 U/ml; NEB, Ipswich, MA; Cat#M0243L) and was allowed to incubate in a thermomixer set to 1200 RPM at 37˚C for 3 min. The lysate was then centrifuged at 20,000 x g for 20 min at 4°C and kept on ice until use.

For RNA-immunoprecipitation, 133.3 μl of MyOne Streptavidin T1 beads (Invitrogen, Waltham, MA; Cat#65602) were incubated with 5.8 μl of 1 mg/ml of Pierce™ biotinylated Protein G (ThermoFisher Scientific, Waltham, MA; Cat#29988) and 20 μg of either the hnRNP H antibody (Bethyl, Montgomery, TX; Cat#A300-511A) or the rabbit IgG antibody (EMD Millipore, Burlington, MA; Cat#12-370) for 1 h. The antibody-coupled beads were washed five times with 0.5% IgG-free BSA (Jackson ImmunoResearch, West Grove, PA; Cat# 001-000-162) in 1X PBS, followed by three washes in lysis buffer. The lysate that was clarified by centrifugation was added to the coated and washed beads and incubated with end-to-end rotation at 4°C for 2 h followed by 2X

bioRxiv preprint doi: https://doi.org/10.1101/2021.07.06.451358; this version posted November 28, 2022. The copyright holder for this preprint (which was not certified by peer review) is the author/funder, who has granted bioRxiv a license to display the preprint in perpetuity. It is made available under aCC-BY-NC-ND 4.0 International license.

wash with 500 μl of wash buffer (end-over-end rotation at 4°C for 5 min each) and another 2X wash with 500 μl of high salt wash buffer (end-over-end rotation at 4°C for 5 min each). The components of the wash buffer are as follows: 20 mM Tris-HCl pH7.4, 10 mM $MgCl_2$, 0.2% Tween-20, and recombinant RNasin ribonuclease Inhibitor (1 uL/ml, Promega, Cat#N2511). The components of the high salt wash buffer are as follows: 50 mM Tris-HCl pH7.4, 1M NaCl, 1 mM EDTA, 1% NP-40, 0.1% SDS, 0.5% sodium deocxycholate, and recombinant RNasin ribonuclease inhibitor (1 uL/ml; Promega, Madison, WI; Cat#N2511). These washes were followed by an additional wash with 500 μl each of both wash buffer and high salt wash buffer. Two additional final washes were performed with 500 μl of wash buffer. The rest of the wash buffer was removed, and beads resuspended in 20 μl of 1X Bolt LDS non-reducing sample buffer (ThermoFisher Scientific, Waltham, MA; Cat#B0007). The beads in sample buffer were then heated at 70°C for 10 min prior to SDS-PAGE on a 4-12% gradient NuPAGE Bis/Tris gels (ThermoFisher Scientific, Waltham, MA; Cat#NP0322BOX) followed by transfer to nitrocellulose membrane with 10% methanol for 6 hours at constant 150 mA. The radiolabeling experiments for determining the optimal CLIP conditions were performed as described in Rieger et al., 2020.

CLIP-seq and total RNA-seq library preparation

Following the completion of membrane transfer, the membrane was cut with a clean razor to obtain a vertical membrane slice per lane from 50 kDa (molecular weight of hnRNP H) to 75 kDa, which translates to 30 to 70 nucleotide RNA fragments crosslinked to the protein. RNA was then extracted from the membrane slices following a previously described procedure (Rieger et al., 2020). The same extraction procedure (starting with the addition of 7M urea) was used to isolate RNA from samples previously stored for total RNA-seq. Following RNA extraction, sample concentration was quantified with Agilent Bioanalyzer and approximately 0.2 ng of RNA was used to prepare next-generation sequencing libraries following a following the eCLIP procedure (van Nostrand et al., 2016) with minor modifications according to Rieger et al., 2020. Because the RNA adapter on each sample contained a unique barcode, the cDNA libraries generated from the sample (12 CLIP-seq and 12 RNA-seq libraries) were multiplexed and pooled for increased throughput. A pooled library at a concentration of 10 nM was shipped to the University of Chicago Sequencing core and subjected to 100 bp paired-end 2 x 100 sequencing in a single lane on Illumina HiSEQ4000. To increase read coverage for the RNA-seq samples, those 12 cDNA libraries were pooled (10 nM concentration) for sequencing for a second time in one lane using Illumina HiSEQ4000. The read coverage for each sample is shown in **Table 1**.

bioRxiv preprint doi: https://doi.org/10.1101/2021.07.06.451358; this version posted November 28, 2022. The copyright holder for this preprint (which was not certified by peer review) is the author/funder, who has granted bioRxiv a license to display the preprint in perpetuity. It is made available under aCC-BY-NC-ND 4.0 International license.

CLIP-seq and total RNA-seq data processing

Reads were trimmed for quality using Trimmomatic (Bolger et al., 2014). Unique Molecular Identifier (UMI) sequences were extracted from Read 2 for removal of PCR amplification duplicates using the 'extract' command in UMI-tools (Smith et al., 2017). After the reads were trimmed and UMI extracted, we used STAR (Dobin et al., 2013) to map reads to mouse genome, version GRCm38/mm10. Even though the samples had undergone ribosomal RNA (rRNA) depletion prior to library preparation, we used BEDtools (Quinlan and Hall, 2010) to intersect the bam files with the RNA annotation bed file exported from UCSC Table browser (Karolchik et al., 2004) to remove rRNAs and other repetitive RNAs. Using the 'dedup' command in UMI_tools (Smith et al., 2017), PCR duplicates from the rRNA-depleted bam files were removed based on UMI extracted in the previous step.

Peak calling using CLIP-seq Analysis of Multi-mapped reads (CLAM)

To define the binding sites for hnRNP H for each of the four conditions separately, we used deduplicated bam files for the three replicates of each condition for peak calling in CLAM (Zhang and Xing, 2017). The BAM file for the CLIP sample and the BAM file for input (corresponding RNA-seq sample) were used as input along with a gene annotation file in Gene Transfer Format downloaded from GENCODE. Following the steps described in CLAM (Zhang and Xing, 2017), in order to allow for peak calling of multi-mapped reads, BAM files were preprocessed ('preprocessor' command) first to separate multi-mapped reads and uniquely mapped reads followed by realigning ('realigner' command) and then peak calling ('peakcaller' command) on a gene-by-gene basis in 100-bp bins. The called peaks were then annotated to the genomic regions using the 'peak_annotator' command to examine binding site distributions across the 5'UTR, 3'UTR, CDS, and introns. The genomic region annotated peaks for each condition can be found in the supplementary files associated with Gene Expression Omnibus (**GEO**) accession number GSE160682.

Homer *de novo* Motif Discovery

To identify the top over-represented motifs in the peaks (those peaks with CLIP peak intensity > 1.5) that were identified in CLAM, Homer software (Heinz et al., 2010) was used for *de novo* motif discovery by using "findMotifsGenome.pl" function. The input file comprised a list of hnRNP H associated peaks containing the genomic coordinates. The "annotatePeak.pl" function was then used to identify motif locations to find genes containing a particular motif.

bioRxiv preprint doi: https://doi.org/10.1101/2021.07.06.451358; this version posted November 28, 2022. The copyright holder for this preprint (which was not certified by peer review) is the author/funder, who has granted bioRxiv a license to display the preprint in perpetuity. It is made available under aCC-BY-NC-ND 4.0 International license.

Pathway and Gene Ontology Enrichment Analysis

To examine the biological function of the hnRNP H targets (peak signal value defined by a CLAM value greater than 1.5 for each target), we performed pathway and gene ontology (**GO**) enrichment analysis of those targets in g:Profiler (Raudvere et al., 2019) against the following data sources: Reactome, WikiPathways, GO molecular function, GO cellular component, and GO biological process. The top 10 pathways and GO terms from each these 5 databases (a list of 50 gene sets) were used for network analysis in Cytoscape using the EnrichmentMap module (Merico et al., 2010). Highly redundant gene sets were grouped together as clusters for clear visualization and easy interpretation. The same pathway and GO enrichment analyses were performed in g:Profiler for the hnRNP H targets with Genotype and Treatment interaction to generate an EnrichmentMap (Reimand et al., 2019). To examine the biological relevance separately for each subgenic region of hnRNP H targets, we performed KEGG (Kanehisa et al., 2019) pathway enrichment analysis in WebGestalt (Liao et al., 2019).

3'UTR usage for *Cacna2d2* using real-time quantitative PCR (RT-qPCR)

Striatal tissue for RT-qPCR validation was collected 30 min after saline or methamphetamine injections as described above. The left striatum was dissected as previously described (Ruan et al., 2020a) and subsequently stored in RNAlater (ThermoFisher Scientific, Cat#AM7020) following manufacturer's instructions to stabilize the RNA. Following RNA extraction with TRIzol reagent (Invitrogen, Cat#15596026), oligo-DT primers were used to synthesize cDNA from the extracted total RNA using a high-capacity cDNA reverse transcription kit (ThermoFisher Scientific, Cat#4368814). RT-qPCR using PowerUP SYBR Green (ThermoFisher Scientific, Cat#A25741) was then performed to evaluate differential 3'UTR usage of *Cacna2d2*. The primer sequences are listed here:

- Proximal end of the 3'UTR of *Cacna2d2* (forward primer): 5'-TTGGCCACTCTCTCCTGAAG-3'
- Proximal end of the 3'UTR of *Cacna2d2* (reverse primer): 5'-ACTAGTGGCCTCCTGTCCTA-3'
- Distal end of the 3'UTR of *Cacna2d2* (forward primer): 5'-CCCCATCAGGTAGTTGTCCA-3'
- Distal end of the 3'UTR of *Cacna2d2* (reverse primer): 5'-TGTCGCTGTTGTTTTCCCAA-3'
- Exons 37-38 of *Cacna2d2* (forward primer): 5'-GGTCCGCACATCTGTTTTGA-3'
- Exons 37-38 of *Cacna2d2* (reverse primer): 5'-GAAGGAGTGGACTTGAGGCT-3'
- Exons 3-4 of *Cacna2d2* (forward primer): 5'-AATTGGTGGAGAAAGTGGCA-3'

bioRxiv preprint doi: https://doi.org/10.1101/2021.07.06.451358; this version posted November 28, 2022. The copyright holder for this preprint (which was not certified by peer review) is the author/funder, who has granted bioRxiv a license to display the preprint in perpetuity. It is made available under aCC-BY-NC-ND 4.0 International license.

- Exons 3-4 of *Cacna2d2* (reverse primer): 5'-GGCTTTCTGGAAATTCTCTGC-3'
- Exons 5-6 of *Gapdh* (forward primer): 5'-GCCTTCCGTGTTCCTACC-3'
- Exons 5-6 of *Gapdh* (reverse primer): 5'-CCTCAGTGTAGCCCAAGATG-3'

SDS-PAGE and immunoblotting for CACNA2D2 protein quantification

The right striatum from the same mice used for the RT-qPCR analysis was processed for Western blots for quantification of CACNA2D2 protein level 30 min after methamphetamine or saline injections in *Hnrnph1* mutants and wild-types. The flash-frozen striatal tissues were homogenized using a hand-held homogenizer in RIPA buffer which included protease and phosphatase inhibitor cocktail (1:100; ThermoFisher Scientific, Cat#78444) followed by sonication. For each sample, 30 μg of protein was heated in a 70ºC water bath for 10 min prior to loading into into a 4-15% Criterion TGX precast Midi protein gel (Bio-Rad, Cat#5671094) for SDS-PAGE followed by wet transfer to a nitrocellulose membrane. Following the transfer, membranes were stained with ponceau S solution (0.1% ponceau S in 1% (v/v) acetic acid for 1 minute de-stained in water to remove non-specific binding. The membranes were then imaged with BioRad ChemiDoc XRS+ system. Following the imaging, the membranes were blocked with 5% milk for 1 hand probed with anti-CACNA2D2 (1:1000; alomone, Cat#ACC-102) over night at 4°C followed by 1 hour probing with donkey anti-rabbit HRP (1:10,000; Jackson ImmunoResearch Labs Cat#711-035-152). The membrane were imaged via enhanced chemiluminescence photodetection with the BioRad ChemiDoc XRS+ system.

Effect of Pregabalin pre-treatment on locomotor responses following saline and methamphetamine treatment and striatum dissections

To habituate mice to the testing environment, on Days 1 and 2, mice were pretreated with a saline injection (10 ml/kg, i.p.) and placed back into their home cages. Thirty min later, mice were administered a second saline injection (10 ml/kg, i.p.) and were recorded for locomotor activity in Plexiglas chambers (40 cm length x 20 cm width x 45 cm height) for 1 h. On Day 3, mice were pretreated with either saline (10 ml/kg, i.p.) or pregabalin (30 mg/kg, i.p., Biosynth Carbosynth, San Diego, CA; Cat#FA27139), a dose previously shown to attenuate cocaine intravenous self-administration (de Guglielmo et al., 2013) without inducing addiction-relevant behaviors on its own (Coutens et al., 2019). All mice within the same cage received the same pretreatment. Thirty min later, mice were injected with methamphetamine (2 mg/kg, i.p.). Sixty min following methamphetamine (or saline), whole striata (left and right sides) were dissected from each mouse (Ruan et al., 2020a), which is 90 min post-

bioRxiv preprint doi: https://doi.org/10.1101/2021.07.06.451358; this version posted November 28, 2022. The copyright holder for this preprint (which was not certified by peer review) is the author/funder, who has granted bioRxiv a license to display the preprint in perpetuity. It is made available under aCC-BY-NC-ND 4.0 International license.

pregabalin injection. Because pregabalin inhibits CACNA2D2 and because Cacna2d2 is an hnRNP H target, we wanted to know if pregabalin pre-treatment would lead to a cellular adaptive response as measured via changes in *Cacna2d2* levels under saline and methamphetamine conditions and whether any adaptive response observed would depend on *Hnrnph1* genotype. Dissected left striata were stored in RNAlater following manufacturer's instructions to stabilize the RNA and for quantification of *Cacna2d2* 3'UTR usage, while dissected right striata were flash-frozen for subsequent CACNA2d2 protein quantification as previously described.

Experimental Design and Statistical Analyses

Locomotor activity in 5-min bins

To replicate our findings of reduced methamphetamine-induced locomotor activity in *Hnrnph1* mutants(Yazdani et al., 2015; Ruan et al., 2020a), we analyzed total distance traveled in 5-min bin separately for Days 1, 2, and 3 using mixed effects ANOVA with Genotype, Sex, and Treatment (saline, methamphetamine) as between-subject factors and Time as a repeated measure. For Day 3, the significant three-way (Genotype x Treatment x Time) interaction was decomposed into a simple two-way (Genotype x Treatment) interaction at each time level. The significant simple two-way interaction was then followed up with simple main effects to investigate the effect of Genotype on distance traveled at every level of Time in each Treatment. The significant simple main effect was then followed up with Bonferroni-adjusted multiple pairwise comparisons to identify genotypic differences in each 5-min time bin.

To determine the effect of pregabalin pretreatment on methamphetamine-induced locomotor in *Hnrnph1* mutants versus wildtypes, total distance traveled in 5-min bins was analyzed separately for Days 1, 2, and 3 using mixed effects ANOVA with Genotype, Sex, and Treatment (saline, pregabalin) as between-subject factors and Time as the repeated-measure factor. For Day 3, the significant two-way (Genotype x Treatment) interaction was followed up with simple main effects to investigate the effect of Treatment on distance traveled at every level of Time in each Genotype. The significant main effect for the wild-types was then followed up with Bonferroni-adjusted multiple pairwise comparisons to identify difference between saline versus pregabalin in each 5-min time bin.

Effect of Genotype, Treatment, and their interaction on hnRNP H binding

Deduplicated BAM files were merged across all 12 CLIP samples and deduplicated BAM files were merged across all 12 input (bulk RNA-seq) samples to generate two merged BAM files as the input for peak calling in

bioRxiv preprint doi: https://doi.org/10.1101/2021.07.06.451358; this version posted November 28, 2022. The copyright holder for this preprint (which was not certified by peer review) is the author/funder, who has granted bioRxiv a license to display the preprint in perpetuity. It is made available under aCC-BY-NC-ND 4.0 International license.

CLAM as described above. The called peaks were then annotated to the genomic regions as described above. The file containing all of the peaks was formatted into a file in GTF format that was used for strand-specific feature counting in individual BAM files from the 12 CLIP samples using featureCounts in SubRead (Liao et al., 2014). Only peaks with peak intensity > 1.5 and FDR < 0.05 as defined by CLAM were included as 'features' for read counting. Reads were summed for each significant peak to produce a count table containing peaks as rows and samples in columns for differential analysis. To examine the effect of Genotype, Treatment, and their interactive effects on hnRNP H binding, differential analysis was performed using limma (Ritchie et al., 2015) and edgeR (Robinson et al., 2009) based on summed read counts for each peak derived from Subread featureCount. The Genotype x Treatment is expressed as: I = (MUT_MA – MUT_SAL) – (WT_MA – WT_SAL). The positions of the peaks and the corresponding gene targets for effect of Genotype, Treatment, and Genotype x Treatment interaction are provided in the supplementary files associated with GEO accession number GSE160682. The correlation between methamphetamine-induced hnRNP H-associated CLIP peaks in *Hnrnph1* mutants versus wild-types was determined by calculating the Pearson's correlation coefficient.

Differential gene expression and differential exon and intron usage analyses

To triangulate on the CLIP-seq and RNA-seq datasets and associate the downstream effects of hnRNP H binding on gene expression and alternative splicing, we used ASpli (Mancini et al., 2020) to analyze differential gene expression and differential exon/intron usage. Deduplicated BAM files from the 12 total RNA-seq samples were used as inputs for alternative splicing and overall gene expression analysis. To test the general hypothesis that target genes of hnRNP H binding interact with Genotype in response to methamphetamine treatment at the expression or splicing level, the interaction was calculated using the following contrast: I = (MUT_MA – MUT_SAL) – (WT_MA – WT_SAL). The outputs from ASpli are provided in the supplementary files associated with GEO accession number GSE160682.

Validation of alternative splicing at the 3'UTR of Cacna2d2

For analyzing differential polyadenylation of *Cacna2d2*, the fold-change for each condition relative to saline-treated wild-types was calculated using the $2^{-\Delta\Delta CT}$ method (Livak and Schmittgen, 2001). Samples were plated in triplicate as technical replicates. Significance of the RT-qPCR results was determined with a two-way ANCOVA with Genotype and Treatment as between-subject factors with Batch as the co-variate. The significant main

bioRxiv preprint doi: https://doi.org/10.1101/2021.07.06.451358; this version posted November 28, 2022. The copyright holder for this preprint (which was not certified by peer review) is the author/funder, who has granted bioRxiv a license to display the preprint in perpetuity. It is made available under aCC-BY-NC-ND 4.0 International license.

effect of Treatment was followed up with Bonferroni-adjusted pairwise comparisons separately between wild-types and *Hnrnph1* mutants.

Quantification of CACNA2D2 protein level

The chemiluminescence intensity signal from the immunoblots was quantified using image analysis software, ImageJ. Total pixel intensity from brightfield images of Ponceau S stain was used for normalization of total protein loading for determining CACNA2D2 protein levels (Aldridge et al., 2009; Gilda and Gomes, 2013). Significance of the immunoblot results was determined using a two-way ANCOVA with Genotype and Treatment as between-subject factors with Batch as the co-variate with the rstatix package in R.

Code/Software

Raw and processed sequencing data from CLIP-seq and RNA-seq can be accessed through the National Center for Biotechnology Information's GEO under the accession number GSE160682. Codes associated with analyses mentioned in Method Details can be found at: https://github.com/camronbryant/hnrnph1_clip.

bioRxiv preprint doi: https://doi.org/10.1101/2021.07.06.451358; this version posted November 28, 2022. The copyright holder for this preprint (which was not certified by peer review) is the author/funder, who has granted bioRxiv a license to display the preprint in perpetuity. It is made available under aCC-BY-NC-ND 4.0 International license.

RESULTS

Hnrnph1 mutants showed reduced methamphetamine-induced locomotor activity

Mice were subjected to a 3-day behavioral protocol to assess methamphetamine-induced locomotor activity prior to tissue collection on Day 3. Performing CLIP specifically in the striatum required a large quantity of tissue. For this reason, we pooled striata (left and right) from four mice (2 females and 2 males per pooled sample) for each condition (**Table 1**). The data reported here represent the average locomotor activity from four mice per replicate for each of the four conditions listed. On the saline-treated Days (Days 1 and 2), there was no genotypic difference in locomotor activity (**Figures 1A-B**). On Day 3, following an acute dose of methamphetamine at 2 mg/kg, *Hnrnph1* mutants showed reduced locomotor activity relative to wild-types (**Figure 1C**) (Yazdani et al., 2015; Ruan et al., 2020a). Importantly, there was no effect of Genotype in response to saline on Day 3 (**Figure 1C**), indicating that the Genotype effect was specific to methamphetamine treatment. The striata were then immediately harvested from each mouse at 30 min post-injection on Day 3 for CLIP-seq processing.

hnRNP H binding sites contain G-rich binding motifs that are enriched in the intronic regions

Accumulating evidence from our lab indicates a role for hnRNP H in methamphetamine addiction liability (Ruan et al., 2020a; Borrelli et al., 2021). Defining the set of RNA targets in brain tissue that are differentially regulated by hnRNP H in *Hnrnph1* mutants in response to methamphetamine could inform key mechanisms underlying decreased dopamine release and behavior. To identify the *in vivo* hnRNP H targets, we performed CLIP using an antibody specific for hnRNP H in the striatum of *Hnrnph1* mutants versus wild-types, 30 min following saline or methamphetamine treatment. We previously validated this antibody to be specific for the C-terminus of hnRNP H via immunoadsorption with a blocking peptide for the epitope (Ruan et al., 2018). Here, we show that the antibody specifically pulled down hnRNP H at 50 kDa with no signal detected using rabbit IgG (**Figure 2A**; Lane 6 versus Lane 3). Importantly, we used stringent lysis and wash conditions as published (van Nostrand et al., 2016). Twenty μg of hnRNP H antibody was the optimal amount needed as indicated by visual inspection of the band intensity (**Figure 2B**).

Our CLIP procedure resulted in RNA-specific pulldown of hnRNP H-RNA complexes. RNAse fragmented the CLIP samples into different sizes in a concentration-dependent manner (**Figure 3A**; from left to right, lanes 3 – 6) indicating the hnRNP H CLIP was RNA-dependent. Longer incubation of CLIP samples with RNase yielded

bioRxiv preprint doi: https://doi.org/10.1101/2021.07.06.451358; this version posted November 28, 2022. The copyright holder for this preprint (which was not certified by peer review) is the author/funder, who has granted bioRxiv a license to display the preprint in perpetuity. It is made available under aCC-BY-NC-ND 4.0 International license.

a lower amount of RNA, providing further support that hnRNP H CLIP was RNA-dependent (**Figure 2C**; Lanes 2-5). Negative controls included immunoprecipitation (**IP**) from uncrosslinked sample (**Figure 3A**; Lane 1) and immunoprecipitation using rabbit IgG from wild-type striatal tissues (**Figure 3A**; Lane 2). No RNA was detected in these two negative control samples (**Figure 3A**; lanes 1 and 2), indicating the need for UV-crosslinking for RNA pull down and demonstrating the specificity of hnRNP H pull down. We chose a region 30 – 70 nucleotides in size (50 – 80 kDa) for RNA extraction to capture the targets of hnRNP H *in vivo* (**Figure 3A**). The cDNA libraries generated from the CLIP samples of the IgG IPs did not yield any detectable PCR bands using gel electrophoresis (only dimers from the sequencing adapter libraries), even after 28 PCR cycles (**Figure 4A**). For this reason, none of the four IgG cDNA libraries were subjected to sequencing. However, for the CLIP samples, DNA bands corresponded to the correct size of the cDNA library (>150 bp) and were detected after 18 PCR cycles (**Figure 4B**). We subjected the same samples used in CLIP for total RNA-seq and measured starting transcript abundance, which permitted normalization to account for differences in RNA abundance (**Table 1**).

To define the targets of hnRNP H under basal conditions, we first focused our analysis on the wild-types treated with saline. Specific hnRNP H sites were identified using Peakcaller subcommand in CLAM (Zhang and Xing, 2017) to perform peak calling throughout the whole genome. The peak calling process was done on a gene-by-gene basis by breaking down each gene into 100 nucleotide bins and testing for enrichment of mapped reads over control (or total RNA-seq mapped reads) and specifying a negative-binomial model on observed read counts. Importantly, CLAM calls peaks using a combination of uniquely- and multi-mapped reads for inclusion of RNA-binding sites that are repetitive elements (Zhang and Xing, 2017). hnRNP H-associated peaks were defined as enriched ($p < 0.05$ and peak signal intensity >1.5) in CLIP samples over input RNA-seq samples. Analysis of the peaks across gene subregions revealed enriched intronic binding of hnRNP H, comprising about 70% of total distribution (**Figure 3B**). This finding is consistent with previous characterization of hnRNP H in HeLa cells (Huelga et al., 2012; Uren et al., 2016), supporting successful isolation of hnRNP H-bound RNAs in mouse striatal tissue.

De novo motif discovery of significant hnRNP H-associated binding sites using the Homer database (Heinz et al., 2010) detected the top over-represented motif to be G-rich (**Figure 3C**) and was more prevalent in intronic regions (**Table 2**) which agrees with the prior literature (Lefave et al., 2011; Uren et al., 2016) and indicates that our CLIP procedure successfully isolated hnRNP H targets in mouse brain striatal tissue. Intronic

bioRxiv preprint doi: https://doi.org/10.1101/2021.07.06.451358; this version posted November 28, 2022. The copyright holder for this preprint (which was not certified by peer review) is the author/funder, who has granted bioRxiv a license to display the preprint in perpetuity. It is made available under aCC-BY-NC-ND 4.0 International license.

poly G-stretches can enhance hnRNP H binding (Han et al., 2005) and their length predicts splicing (Katz et al., 2010). Pathway enrichment analysis of the hnRNP H RNA targets containing these G-rich genomic locations identified "presynaptic depolarization and calcium channel opening," comprising of subunits of calcium channels encoded by *Cacna1a, Cacnb4, Cacna1e, Cacng4, Cacna1b, Cacng2, and Cacnb2* (**Figure 3D and Table 3**), all of which are important for neurotransmission (Dolphin and Lee, 2020). FMRP is an RBP that was previously shown to bind to mRNA transcripts that encode for ion channels is FMRP (Darnell et al., 2011). Thus, like FMRP, our findings identify hnRNP H as another RBP that binds to calcium channel subunit transcripts to regulate gene splicing and expression that plausibly influences neurotransmission and behavior (**Tables 3 and 4**).

hnRNP H regulates gene networks important for synaptic function

To determine whether hnRNP H regulates a subset of targets in the striatum, pathway and gene ontologies (**GO**) analyses were performed to examine the biological and molecular functions of hnRNP H targets. Gene sets along with the associated genes are provided in the supplementary files associated with GEO accession number GSE160682. The enriched gene sets are represented in an enrichment map network (**Figure 5)** and their connections depend on the number of shared genes where highly related gene sets are clustered together. The enrichment map network clearly revealed gene sets related to synaptic functions (**Figure 5**). The top five enriched gene sets include "transmission across chemical synapse", "neuronal system", "axon guidance", "muscle contraction", and "mRNA processing" (*nodes, **Figure 5**). Thus, hnRNP H regulates pre-mRNAs and mRNAs coding for proteins involved in synaptic function.

***Hnrnph1* mutation and methamphetamine treatment induce changes in RNA-binding targets of hnRNP H**

To test the hypothesis that hnRNP H exhibits a functional response to methamphetamine treatment (i.e., a change in the hnRNP H targetome), we examined the baseline and methamphetamine-induced targetome of hnRNP H in *Hnrnph1* mutants versus wild-types. Comparing changes in binding across subregions of the mRNA transcripts revealed the extent to which the *Hnrnph1* mutation and methamphetamine impact splicing function versus mRNA stability and/or translation.

In using the 2 x 2 design (Genotype x Treatment) to analyze the read distribution separately across the 3'UTR, introns, CDS, and 5'UTR for each of the four conditions, we again discovered over-representation of binding sites for intronic regions of the mRNA transcripts across all four conditions (**Figure 6A**). In comparison

bioRxiv preprint doi: https://doi.org/10.1101/2021.07.06.451358; this version posted November 28, 2022. The copyright holder for this preprint (which was not certified by peer review) is the author/funder, who has granted bioRxiv a license to display the preprint in perpetuity. It is made available under aCC-BY-NC-ND 4.0 International license.

to the hnRNP H binding targets at baseline (WT_SAL), changes in hnRNP H binding at 3'UTR and introns as a function of Genotype and Treatment were more variable compared to binding in the CDS and 5'UTR than would be expected by chance (**Table 5**). Thus, methamphetamine treatment induced a signaling response that ultimately shifted the binding of hnRNP H to its intronic targets that are predicted to perturb mRNA splicing. Notably, following methamphetamine, wild-types showed an *increase* in the percentage of 3'UTR binding sites whereas *Hnrnph1* mutants showed a *decrease* in the percentage of 3'UTR binding sites (**Figure 6A**). These results suggest that methamphetamine-induced signaling within the striatum induces opposing alterations in *Hnrnph1* mutants versus wild-types in hnRNP H-mediated regulation of mRNA stability, polyadenylation site usage, and/or translation.

Opposing methamphetamine-induced changes in the 3'UTR targetome between *Hnrnph1* mutants versus wild-types prompted further examination. In plotting changes in hnRNP H-associated CLIP peaks in each of the four groups (Genotype x Treatment), we found that hnRNP H CLIP peaks showing methamphetamine-induced *increased* binding in wild-types were more likely to show methamphetamine-induced *decreased* binding in *Hnrnph1* mutants (**Figure 6B**). Thus, the hnRNP H shift in binding was generally in the opposite direction between the two genotypes in response to methamphetamine (**Figure 6B**). This negative correlation potentially indicates that the heterozygous *Hnrnph1* mutation exerts an overall dominant negative effect on hnRNP H1 function, especially in response to methamphetamine.

Our CLIP-seq dataset identified more than 1000 mRNA transcripts associated with genotype and methamphetamine effects (**Figure 7A-B**). To narrow the list of transcript targets to those that were most relevant to genotypic differences in methamphetamine-induced dopamine release and behavior, we focused specifically on targets showing a Genotype x Treatment interaction. These targets were enriched for pathways associated with psychostimulant-induced synaptic plasticity including "amphetamine addiction," "long-term potentiation," and "dopaminergic synapse" (**Figure 6C; Table 6A**). The targets were also enriched for cellular components of "ATPase complex", "myelin sheath," "neuron spine", and "nuclear chromatin", which all represent cellular adaptations in response to methamphetamine (**Figure 6D; Table 6B**). Furthermore, the enrichment map network of the top over-represented pathways and GO terms for these targets revealed clustering of nodes associated with synaptic function (**Figure 7C**). Post-transcriptional regulation of these mRNA targets by hnRNP H could

bioRxiv preprint doi: https://doi.org/10.1101/2021.07.06.451358; this version posted November 28, 2022. The copyright holder for this preprint (which was not certified by peer review) is the author/funder, who has granted bioRxiv a license to display the preprint in perpetuity. It is made available under aCC-BY-NC-ND 4.0 International license.

contribute to reduced methamphetamine-induced dopamine release in *Hnrnph1* mutants and/or reduced post-synaptic dopaminergic signaling, either of which could underlie reduced methamphetamine-induced behaviors.

3'UTR and intronic targets of hnRNP H show enrichment for excitatory and psychostimulant-induced synaptic plasticity

Both genotype and methamphetamine treatment modulate *Hnrnph1* binding events within the introns and 3'UTRs (**Figure 6A**). We reasoned that those targets showing Genotype x Treatment interactions in hnRNP H binding are potential mechanistic targets that warrant further investigation. We partitioned the hnRNP H-interactive CLIP peaks into separate subgenic regions (5'UTR, 3'UTR, intron, or CDS), which allowed us to characterize the impact of changes in binding on specific types of hnRNP H-dependent post-transcriptional processing that could refine which subgenic targets are most relevant in driving the enrichment scores related to synaptic function.

We examined binding of hnRNP H across transcripts by plotting normalized $\log_2$CPM (counts per million) mapped reads to subgenic regions (**Figure 8**). We observed an opposing pattern of methamphetamine-induced changes in hnRNP H binding to 3'UTR targets between *Hnrnph1* mutants and wild-types whereby wild-types showed an increase in hnRNP H binding to the 3'UTR whereas *Hnrnph1* mutants showed a decrease in hnRNP H binding to the 3'UTR. This negative correlation between methamphetamine treatment and binding was also observed for the 5'UTR, CDS, and introns (**Figure 9**) but was most pronounced for the most robust 3'UTR targets (**Figure 8**).

To gain additional mechanistic insight into the 3'UTR targets showing a Genotype x Treatment interaction in binding, KEGG enrichment analysis of subgenic regions revealed that only the 3'UTR targets showed significant enrichment for pathways associated with psychostimulant-induced synaptic plasticity (**Table 7**). Some of these 3'UTR targets, including *Gnas, Prkcb, Gria2, Grin2a,* and *Calm2* are associated with "dopaminergic synapse" whereas other 3'UTR targets including *Atp6v1b2, Atp60C, Slc6a1, Slc1a3, and Slc1a2* are associated with "synaptic vesicle cycling." Once again, closer examination of these enriched targets revealed opposing changes in hnRNP H binding as a function of Genotype and methamphetamine treatment (**Figure 10**). Binding of RBPs to 3'UTRs of transcripts provides a rapid means for regulating mRNA translation at sites distance from the cell body such as the synapse (Mayr, 2017; Harvey et al., 2018). Thus, in response to methamphetamine, hnRNP H has the potential to rapidly regulate translation of proteins involved in synaptic function via changes in

bioRxiv preprint doi: https://doi.org/10.1101/2021.07.06.451358; this version posted November 28, 2022. The copyright holder for this preprint (which was not certified by peer review) is the author/funder, who has granted bioRxiv a license to display the preprint in perpetuity. It is made available under aCC-BY-NC-ND 4.0 International license.

3'UTR binding to mRNA transcripts. Intronic targets also showed very similar enriched pathways as those found for 3'UTR targets, thus also implicating hnRNP H in splicing in functional regulation of transcripts and proteins involved in synaptic function as well (**Table 8**).

Cacna2d2 is a methamphetamine-induced binding target of hnRNP H that is differentially regulated at the whole transcript and exon levels in *Hnrnph1* mutants versus wild-types

We next sought to determine the functional consequences of changes in binding on mRNA transcript levels. To integrate striatal hnRNP H binding with gene expression and alternative splicing, we analyzed the transcriptome of striatal tissue from the same samples used in CLIP-seq. We performed both gene- and exon/intron-level transcriptome analyses to identify differentially expressed genes (**Figure 11**) and genes showing evidence for alternative splicing, namely genes showing significant differential exon or intron usage. The genes can be found in the supplementary files associated with GEO accession number GSE160682. *Cacna2d2* was one gene that consistently showed up in our convergent analyses. Specifically, Cacna2d2 was identified as 1) a binding target of hnRNP H; 2) a differentially expressed transcript (Genotype x Treatment); and 3) a transcript showing differential exon/intron usage (Genotype x Treatment; **Figure 12A**). *Cacna2d2* showed a methamphetamine-induced increase in expression in *Hnrnph1* mutants and a methamphetamine-induced decrease in wild-types (**Figure 12B**). A total of 19 genes showed a Genotype x Treatment interaction in differential gene expression (**Figure 12B**) with 6 of them (including *Cacna2d2*) overlapping with hnRNP H targets identified in CLIP-seq (circled in **Figure 12B** and listed in **Table 9**) – a 30% overlap in binding targets and differential expression is much greater than would be expected by chance (Fisher's exact test p = 6.11E-08). One of these 6 genes was the long noncoding RNA *Malat1* which is involved in synapse formation and synaptic transmission (Zhang et al., 2017). Interestingly, multiple studies demonstrated that hnRNP H binds to *Malat1* (Uren et al., 2016; Arun et al., 2020; Scherer et al., 2020). We previously identified a trans-eQTL for *Malat1* that originates within the *Hnrnph1* behavioral QTL for reduced MA-induced locomotor activity (Yazdani et al., 2015). Other overlapping hnRNP H targets showing differential expression include *Mir124*, *Gtf2e2*, *Unc13*, and *Camta1* (**Figures 12A-B**).

Cacna2d2 codes for the voltage-dependent calcium channel subunit $\alpha 2\delta 2$. Our CLIP analysis shows that hnRNP H binds to the 3'UTR of *Cacna2d2* and thus could plausibly regulate synaptic localization, polyadenylation site selection, mRNA stability at the 3'UTR, and ultimately CACNA2D2 protein levels (**Figure**

bioRxiv preprint doi: https://doi.org/10.1101/2021.07.06.451358; this version posted November 28, 2022. The copyright holder for this preprint (which was not certified by peer review) is the author/funder, who has granted bioRxiv a license to display the preprint in perpetuity. It is made available under aCC-BY-NC-ND 4.0 International license.

12C). Three putative *Cacna2d2* isoforms, harboring different 3'UTR lengths, have been annotated by GENCODE. The MEME suite tools (Bailey et al., 2009) identified G-rich motifs (canonical for hnRNP H) within the 3'UTR of *Cacna2d2* (**Figure 12D**). Correspondingly, we detected evidence for alternate usage at the 3'UTR as revealed by a Genotype x Treatment Interaction ($\log_2$FC = -1.37, p = 0.033) in the number of reads mapped to the 3'UTR region. For wild-types, decreased methamphetamine-induced hnRNP H binding was associated with increased 3'UTR usage and decreased *Cacna2d2* expression (**Figure 12E**). However, in *Hnrnph1* mutants, increased binding of hnRNP H was associated with decreased 3'UTR usage and increase in Cacna2d2 transcript levels (**Figure 12E**).

We designed primers to validate this detected differential 3'UTR usage of *Cacna2d2* via qPCR (**Figure 13A**). There was a methamphetamine-induced decrease in usage of the distal end of 3'UTR of *Cacna2d2* in *Hnrnph1* mutants, with no significant change observed in wild-types (right most panel, **Figure 13B**). Notably, according to our CLIP-seq analysis, this distal region in *Cacna2d2* is the binding site for hnRNP H (**Figure 12C**). Immunoblotting of the opposite hemisphere from the same samples as in **Figure 13B** revealed no significant change in CACNA2D2 protein after methamphetamine treatment relative to saline in the wild-types and *Hnrnph1* mutants (**Figures 13C and 14**).

The methamphetamine-induced opposing differences in hnRNP H-Cacna2d2 interactions in *Hnrnph1* mutants and wild-types regarding differential 3'UTR usage and *Cacna2d2* expression warranted further functional investigation at the behavioral level. First, to determine if perturbing CACNA2D2 would have a genotype-specific effect on basal locomotion, we tested the consequence of administration of the a2d2/a2d1 inhibitor pregabalin on basal locomotor activity following saline injections and the potential influence of *Hnrnph1* genotype on the effects of pregabalin (**Figure 15A**). There was no effect of pregabalin on basal locomotion in response to saline (**Figure 15B**).

Next, in a separate set of experimental cohorts of mice, we tested the effect of pregabalin on methamphetamine-induced locomotor activity and the potential influence of *Hnrnph1* genotype on this outcome measure. There was a Sex x Time x pregabalin Treatment effect (p = 0.03) that warranted separate analyses in females and males. For females, there was a Genotype x Treatment interaction (p = 0.037) that was explained by pregabalin treatment inducing a large reduction in methamphetamine-induced locomotor activity in wild-types, while having no effect in *Hnrnph1* mutants (**Figure 15C**). In males, there was no significant effect of pregabalin

bioRxiv preprint doi: https://doi.org/10.1101/2021.07.06.451358; this version posted November 28, 2022. The copyright holder for this preprint (which was not certified by peer review) is the author/funder, who has granted bioRxiv a license to display the preprint in perpetuity. It is made available under aCC-BY-NC-ND 4.0 International license.

on methamphetamine behavior in either genotype (**Figure 15D**). There was no baseline locomotion detected on the two habituation days (**Figure 16**). Overall, these behavioral pharmacological results support the hypothesis that wild-type hnRNP H-Cacna2d2 interactions contribute to methamphetamine-induced behavior and that this contribution is disrupted in *Hnrnph1* mutants.

Because the CLIP and gene expression data implicated differential 3'UTR usage of *Cacna2d2* in *Hnrnph1* mutants vs. wild-types (**Figure 13**), we once again examined 3'UTR usage in whole striatal tissue in response to pregabalin in saline- and methamphetamine-treated wild-types and *Hnrnph1* mutants. Because pregabalin inhibits CACNA2D2 and because Cacna2d2 is an hnRNP H target, we wanted to know if pregabalin pre-treatment would lead to a cellular adaptive response as measured via changes in *Cacna2d2* transcripts under saline and methamphetamine conditions and whether any adaptive response observed would depend on *Hnrnph1* genotype. We hypothesized that because hnRNP H targets the 3' UTR of *Cacna2d2*, then pregabalin could interact with *Hnrnph1* genotype to affect 3'UTR usage of *Cacna2d2*. There was no effect of pregabalin on proximal or distal 3'UTR *Cacna2d2* usage between genotypes in mice administered pregabalin followed by saline (**Figures 17A, C)**. Following methamphetamine, pregabalin induced a significant increase in proximal 3'UTR usage of *Cacna2d2* in wild-type mice, but not in the *Hnrnph1* mutants (**Figure 17B**). Intriguingly, there was no effect of pregabalin on distal 3'UTR usage in either genotype following methamphetamine (**Figure 17D**). Finally, there was no effect of pregabalin on whole striatal CACNA2D2 protein levels under saline or methamphetamine conditions in either genotype (**Figures 17E-F**). Overall, our results provide evidence that under methamphetamine treatment, pharmacological inhibition of $\alpha 2\delta 2$ leads to increased proximal 3'UTR usage of *Cacna2d2* which could ultimately affect cellular responses and behavior.

bioRxiv preprint doi: https://doi.org/10.1101/2021.07.06.451358; this version posted November 28, 2022. The copyright holder for this preprint (which was not certified by peer review) is the author/funder, who has granted bioRxiv a license to display the preprint in perpetuity. It is made available under aCC-BY-NC-ND 4.0 International license.

DISCUSSION

This study defined the basal and methamphetamine-induced hnRNP H striatal targetome *in vivo* in wild-types versus *Hnrnph1* mutants showing deficits in methamphetamine-induced dopamine release and behavior. The hnRNP H targetome shows rapid plasticity and provides a unique analysis where CLIP-seq aided in our understanding of gene regulation induced by drugs of abuse via a behaviorally relevant RNA-binding protein.

The *Hnrnph1* mutation had a global effect on the hnRNP H targetome at baseline and opposite methamphetamine-induced perturbations versus wild-types. This result mirrors the opposite methamphetamine-induced changes in synaptic mitochondrial proteins in striatal synaptosomal fractions in *Hnrnph1* mutants versus wildtypes (Ruan et al., 2020a) and predicts genotype-dependent treatment effects on synaptic transmission, signaling, and behavior. Differential 3'UTR usage, exon usage, and gene expression triangulated on *Cacna2d2* as a methamphetamine-induced RNA-binding target of hnRNP H that could modulate behavior. Pharmacological inhibition of CACNA2D2 with pregabalin recapitulated the mutant behavior by decreasing methamphetamine-induced locomotor activity in female wild-types, supporting CACNA2D2 as an RNA target linking hnRNP H with methamphetamine behavior.

hnRNP H localizes primarily to the nucleus of neurons in adult mice (Kamma et al., 1995; van Dusen et al., 2010; Ruan et al., 2020a), with low levels in cytoplasm (Wall et al., 2020). Nuclear binding of RBPs to 3'UTRs guides cytoplasmic localization and translation of mRNAs (Guramrit et al., 2015). Thus, nuclear hnRNP H binding to 3'UTRs of mRNAs could recruit other proteins necessary for export of mRNAs to cytoplasm for translation. Accordingly, most striatal hnRNP H targets were enriched for excitatory synaptic transmission and psychostimulant addiction (**Figure 5**). RBP-bound mRNAs are often functionally related because they share sequence elements recognized by the RBP and are post-transcriptionally regulated in concert (Keene and Tenenbaum, 2002). For hnRNP H, the core motifs in most target mRNAs were G-rich sequences (**Figure 3C**), consistent with prior reports (Russo et al., 2010; Lefave et al., 2011; Huelga et al., 2012; Uren et al., 2016). Interestingly, most target mRNAs containing these G-rich motifs code for pre-synaptic calcium channel subunits (**Figure 3D**) that are enriched for pre-synaptic neurotransmitter release and psychostimulant-induced post-synaptic excitatory plasticity (**Table 7**). Strikingly, 3'UTR targets showed large genotypic differences in baseline binding (increased in *Hnrnph1* mutants) and opposite methamphetamine-induced changes in hnRNP H binding (decreased in *Hnrnph1* mutants; **Figure 10**). Increased basal binding of hnRNP H to 3'UTR targets in *Hnrnph1*

bioRxiv preprint doi: https://doi.org/10.1101/2021.07.06.451358; this version posted November 28, 2022. The copyright holder for this preprint (which was not certified by peer review) is the author/funder, who has granted bioRxiv a license to display the preprint in perpetuity. It is made available under aCC-BY-NC-ND 4.0 International license.

mutants might be explained by the robust increase in synaptic hnRNP H in the striatum in the mutants (Ruan et al., 2020a). The enrichment terms of 3'UTR-bound mRNAs support synaptically localized/destined mRNAs poised for rapid translation (Bae and Miura, 2020).

Cacna2d2 emerged as an interesting hnRNP H target showing a methamphetamine-induced decrease in binding and usage of the 3'UTR and an increase in *Cacna2d2* transcript in *Hnrnph1* mutants (**Figure 12E**). *Cacna2d2* is expressed in cerebellum, striatum, and hippocampus (Dolphin, 2012), and codes for a pre-protein that is processed into $\alpha2$ and $\delta2$ subunits of voltage-gated calcium channels (**VGCCs**) (Dolphin and Lee, 2020). $\alpha2\delta2$ subunits localize VGCCs to the active zone and promote neurotransmitter release (Dolphin, 2013). The effects of $\alpha2\delta2$ subunits on synaptic transmission are complex. Overexpression of $\alpha2\delta2$ subunits decreased presynaptic calcium elevation following an action potential, yet increased vesicular release (Hoppa et al., 2012). Additionally, overexpression of *Cacna2d2* disrupted intracellular calcium signaling and mitochondrial function (Carboni et al., 2003). Following calcium influx, mitochondria can buffer intracellular calcium (Rizzuto et al., 2012). Our previous proteomic analysis of the striatal synaptosome showed opposite baseline and methamphetamine-induced changes in mitochondrial protein levels in *Hnrnph1* mutants versus wild-types (Ruan et al., 2020a). Methamphetamine inhibits calcium entry into L-type and N-type VGCCs and longer exposure induces a compensatory upregulation of *Cacna1c* transcript in SH-SY5Y cells (Andres et al., 2015). Intracellular and extracellular calcium contribute to methamphetamine-induced dopamine release in the ventral striatum (Yorgason et al., 2020). The *Cacna2d2* dynamics at multiple levels following methamphetamine treatment implicates regulation of calcium channel subunits (**Table 4**) as a rapid, adaptive means for controlling calcium entry following the methamphetamine-induced surge in dopamine release.

RNA-seq identified a methamphetamine-induced *increase* in *Cacna2d2* transcript levels in *Hnrnph1* mutants and a *decrease* in wild-types **(Figure 12E);** however, we did not replicate this finding via RT-qPCR in independent samples using primers against *Cacna2d2* coding exons 3-4 or 37-38 **(Figure 13B).** We used random hexamers to generate cDNA for RNA-seq versus oligo dTs to generate cDNA for qPCR in new samples which could explain the lack of replication. We chose oligo dTs for qPCR validation because we were most interested in mRNAs associated with protein translation. We also did not observe any genotypic difference in CACNA2D2 protein at baseline or following methamphetamine (**Figure 13C**). Similar to hnRNP H protein, the lack of genotypic differences in CACNA2D2 protein could be explained by its synaptic localization and the fact

bioRxiv preprint doi: https://doi.org/10.1101/2021.07.06.451358; this version posted November 28, 2022. The copyright holder for this preprint (which was not certified by peer review) is the author/funder, who has granted bioRxiv a license to display the preprint in perpetuity. It is made available under aCC-BY-NC-ND 4.0 International license.

that we examined whole tissue striatum rather than synaptosomes (Ruan et al., 2020a) - an important question for future investigation of the synaptosomal hnRNP H targetome.

In testing CACNA2D2 as a candidate target linking hnRNP H binding to gene regulation and behavior, pregabalin recapitulated the *Hnrnph1* mutant phenotype of reduced methamphetamine locomotion in wild-type females without having any effect in mutants (**Figure 15C**) or in males **(Figure 15D)**. Pregabalin is used to treat seizures (Panebianco et al., 2019), neuropathic pain (Attal et al., 2010), and anxiety (Slee et al., 2019). Our findings are the first to show that pregabalin can attenuate methamphetamine-induced behavior and compliment studies showing pregabalin-induced decrease in ketamine- (Nunes et al., 2012) and morphine-induced locomotion (Vashchinkina et al., 2018) and in cocaine oral self-administration (de Guglielmo et al., 2013). Prior work with gabapentin, a CACNA2D1 inhibitor, showed a reduction in methamphetamine-induced locomotor sensitization (Kurokawa et al., 2010).

The female-specific reduction in methamphetamine-induced locomotor activity by pregabalin in wild-type mice was surprising. One study found that pregabalin induced conditioned place preference at lower doses in females versus males (Alsaab et al., 2020), suggesting females are more sensitive to pregabalin. Another unanticipated finding in the pregabalin study was the lack of methamphetamine behavioral phenotype in *Hnrnph1* mutants that we replicated in multiple studies (Yazdani et al., 2015; Ruan et al., 2020a), including here (**Figure 1C**). We suspect that the extra saline injection procedure 30 min prior to methamphetamine administration led to the loss of *Hnrnph1* Genotype effect. We have observed other such disruptions of main effects with extra saline injections in other behavioral models (e.g., placebo analgesia.)

To assess the effect of pregabalin on *Cacna2d2* expression, we quantified Cacna2d2 mRNA and protein at 60 min post-methamphetamine injection (instead of 30 min; **Figure 17**) and (90 min post-pregabalin). This was a strategic decision upfront to ensure we would not miss any time window where pregabalin might have an effect. In retrospect, pregabalin's behavioral effects were most pronounced within the first 30 min; thus, analyzing *Cacna2d2* expression at 30 min post-methamphetamine might yield more robust results. Furthermore, a limitation of our design was that we could not directly compare methamphetamine treatment effects on *Cacna2d2* expression. Our rationale for separate methamphetamine and saline experiments was that we first wanted to determine if there was an effect of pregabalin on methamphetamine behavior. Upon observing a significant

bioRxiv preprint doi: https://doi.org/10.1101/2021.07.06.451358; this version posted November 28, 2022. The copyright holder for this preprint (which was not certified by peer review) is the author/funder, who has granted bioRxiv a license to display the preprint in perpetuity. It is made available under aCC-BY-NC-ND 4.0 International license.

behavioral result, we then ran the experiment involving saline-treated mice, to rule out non-specific effects of pregabalin on locomotion.

Despite these limitations, we observed an increase of Cacna2d2 proximal 3'UTR mRNA in wild-types, but not *Hnrnph1* mutants injected with pregabalin and methamphetamine (**Figure 17B**) and not in either genotype when saline was administered (**Figure 17A**). This pattern fits the behavioral findings (in females, at least) whereby increased 3' proximal UTR usage associated with decreased methamphetamine behavior. Pregabalin binds to $\alpha2\delta1$ and $\alpha2\delta2$ subunits with similar affinities and in several brain regions, including striatum (Li et al., 2011). As both $\alpha2\delta1$ and $\alpha2\delta2$ subunits are expressed in the rodent striatum (Barclay and Rees, 2000; Taylor and Garrido, 2008), pregabalin could also influence *Cacna2d1* expression, which, along with binding to $\alpha2\delta1$, could also contribute to the pregabalin-induced reduction in methamphetamine behavior.

To conclude, we provide the first methamphetamine-induced RNA targetome on an RBP, hnRNP H. Analysis of drug-induced RBP targetomes, especially drugs of abuse, is a novel, understudied approach for understanding rapid, synaptic gene regulation as it relates to cell biological adaptations in neuronal excitability, neurotransmitter release, plasticity, and behavior. We focused on hnRNP H, given the evidence for its role in methamphetamine-induced dopamine release and addiction model behaviors (Yazdani et al., 2015; Bryant and Yazdani, 2016; Ruan et al., 2020a, 2020b) across multiple substances (Bryant et al., 2020; Fultz et al., 2021). We established hnRNP H as a novel gene regulatory link among several target mRNAs coding for proteins known to mediate psychostimulant-induced neurotransmission and plasticity. Finally, we pharmacologically validated CACNA2D2 as a functional mechanistic target linking the *Hnrnph1* mutation with methamphetamine behavior. Our study design represents a powerful approach for triangulating complementary -omics datasets that can be broadly applied to the study of drug-induced RBP-RNA dynamics and discovery of RNA-binding targets underlying cell biological responses and neurobehavioral adaptations that can be leveraged for novel therapeutics.

bioRxiv preprint doi: https://doi.org/10.1101/2021.07.06.451358; this version posted November 28, 2022. The copyright holder for this preprint (which was not certified by peer review) is the author/funder, who has granted bioRxiv a license to display the preprint in perpetuity. It is made available under aCC-BY-NC-ND 4.0 International license.

REFERENCES

Agarwal V, Bell GW, Nam JW, Bartel DP (2015) Predicting effective microRNA target sites in mammalian mRNAs. Elife 4:1–38.

Aldridge GM, Podrebarac DM, Greenough WT, Weiler IJ (2009) The use of total protein stains as loading controls: an alternative to high-abundance single protein controls in semi-quantitative immunoblotting Georgina. J Neurosci Methods 172:250–254.

Alsaab HO, Altowairqi E, Alzahrani N, Alzahrani R, Alshehri FS, Almalki AH, Alsanie WF, Gaber A, Alkhalifa T, Almalki A, Shah ZA, Althobaiti YS (2020) Sex differences in pregabalin-seeking like behavior in a conditioned place preference paradigm. Saudi Pharmaceutical Journal 28:1749–1755.

Andres MA, Cooke IM, Bellinger FP, Berry, MJ, Zaporteza M, Rueli RH, Barayuga SM, Chang L (2015) Methamphetamine acutely inhibits voltage-gated calcium channels but chronically upregulates L-type channels. J Neurochem 134:56–65.

Arhin GGK, Boots M, Bagga PPS, Milcarek C, Wilusz J (2002) Downstream sequence elements with different affinities for the hnRNP H/H' protein influence the processing efficiency of mammalian polyadenylation signals. Nucleic Acids Res 30:1842–1850.

Arun G, Aggarwal D, Spector DL (2020) MALAT1 Long Non-Coding RNA: Functional Implications. Noncoding RNA 6:22.

Attal N, Cruccu G, Baron R, Haanpa M, Hansson P, Jensen T, Nurmikko T (2010) EFNS GUIDELINES EFNS guidelines on the pharmacological treatment of neuropathic pain: 2010 revision. Eur J Neurol 17:1113-e88.

Bae B, Miura P (2020) Emerging roles for 3' UTRs in neurons. Int J Mol Sci 21:1–24.

Bailey TL, Boden M, Buske FA, Frith M, Grant CE, Clementi L, Ren J, Li WW, Noble WS (2009) MEME Suite: Tools for motif discovery and searching. Nucleic Acids Res 37:202–208.

Barclay J, Rees M (2000) Genomic organization of the mouse and human α2δ2 voltage-dependent calcium channel subunit genes. Mammalian Genome 11:1142–1144.

Baumann MH, Ayestas MA, Sharpe LG, Lewis DB, Rice KC, Rothman RB (2002) Persistent antagonism of methamphetamine-induced dopamine release in rats pretreated with GBR12909 decanoate. Journal of Pharmacology and Experimental Therapeutics 301:1190–1197.

bioRxiv preprint doi: https://doi.org/10.1101/2021.07.06.451358; this version posted November 28, 2022. The copyright holder for this preprint (which was not certified by peer review) is the author/funder, who has granted bioRxiv a license to display the preprint in perpetuity. It is made available under aCC-BY-NC-ND 4.0 International license.

Bolger AM, Lohse M, Usadel B (2014) Trimmomatic: A flexible trimmer for Illumina sequence data. Bioinformatics 30:2114–2120.

Borrelli KN, Langan CR, Dubinsky KR, Szumlinski KK, Carlezon WA, Chartoff EH, Bryant CD (2021) Intracranial self-stimulation and concomitant behaviors following systemic methamphetamine administration in Hnrnph1 mutant mice. Psychopharmacology (Berl) 238:2031–2041.

Bryant CD, Healy AF, Ruan QT, Coehlo MA, Lustig E, Yazdani N, Luttik KP, Tran T, Swancy I, Brewin LW, Chen MM, Szumlinski KK (2020) Sex-dependent effects of an Hnrnph1 mutation on fentanyl addiction-relevant behaviors but not antinociception in mice. Genes Brain Behav 20:1–37.

Bryant CD, Yazdani N (2016) RNA binding proteins, neural development and the addictions. Genes Brain Behav 15:169–186.

Carboni GL, Gao B, Nishizaki M, Xu K, Minna JD, Roth JA, Ji L (2003) CACNA2D2-mediated apoptosis in NSCLC cells is associated with alterations of the intracellular calcium signaling and disruption of mitochondria membrane integrity. Oncogene 22:615–626.

Coutens B, Mouledous L, Stella M, Rampon C, Lapeyre-mestre M, Roussin A, Guiard BP, Jouanjus E (2019) Lack of correlation between the activity of the mesolimbic dopaminergic system and the rewarding properties of pregabalin in mouse. Psychopharmacology (Berl) 236:2069–2082.

Darnell JC, Driesche SJ Van, Zhang C, Hung KYS, Mele A, Fraser CE, Stone EF, Chen C, Fak JJ, Chi SW, Licatalosi DD, Richter JD, Darnell RB (2011) FMRP stalls ribosomal translocation on mRNAs linked to synaptic function and autism. Cell 146:247–261.

Darnell RB (2013) RNA Protein Interaction in Neurons. Annu Rev Neurosci 36:243–270.

de Guglielmo G, Cippitelli A, Somaini L, Gerra G, Li H, Stopponi S, Ubaldi M, Kallupi M, Ciccocioppo R (2013) Pregabalin reduces cocaine self-administration and relapse to cocaine seeking in the rat. Addiction Biology 18:644–653.

Dobin A, Davis CA, Schlesinger F, Drenkow J, Zaleski C, Jha S, Batut P, Chaisson M, Gingeras TR (2013) STAR: Ultrafast universal RNA-seq aligner. Bioinformatics 29:15–21.

Dolphin AC (2012) Calcium channel auxiliary α2δ and β subunits: Trafficking and one step beyond. Nat Rev Neurosci 13:542–555.

bioRxiv preprint doi: https://doi.org/10.1101/2021.07.06.451358; this version posted November 28, 2022. The copyright holder for this preprint (which was not certified by peer review) is the author/funder, who has granted bioRxiv a license to display the preprint in perpetuity. It is made available under aCC-BY-NC-ND 4.0 International license.

Dolphin AC (2013) The α2δ subunits of voltage-gated calcium channels. Biochim Biophys Acta Biomembr 1828:1541–1549.

Dolphin AC, Lee A (2020) Presynaptic calcium channels: specialized control of synaptic neurotransmitter release. Nat Rev Neurosci 21:213–229.

Fish EW, Krouse MC, Stringfield SJ, DiBerto JF, Robinson JE, Malanga CJ (2013) Changes in Sensitivity of Reward and Motor Behavior to Dopaminergic, Glutamatergic, and Cholinergic Drugs in a Mouse Model of Fragile X Syndrome. PLoS One 8:1–14.

Fleckenstein AE, Volz TJ, Hanson GR (2009) Psychostimulant-induced alterations in vesicular monoamine transporter-2 function: Neurotoxic and therapeutic implications. Neuropharmacology 56:133–138.

Fukuda T, Naiki T, Saito M, Irie K (2009) hnRNP K interacts with RNA binding motif protein 42 and functions in the maintenance of cellular ATP level during stress conditions. Genes to Cells 14:113–128.

Fukunaga T, Iwakiri J, Ono Y, Hamada M (2019) Lncrrisearch: A web server for lncRNA-RNA interaction prediction integrated with tissue-specific expression and subcellular localization data. Front Genet 10:1–6.

Fulks JL, Obryhim BE, Wenzel SK, Fowler SC, Vorontsova E, Pinkston JW, Ortiz AN, Johnson MA (2010) Dopamine release and uptake impairments and behavioral alterations observed in mice that model fragile X mental retardation syndrome. ACS Chem Neurosci 1:679–690.

Fultz EK, Coelho MA, Lieberman D, Jimenez-Chavez L, Bryant CD, Szumlinski KK (2021) Hnrnph1 is a Novel Regulator of Alchohol Reward. Drug Alcohol Depend 220:1–27.

Galbraith N (2015) The methamphetamine problem. BJPsych Bull 39:218–220.

Geuens T, Bouhy D, Timmerman V (2016) The hnRNP family: insights into their role in health and disease. Hum Genet 135:851–867.

Gilda JE, Gomes A V. (2013) Stain Free Total Protein Staining is a Superior Loading Control to β-Actin for Western Blots. Anal Biochem 440:1–6.

Guil S, Long JC, Cáceres JF (2006) hnRNP A1 Relocalization to the Stress Granules Reflects a Role in the Stress Response. Mol Cell Biol 26:5744–5758.

Guramrit S, Gabriel P, Gene W. Y, Melissa J. M (2015) The Clothes Make the mRNA: Past and Present Trends in mRNP Fashion. Annu Rev Biochem:229–262.

bioRxiv preprint doi: https://doi.org/10.1101/2021.07.06.451358; this version posted November 28, 2022. The copyright holder for this preprint (which was not certified by peer review) is the author/funder, who has granted bioRxiv a license to display the preprint in perpetuity. It is made available under aCC-BY-NC-ND 4.0 International license.

Han K, Yeo G, An P, Burge CB, Grabowski PJ (2005) A combinatorial code for splicing silencing: UAGG and GGGG motifs. PLoS Biol 3:0843–0860.

Han SP, Tang YH, Smith R (2010) Functional diversity of the hnRNPs: past, present and perspectives. Biochem J 430:379–392.

Harvey RF, Smith TS, Mulroney T, Queiroz RML, Pizzinga M, Dezi V, Villenueva E, Ramakrishna M, Lilley KS, Willis AE (2018) Trans-acting translational regulatory RNA binding proteins. Wiley Interdiscip Rev RNA 9:1–19.

Hedegaard H, Miniño AM, Warner M (2020) Drug Overdose Deaths in the United States, 1999-2018. NCHS Data Brief:1–8.

Heinz S, Benner C, Spann N, Bertolino E, Lin YC, Laslo P, Cheng JX, Murre C, Singh H, Glass CK (2010) Simple combinations of lineage-determining transcription factors prime cis-regulatory elements required for macrophage and B cell identities. Mol Cell 38:576–589.

Hentze MW, Castello A, Schwarzl T, Preiss T (2018) A brave new world of RNA-binding proteins. Nat Rev Mol Cell Biol 19:327–341.

Honoré B, Rasmussen HH, Vorum H, Dejgaard K, Liu X, Gromov P, Madsen P, Gesser B, Tommerup N, Celis JE (1995) Heterogeneous nuclear ribonucleoproteins H, H′, and F are members of a ubiquitously expressed subfamily of related but distinct proteins encoded by genes mapping to different chromosomes. Journal of Biological Chemistry 270:28780–28789.

Hoppa MB, Lana B, Margas W, Dolphin AC, Ryan TA (2012) α2δ Expression Sets Presynaptic Calcium Channel Abundance and Release Probability. Nature 486:122–125.

Huebschman JL, Davis MC, Tovar Pensa C, Guo Y, Smith LN (2021) The fragile X mental retardation protein promotes adjustments in cocaine self-administration that preserve reinforcement level. European Journal of Neuroscience 54:4920–4933.

Huelga SC, Vu AQ, Arnold JD, Liang TD, Liu PP, Yan BY, Donohue JP, Shiue L, Hoon S, Brenner S, Ares M, Yeo GW (2012) Integrative Genome-wide Analysis Reveals Cooperative Regulation of Alternative Splicing by hnRNP Proteins. Cell Rep 1:167–178.

Kamma H, Portman DSDS, Dreyfuss G (1995) Cell Type-Specific Expression of hnRNP Proteins. Exp Cell Res 221:187–196.

bioRxiv preprint doi: https://doi.org/10.1101/2021.07.06.451358; this version posted November 28, 2022. The copyright holder for this preprint (which was not certified by peer review) is the author/funder, who has granted bioRxiv a license to display the preprint in perpetuity. It is made available under aCC-BY-NC-ND 4.0 International license.

Kanehisa M, Sato Y, Furumichi M, Morishima K, Tanabe M (2019) New approach for understanding genome variations in KEGG. Nucleic Acids Res 47:D590–D595.

Karolchik D, Hinrichs AS, Furey TS, Roskin KM, Sugnet CW, Haussler D, Kent WJ, Center (2004) The UCSC Table Browser data retrieval tool. Nucleic Acids Res 32:D493–D496.

Katz Y, Wang ETT, Airoldi EMM, Burge CBB (2010) Analysis and design of RNA sequencing experiments for identifying isoform regulation. Nat Methods 7:1009–1015.

Keene JD, Tenenbaum SA (2002) Eukaryotic mRNPs may represent posttranscriptional operons. Mol Cell 9:1161–1167.

Keleta YB, Martinez JL (2012) Brain Circuits of Methamphetamine Place Reinforcement Learning: The Role of the Hippocampus-VTA Loop. Brain Behav 2:128–141.

Kish SJ (2008) Pharmacologic mechanisms of crystal meth. CMAJ 178:1679–1682.

Kurokawa K, Shibasaki M, Ohkuma S (2010) Methamphetamine-induced up-regulation of α2/δ subunit of voltage-gated calcium channels is regulated by DA receptors. Synapse 64:822–828.

Lefave C V, Squatrito M, Vorlova S, Rocco GL, Brennan CW, Holland EC, Pan Y, Cartegni L (2011) Splicing factor hnRNPH drives an oncogenic splicing switch in gliomas. EMBO J 30:4084–4097.

Li Z, Taylor CP, Weber M, Piechan J, Prior F, Bian F, Cui M, Hoffman D, Donevan S (2011) Pregabalin is a potent and selective ligand for α 2δ-1 and α 2δ-2 calcium channel subunits. Eur J Pharmacol 667:80–90.

Liao Y, Smyth GK, Shi W (2014) FeatureCounts: An efficient general purpose program for assigning sequence reads to genomic features. Bioinformatics 30:923–930.

Liao Y, Wang J, Jaehnig EJ, Shi Z, Zhang B (2019) WebGestalt 2019: gene set analysis toolkit with revamped UIs and APIs. Nucleic Acids Res 47:W199–W205.

Livak KJ, Schmittgen TD (2001) Analysis of relative gene expression data using real-time quantitative PCR and the 2-ΔΔCT method. Methods 25:402–408.

Lominac KD, McKenna CL, Schwartz LM, Ruiz PN, Wroten MG, Miller BW, Holloway JJ, Travis KO, Rajasekar G, Maliniak D, Thompson AB, Urman LE, Phillips TJ, Szumlinski KK (2014) Mesocorticolimbic monoamine correlates of methamphetamine sensitization and motivation. Front Syst Neurosci 8:1–19.

Mancini E, Rabinovich A, Iserte J, Yanovsky M (2020) ASpli: Analysis of alternative splicing using RNA-Seq. R package version 1140.

bioRxiv preprint doi: https://doi.org/10.1101/2021.07.06.451358; this version posted November 28, 2022. The copyright holder for this preprint (which was not certified by peer review) is the author/funder, who has granted bioRxiv a license to display the preprint in perpetuity. It is made available under aCC-BY-NC-ND 4.0 International license.

Markmiller S, Soltanieh S, Server KL, Mak R, Jin WJ, Fang MY, Luo E-C, Krach F, Yang D, Sen A, Fulzele A, Yeo GW, Wozniak JM, Gonzalez DJ, Kankel MW, Gao F-B, Bennett EJ, Lécuyer E (2018) Context-Dependent and Disease-Specific Diversity in Protein Interactions within Stress Granules. Cell 172:590–604.

Mayr C (2017) Regulation by 3 -Untranslated Regions. Annual Reviews 51:171–194.

Merico D, Isserlin R, Stueker O, Emili A, Bader GD (2010) Enrichment map: A network-based method for gene-set enrichment visualization and interpretation. PLoS One 5:e13984.

Nunes EA, Canever L, Oliveira L De, Luca RD De, Quevedo J, Zugno A, Peregrino A, Crippa JAS, Dursun SM, Baker GB, Hallak JEC (2012) Effects of pregabalin on behavioral alterations induced by ketamine in rats. Braz J Psychiatry 34:329–333.

Panebianco M, Bresnahan R, Hemming K, Marson A (2019) Pregabalin add-on for drug-resistant focal epilepsy (Review). Cochrane Database Syst Rev 7:CD005612.

Pilch J, Koppolu AA, Walczak A, Murcia Pienkowski VA, Biernacka A, Skiba P, Machnik-Broncel J, Gasperowicz P, Kosińska J, Rydzanicz M, Emich-Widera E, Płoski R (2018) Evidence for HNRNPH1 being another gene for Bain type syndromic mental retardation. Clin Genet 94:381–385.

Quinlan AR, Hall IM (2010) BEDTools: A flexible suite of utilities for comparing genomic features. Bioinformatics 26:841–842.

Raudvere U, Kolberg L, Kuzmin I, Arak T, Adler P, Peterson H, Vilo J (2019) G:Profiler: A web server for functional enrichment analysis and conversions of gene lists (2019 update). Nucleic Acids Res 47:W191–W198.

Reichert SC et al. (2020) HNRNPH1-related syndromic intellectual disability: Seven additional cases suggestive of a distinct syndromic neurodevelopmental syndrome. Clin Genet 98:91–98.

Reimand J, Isserlin R, Voisin V, Kucera M, Tannus-Lopes C, Rostamianfar A, Wadi L, Meyer M, Wong J, Xu C, Merico D, Bader GD (2019) Pathway enrichment analysis and visualization of omics data using g:Profiler, GSEA, Cytoscape and EnrichmentMap. Nat Protoc 14:482–517.

Rieger MA, King DM, Crosby H, Liu Y, Cohen BA, Dougherty JD (2020) CLIP and Massively Parallel Functional Analysis of CELF6 Reveal a Role in Destabilizing Synaptic Gene mRNAs through Interaction with 3′ UTR Elements. Cell Rep 33:108531 Available at: https://doi.org/10.1016/j.celrep.2020.108531.

bioRxiv preprint doi: https://doi.org/10.1101/2021.07.06.451358; this version posted November 28, 2022. The copyright holder for this preprint (which was not certified by peer review) is the author/funder, who has granted bioRxiv a license to display the preprint in perpetuity. It is made available under aCC-BY-NC-ND 4.0 International license.

Ritchie ME, Phipson B, Wu D, Hu Y, Law CW, Shi W, Smyth GK (2015) Limma powers differential expression analyses for RNA-sequencing and microarray studies. Nucleic Acids Res 43:e47.

Rizzuto R, De Stefani D, Raffaello A, Mammucari C (2012) Mitochondria as sensors and regulators of calcium signalling. Nat Rev Mol Cell Biol 13:566–578.

Robinson MD, McCarthy DJ, Smyth GK (2009) edgeR: A Bioconductor package for differential expression analysis of digital gene expression data. Bioinformatics 26:139–140.

Ruan QT et al. (2020a) A mutation in hnRNPH1 that decreases methamphetamine-induced reinforcement, reward, and dopamine release and increases synaptosomal hnRNP H and mitochondrial proteins. Journal of Neuroscience 40:107–130.

Ruan QT, Yazdani N, Beierle JA, Hixson KM, Hokenson KE, Apicco DJ, Luttik KP, Zheng K, Maziuk BF, Ash PEA, Szumlinski KK, Russek SJ, Wolozin B, Bryant CD (2018) Changes in neuronal immunofluorescence in the C- versus N-terminal domains of hnRNP H following D1 dopamine receptor activation. Neurosci Lett 684:109–114.

Ruan QT, Yazdani N, Reed ER, Beierle JA, Peterson LP, Luttik KP, Szumlinski KK, Johnson WE, Ash PEA, Wolozin B, Bryant CD (2020b) 5′ UTR variants in the quantitative trait gene Hnrnph1 support reduced 5′ UTR usage and hnRNP H protein as a molecular mechanism underlying reduced methamphetamine sensitivity. FASEB Journal 34:9223–9244.

Russo A, Siciliano G, Catillo M, Giangrande C, Amoresano A, Pucci P, Pietropaolo C, Russo G (2010) hnRNP H1 and intronic G runs in the splicing control of the human rpL3 gene. Biochim Biophys Acta Gene Regul Mech 1799:419–428.

Scherer M, Levin M, Butter F, Scheibe M (2020) Quantitative proteomics to identify nuclear rna- binding proteins of malat1. Int J Mol Sci 21:1–12.

Siciliano CA, Calipari ES, Ferris MJ, Jones SR (2014) Biphasic mechanisms of amphetamine action at the dopamine terminal. Journal of Neuroscience 34:5575–5582.

Slee A, Nazareth I, Bondaronek P, Liu Y, Cheng Z, Freemantle N (2019) Articles Pharmacological treatments for generalised anxiety disorder : a systematic review and network meta-analysis. The Lancet 6736:1–10.

Smith LN, Jedynak JP, Fontenot MR, Hale CF, Dietz KC, Taniguchi M, Thomas FS, Zirlin BC, Birnbaum SG, Huber M, Thomas MJ, Cowan CW, Smith LN, Jedynak JP, Fontenot MR (2014) Fragile X mental

bioRxiv preprint doi: https://doi.org/10.1101/2021.07.06.451358; this version posted November 28, 2022. The copyright holder for this preprint (which was not certified by peer review) is the author/funder, who has granted bioRxiv a license to display the preprint in perpetuity. It is made available under aCC-BY-NC-ND 4.0 International license.

retardation protein regulates synaptic and behavioral plasticity to repeated cocaine administration. Neuron 82:645–658.

Smith T, Heger A, Sudbery I (2017) UMI-tools: Modelling sequencing errors in Unique Molecular Identifiers to improve quantification accuracy. Genome Res 27.

Taylor CP, Garrido R (2008) Immunostaining of rat brain, spinal cord, sensory neurons and skeletal muscle for calcium channel alpha2-delta (α2-δ) type 1 protein. Neuroscience 155:510–521.

Thorvaldsdóttir H, Robinson JT, Mesirov JP (2013) Integrative Genomics Viewer (IGV): High-performance genomics data visualization and exploration. Brief Bioinform 14:178–192.

Uren PJ, Bahrami-Samani E, de Araujo PR, Vogel C, Qiao M, Burns SC, Smith AD, Penalva LOF (2016) High-throughput analyses of hnRNP H1 dissects its multi-functional aspect. RNA Biol:1–12.

van Dusen CM, Yee L, McNally LM, McNally MT (2010) A glycine-rich domain of hnRNP H/F promotes nucleocytoplasmic shuttling and nuclear import through an interaction with transportin 1. Mol Cell Biol 30:2552–2562.

van Nostrand EL, Pratt GA, Shishkin AA, Gelboin- C, Fang MY, Sundararaman B, Blue SM, Thai B, Surka C, Elkins K, Stanton R, Rigo F, Yeo GW, Jolla L, Program C, Jolla L, Jolla L, California J, Engineering B (2016) Robust transcriptome-wide discovery of RNA binding protein binding sites with enhanced CLIP (eCLIP). Nat Methods 13:508–514.

Vashchinkina E, Piippo O, Vekovischeva O, Krupitsky E, Ilyuk R, Neznanov N, Kazankov K, Zaplatkin I, Korpi ER (2018) Addiction-related interactions of pregabalin with morphine in mice and humans: reinforcing and inhibiting effects. Addiction Biology 23:945–958.

Wall ML, Bera A, Wong FK, Lewis SM (2020) Cellular stress orchestrates the localization of hnRNP H to stress granules. Exp Cell Res 394:112111.

Wise RA (2004) Dopamine, learning and motivation. Nat Rev Neurosci 5:483–494.

Xu J et al. (2014) A Heroin Addiction Severity-Associated Intronic Single Nucleotide Polymorphism Modulates Alternative Pre-mRNA Splicing of the Opioid Receptor Gene OPRM1 via hnRNPH Interactions. Journal of Neuroscience 34:11048–11066.

bioRxiv preprint doi: https://doi.org/10.1101/2021.07.06.451358; this version posted November 28, 2022. The copyright holder for this preprint (which was not certified by peer review) is the author/funder, who has granted bioRxiv a license to display the preprint in perpetuity. It is made available under aCC-BY-NC-ND 4.0 International license.

Yazdani N, Parker CC, Shen Y, Reed ER, Guido MA, Kole LA, Kirkpatrick SL, Lim JE, Sokoloff G, Cheng R, Johnson WE, Palmer AA, Bryant CD (2015) Hnrnph1 Is A Quantitative Trait Gene for Methamphetamine Sensitivity. PLoS Genet 11:e1005713.

Yorgason JT, Hedges DM, Obray JD, Jang EY, Bills KB, Woodbury M, Williams B, Parsons MJ, Andres MA, Steffensen SC (2020) Methamphetamine increases dopamine release in the nucleus accumbens through calcium-dependent processes. Psychopharmacology (Berl) 237:1317–1330.

Zhang X, Hamblin MH, Yin KJ (2017) The long noncoding RNA Malat1: Its physiological and pathophysiological functions. RNA Biol 14:1705–1714.

Zhang Z, Xing Y (2017) CLIP-seq analysis of multi-mapped reads discovers novel functional RNA regulatory sites in the human transcriptome. Nucleic Acids Res 45:9260–9271.

bioRxiv preprint doi: https://doi.org/10.1101/2021.07.06.451358; this version posted November 28, 2022. The copyright holder for this preprint (which was not certified by peer review) is the author/funder, who has granted bioRxiv a license to display the preprint in perpetuity. It is made available under aCC-BY-NC-ND 4.0 International license.

FIGURE LEGENDS

Figure 1. Replication of decreased methamphetamine-induced locomotor activity in *Hnrnph1* mutants versus wild-types. On Days 1 and 2, mice were injected (i.p.) with saline and placed into testing apparatus for 1 h. On Day 3, mice were injected (i.p.) with 2 mg/kg methamphetamine and placed into testing apparatus for 30 min followed by immediate sacrifice and removal of the striatum. WT_SAL = untreated saline wild-types; WT_MA = methamphetamine-treated wild-types; MUT_SAL = untreated saline *Hnrnph1* mutants; MUT_MA = methamphetamine-treated *Hnrnph1* mutants. **(A-B):** Locomotor activity on Day 1 **(A)** and Day 2 **(B)** for 1 h in 5-min bins. There was no genotypic difference in total distance traveled in response to saline on Day 1 or Day 2 [Day 1: $F(11,616)_{\text{Genotype x Treatment x Time}} = 0.841$, $p = 0.599$; Day 2: $F(11,616)_{\text{Genotype x Treatment x Time}} = 1.181$, $p = 0.296$]. **(C):** Acute methamphetamine-induced locomotor activity on Day 3 for 30 min in 5-min bins. Thirty min post methamphetamine injection, mice were sacrificed and whole striatum from each mouse was dissected and harvested for CLIP-seq processing. *Hnrnph1* mutants showed less locomotor activity compared to wild-types in response to methamphetamine but no difference following saline [$F(5,280)_{\text{Genotype x Treatment x Time}} = 7.354$, $p = 1.70e\text{-}06$]. In considering the time-course of locomotor activity following methamphetamine, there was a significant decrease in distance traveled in *Hnrnph1* mutants relative to wild-types following methamphetamine on Day 3 at 15 – 20 min bin [$t(360) = 3.126$, $*p_{adj} = 0.023$], 20 – 25 min bin [$t(360) = 3.296$, $*p_{adj} = 0.013$], and 25 – 30 min bin [$t(360) = 3.867$, $*p_{adj} = 0.002$]. No effect of Sex or interaction of Sex with other factors was detected for any of the measure reported. Sample size of each group is indicated in the legend. Data are presented as the mean ± S.E.M.

Figure 2. Optimization of the CLIP conditions for hnRNP H. (A): Immunoblot shows the IP condition using the anti-hnRNP H antibody. No nonspecific bands were detected in the rabbit IgG pulldown. In the hnRNP H IP, a band of 50 kDa corresponding to the size of hnRNP H was detected. **(B):** Immunoblot showing IP condition using different concentrations of hnRNP H antibody. A total of 20 ug of antibody was chosen for the IP. **(C):** RNA ^{32}P autoradiogram showing bound RNA under different duration of RNase I_f digestion. Three min was chosen as the optimal length of digestion.

Figure 3. RNA-binding sites of hnRNP H at baseline in saline control wild-types are enriched for introns and G-rich binding motifs. eCLIP-seq revealed transcriptome-wide striatal RNA targets of hnRNP H in saline control wild-types (WT_SAL). Peak calling of both uniquely and multi-mapped reads was performed using CLAM

bioRxiv preprint doi: https://doi.org/10.1101/2021.07.06.451358; this version posted November 28, 2022. The copyright holder for this preprint (which was not certified by peer review) is the author/funder, who has granted bioRxiv a license to display the preprint in perpetuity. It is made available under aCC-BY-NC-ND 4.0 International license.

(Zhang and Xing, 2017). **(A):** RNA ^{32}P autoradiogram of hnRNP H-bound RNA. CLIP conditions are shown for each lane: no crosslinking, IgG mock IP, and four different RNase I_f concentrations from high to low. An increasing amount of RNA was pulled down as the concentration of RNase I_f was decreased. The scissors denote the region above the molecular weight of hnRNP H (50 kDa) that was isolated for sequencing. The region runs from 50 to 80 kDa, which corresponds to 30 to 70 bp for RNA length. The larger bands observed above 100 kDa could represent very long RNAs that are resistant to digestion or large hnRNP H-associated protein-protein complexes bound to RNAs. **(B):** hnRNP H binds primarily to introns of target RNAs. More than 70% of hnRNP H CLIP sites are intronic. The pie chart shows the relative distribution of CLIP sites in 5'UTR, coding sequences (**CDS**), introns, and 3'UTR. Proximal introns indicate less than 200 (proximalx200_intron) or 500 (proximalx500_intron) nucleotides from the 5' or 3' splice sites with the remainder annotated as distal introns. Unannotated exons are referred to as "other exons". **(C):** Poly-G tract is the most prevalent component of the hnRNP H binding motif. *De novo* motif discovery of hnRNP H CLIP sites was performed using Homer (Heinz et al., 2010). **(D):** hnRNP H RNA-binding targets containing G-rich motifs in their binding sites are most highly enriched for "presynaptic depolarization and calcium channel opening" pathway. Pathway enrichment analysis of hnRNP H RNA-binding targets with the poly-G motif was performed in WebGestalt (Liao et al., 2019) using the over-representation analysis methods. The top 10 pathways with FDR < 0.05 are shown, sorted from high to low enrichment ratio.

Figure 4. cDNA libraries generation followed by visualization with DNA gel electrophoresis. (A): No cDNA library was generated from IgG mock IP**.** Even after 28 cycles, no cDNA library (which should be > 200 bp) was detected. For this reason, these four samples were not subjected to RNA-seq. **(B):** In contrast with CLIP cDNA libraries, DNA bands > 200 bp were detected after 20 PCR cycles.

Figure 5. hnRNP H RNA-binding targets at baseline in saline control wild-types are enriched for synaptic function. A list containing all hnRNP H targets meeting the CLAM peak signal threshold cutoff of greater than 1.5 was used as the input for gene ontology and pathway analysis using g:Profiler (Raudvere et al., 2019). The top 10 gene ontology (molecular function, cellular component and biological process) as well Reactome and WikiPathways were selected for visualization and clustering of gene-set enrichment as a network in the EnrichmentMap Cytoscape App (Merico et al., 2010). Gene sets are organized into a network enrichment map as shown. Each square (node) represents a gene set and each edge represents mutual overlaps. A majority of

bioRxiv preprint doi: https://doi.org/10.1101/2021.07.06.451358; this version posted November 28, 2022. The copyright holder for this preprint (which was not certified by peer review) is the author/funder, who has granted bioRxiv a license to display the preprint in perpetuity. It is made available under aCC-BY-NC-ND 4.0 International license.

gene sets are annotated for synaptic functions. The five nodes indicated in asterisk represent the top five most enriched gene sets by p-value.

Figure 6. RNA-binding targets of hnRNP H showing a Genotype x Treatment interaction are enriched for pathways and cellular components involved in drug-evoked synaptic plasticity. CLIP-seq analysis revealed transcriptome-wide striatal RNA-binding targets of hnRNP H in saline and methamphetamine-treated *Hnrnph1* mutants versus wild-types. Peak calling in CLAM (Zhang and Xing, 2017) was performed separately for each of the four conditions. For differential analysis, peak calling was also performed using CLAM (Zhang and Xing, 2017) on the merged bam file across all conditions followed by read counts against the identified peaks and differential analysis of peak intensity. WT_SAL = untreated saline wild-types; WT_MA = methamphetamine-treated wild-types; MUT_SAL = untreated saline *Hnrnph1* mutants; MUT_MA = methamphetamine-treated *Hnrnph1* mutants. **(A):** In comparison to WT_SAL, only the percentages of hnRNP H binding events associated with 3'UTR and introns were significantly different in the other three conditions (See chi-square tests in **Table S5**). The percentage of binding events that comprised 3'UTRs varied drastically between Genotype and Treatment whereby there was an increase in WT_MA compared to WT_SAL and a decrease in MUT_MA compared to MUT_SAL (chi-square test: *$p < 0.001$). All intron binding events (including distal introns and proximal introns) were significantly different from WT_SAL (chi-square test: all p's < 0.001), with the exception of MUT_SAL ($p = 0.453$ for proximalx200_intron). The relative distribution of RNA-binding sites over the gene elements for each of the four conditions in the 2 x 2 (Genotype x Treatment) experimental design is shown. **(B):** An hnRNP H CLIP peak with increased binding in wild-types is more likely to show decreased binding in *Hnrnph1* mutants in response to methamphetamine. The plot shows a negative correlation between $\log_2$FC (WT_MA vs WT_SAL) and $\log_2$FC (MUT_MA vs MUT_SAL) (Pearson's correlation coefficient $r = -0.034$, $p < 2.2e-16$). The hnRNP H CLIP peaks showing Genotype x Treatment interactions (highlighted in magenta) showed a much stronger negative correlation (Pearson's $r = -0.692$, $p < 2.2e-16$). Each data point corresponds to a hnRNP H-associated CLIP peak. **(C):** Strong enrichment scores for "amphetamine addiction", "alcoholism", "long-term potentiation", and "dopaminergic synapse" pathways were detected for those hnRNP H RNA-binding targets showing Genotype x Treatment interaction. GSEA analysis was performed in WebGestalt (Liao et al., 2019) on a ranked list (based on $\log_2$FC) of hnRNP H targets showing Genotype x Treatment interaction. **(D):** Strong

bioRxiv preprint doi: https://doi.org/10.1101/2021.07.06.451358; this version posted November 28, 2022. The copyright holder for this preprint (which was not certified by peer review) is the author/funder, who has granted bioRxiv a license to display the preprint in perpetuity. It is made available under aCC-BY-NC-ND 4.0 International license.

enrichment for "ATPase complex", "myelin sheath", "neuron spine" and "nuclear chromatin" cellular components were detected, specifically for those hnRNP H RNA-binding targets showing Genotype x Treatment interaction.

Figure 7. hnRNP H RNA-binding targets showing Genotype x Treatment interactions are enriched in pathways and gene ontology involved in drug-induced synaptic plasticity. WT_SAL = untreated saline wild-types; WT_MA = methamphetamine-treated wild-types; MUT_SAL = untreated saline *Hnrnph1* mutants; MUT_MA = methamphetamine-treated *Hnrnph1* mutants. **(A):** Venn diagram shows distinct and overlapping hnRNP H targets identified in each of the four conditions. **(B):** Venn diagram shows distinct and overlapping hnRNP H targets as a function of Genotype, Treatment, or Genotype x Treatment interaction. Peak calling was performed using CLAM to identify peaks based on merged bam files across all conditions. Individual bam files were then used to count reads against the identified peaks. Differential peak analysis for Genotype x Treatment interaction was performed using limma/edgeR. The Genotype x Treatment interaction is expressed as (MUT_{MA} – MUT_{SAL}) – (WT_{MA} – WT_{SAL}). **(C):** Pathway analysis of the hnRNP H targets that showed a Genotype x Treatment interaction. The EnrichmentMap Cytoscape App (Merico et al., 2010) was used to build a network of the top 10 gene ontology and pathways enrichment results. Each square (or node) represents a gene set and edge represents mutual overlaps. A majority of gene sets are involved in synaptic function.

Figure 8. 3'UTR targets show opposite changes in methamphetamine-induced binding to hnRNP H between *Hnrnph1* mutants and wild-types. Genotype x Treatment-associated hnRNP H CLIP peaks, stratified across 4 gene elements: 5'UTR, 3'UTR, intron, and CDS. WT_SAL = untreated saline wild-types; WT_MA = methamphetamine-treated wild-types; MUT_SAL = untreated saline *Hnrnph1* mutants; MUT_MA = methamphetamine-treated *Hnrnph1* mutants. Heatmaps show normalized $\log_2$ CPM (count-per-million) read counts for significant peaks demonstrating a Genotype x Treatment interaction. The interaction is expressed as (MUT_MA – MUT_SAL) – (WT_MA – WT_SAL). The row of each heatmap represents a binding site sorted by p-value from smallest to largest, where those with a p-value of less than 0.01 are shown in the heatmap. Relative to saline control wildtypes, saline control *Hnrnph1* mutants showed an increase in baseline binding of hnRNP H to the 3'UTR regions of RNA-binding targets that decreases in response to methamphetamine treatment.

Figure 9. A strong negative correlation is detected between hnRNP H RNA-binding dynamic in the wildtypes and *Hnrnph1* mutant in response methamphetamine in the 3'UTR (A), introns (B), CDS (C), and 5'UTR (D). Correlation plots comparing $\log_2$FC values between various contrast. Each point represents a binding

bioRxiv preprint doi: https://doi.org/10.1101/2021.07.06.451358; this version posted November 28, 2022. The copyright holder for this preprint (which was not certified by peer review) is the author/funder, who has granted bioRxiv a license to display the preprint in perpetuity. It is made available under aCC-BY-NC-ND 4.0 International license.

site or peak. The data points hightlighted in mageneta are those peaks that show significant Genotype x Treatment intereaction.

Figure 10. 3'UTR targets show significant enrichment for both pre- and post-synaptic function. Interaction plots for 3'UTR targets with significant Genotype by Treatment interaction that are enriched for **(A)** synaptic vesicle cycle and **(B)** dopaminergic synapse. The interaction plots are generated from CLIP-seq data showing average values with standard deviation of the means, with n = 3 per condition. WT = wild-types; MUT = *Hnrnph1* mutants; SAL = saline; MA = methamphetamine.

Figure 11. The main effect of Genotype is more significant than the main effect of Treatment. Differential gene expression for interaction of Genotype (MUT – WT) or Treatment (MA – SAL) was performed using limma (Ritchie et al., 2015) and edgeR (Robinson et al., 2009). WT = wild-types; MUT = *Hnrnph1* mutants; SAL = saline; MA = methamphetamine. **(A)**: Volcano plot showing genes that are differentially expressed between Hnrnph1 mutants and wild-types. **(B)**: Volcano plot showing genes that are differential expressed between methamphetamine and saline condition.

Figure 12. Identification of Cacna2d2 as the only RNA target showing a Genotype x Treatment-induced change in hnRNP H1 binding, gene expression, and alternative splicing. Differential gene expression (**DE**) for the interaction of Genotype and Treatment [(MUT_MA – MUT_SAL) – (WT_MA – WT_SAL)] was performed using limma (Ritchie et al., 2015) and edgeR (Robinson et al., 2009). Differential exon and intron usage analysis (alternatively spliced; AS) for interaction of Genotype with Treatment [(MUT_MA – MUT_SAL) – (WT_MA – WT_SAL)] was performed using Aspli (Mancini et al., 2020). WT_SAL = untreated saline wild-types; WT_MA = methamphetamine-treated wild-types; MUT_SAL = untreated saline *Hnrnph1* mutants; MUT_MA = methamphetamine-treated *Hnrnph1* mutants. **(A):** Venn diagram comparing RNA-binding targets of hnRNP H with differential gene expression and differential exon or intron usage. The 19 DE genes and 469 AS genes were then compared with the hnRNP H targets that comprised the Genotype x Treatment interactions. Cacna2d2 was the only RNA-binding target of hnRNP H that was both a DE gene and an AS gene. Only the top overlapping and non-overlapping hnRNP H targets and AS genes are indicated. Out of the 19 DE genes, *Cacna2d2, Elfn1*, *Calb2*, and *Zic1* are putative targets of *Malat1* (predicted by TargetScan; (Agarwal et al., 2015) while *Camta1* and *Pcdh8* are putative targets of *Mir124a* (predicted by LncRRIsearch; (Fukunaga et al., 2019). **(B):** Volcano plot of genes showing a Genotype x Treatment interaction in response to methamphetamine. The interaction is

bioRxiv preprint doi: https://doi.org/10.1101/2021.07.06.451358; this version posted November 28, 2022. The copyright holder for this preprint (which was not certified by peer review) is the author/funder, who has granted bioRxiv a license to display the preprint in perpetuity. It is made available under aCC-BY-NC-ND 4.0 International license.

expressed as (MUT_MA – MUT_SAL) – (WT_MA – WT_SAL). *Cacna2d2* is circled in red. The five overlapping hnRNP H targets and DE genes are circled in purple. **(C):** hnRNP H preferentially binds to the 3'UTR of *Cacna2d2*. Visualization of reads by Integrative Genome Browser (Thorvaldsdóttir et al., 2013) for the hnRNP H CLIP peak at the 3'UTR of *Cacna2d2*. Scale of the plot height is in counts per million (CPM). **(D):** A G-rich motif was detected at the hnRNP H CLIP peak within the 3'UTR of *Cacna2d2*. *De novo* motif discovery of the binding site was performed in MEME (Bailey et al., 2009). **(E):** Interaction plots showing hnRNP H binding to the 3 'UTR of *Cacna2d2* (left), differential usage of the 3'UTR (middle), and differential gene expression of *Cacna2d2* (right) as a function of Genotype and Treatment. The increase in hnRNP H binding to the 3'UTR of *Cacna2d2* was associated with decreased 3'UTR usage and increased gene expression *of Cacna2d2* in *Hnrnph1* mutants. Here, 3'UTR usage is defined as to the number of normalized reads mapped to the 3'UTR portion of *Cacna2d2*. The interaction plots were generated from CLIP-seq and RNA-seq data showing average values with standard deviation of the means, with n = 3 per condition.

Figure 13. RT-qPCR analysis provides further support for decreased usage of the distal end of the 3'UTR of *Cacna2d2* (also the binding site for hnRHP H) in *Hnrnph1* mutants in response to methamphetamine. CLIP-seq analysis identified an increase in hnRNP H binding at the distal end of 3'UTR of *Cacna2d2* in *Hnrnph1* mutants that was associated with decreased usage of the 3'UTR, warranting further validation. SAL = saline; MA = methamphetamine; WT = wild-types; H1 MUT = *Hnrnph1* mutants**. (A):** Three polyadenylation sites (pA-1, pA-2, and pA-3) are present within the 3'UTR of *Cacna2d2* that distinguish isoforms containing 3'UTR of different lengths (UCSC genome browser). Primers were designed to detect differences in usage of the proximal and distal end of the 3'UTR of *Cacna2d2* as well as exons 37-38 and exons 3-4 (UCSB annotations). The schematic indicates the positions of these primers. **(B):** The left striata were harvested in the same manner as in the CLIP-seq study followed by RNA extraction, cDNA library generation with oligo-DT primers, and RT-qPCR to detect differential usage of the regions at the 3'UTR of *Cacna2d2* and upstream of the 3' UTR. No differences were found at exons 3-4 [$F(1,39)_{\text{Genotype x Treatment}} = 0.650$, $p = 0.425$], exons 37-38 [$F(1,39)_{\text{Genotype x Treatment}} = 0.900$, $p = 0.349$], or at the proximal end of the 3'UTR [$F(1,39)_{\text{Genotype x Treatment}} = 0.198$, $p = 0.659$]. Although no significant Genotype x Treatment interaction was detected for the usage of the distal end of the 3'UTR [$F(1,39)_{\text{Genotype x Treatment}} = 1.485$, $p = 0.230$], there was a main effect of Treatment [$F(1,39)_{\text{Treatment}} = 10.772$, $p = 0.002$]. In examining the effect of Treatment at each level of Genotype, a significant, simple main effect of Treatment was found in the

bioRxiv preprint doi: https://doi.org/10.1101/2021.07.06.451358; this version posted November 28, 2022. The copyright holder for this preprint (which was not certified by peer review) is the author/funder, who has granted bioRxiv a license to display the preprint in perpetuity. It is made available under aCC-BY-NC-ND 4.0 International license.

Hnrnph1 mutants [$F(1,40)_{Treatment} = 9.368$, $p = 0.004$] but not in the wild-types [$F(1,40)_{Treatment} = 2.993$, $p = 0.091$]. Subsequent analysis revealed decreased methamphetamine-induced usage of the distal end of 3'UTR in *Hnrnph1* mutants compared to wild-types [$t(40) = -3.061$, $^*p = 0.004$], with no significant genotypic difference between saline groups [$t(40) = -1.730$, $p = 0.091$]. The normalized $2^{-\Delta\Delta CT}$ values from three independent replicates are shown in the plots. **(C):** The right striata from the same mice used in RT-qPCR analysis (**Figure 13B**) were collected for Western blot analysis to assess differences in CACNA2D2 protein expression. Immunoblots from three separate replicates are shown on the left side of the figure panel and quantification is shown on the right. There was no significant genotypic difference in the level of CACNA2D2 protein in saline or methamphetamine treatment groups [$F(1,40)_{Genotype \times Treatment} = 2.587$, $p = 0.117$]. Data are presented as the mean ± S.E.M.

Figure 14. Ponceau S staining for total protein normalization used in immunoblot quantification of CACNA2D2 protein level. Total protein stains via ponceau S instead of a housekeeping gene were used as loading controls. The densitometry value for the total protein level in each lane is indicated below each lane in the immunoblots for each of the three replicates.

Figure 15. Pregabalin pretreatment recapitulates the *Hnrnph1* mutational phenotype of decreased methamphetamine-induced locomotor activity in wild-type females but not in *Hnrnph1* mutants. On Days 1 and 2, thirty min after pretreatment with saline and placement back into the home cage, mice were injected again with saline (i.p.) and placed into testing apparatus for 1 h. On Day 3, one-half of the mice were once again pretreated first with saline (i.p.) while the other one-half received pregabalin (30 mg/kg, i.p.) and were placed back into the home cage for 30 min. Mice were then injected with 2 mg/kg methamphetamine (i.p.) or saline (i.p.) and immediately placed into the testing apparatus for 60 min followed by immediate sacrifice and removal of the striatum. WT_SAL = wild-types pretreated with saline; WT_Pregabalin = wild-types pretreated with pregabalin; MUT_SAL = *Hnrnph1* mutants pretreated with saline; MUT_Pregabalin = *Hnrnph1* mutants pre-treated with pregabalin. **(A):** Injection timeline for those mice pre-treated with pregabalin (30 mg/kg, i.p.) on Day 3. **(B):** Effect of pregabalin pretreatment (-30 min) on saline-induced on Day 3 in 5-min bins over a 60-min period. In response to an acute dose of saline on Day 3 after pretreatment with pregabalin or saline, wild-types and *Hnrnph1* mutants showed no time- or sex-dependent difference in locomotor activity [$F(11,616)_{Treatment \times Sex \times Time} = 1.080$, $p = 0.375$]. **(C-D):** Methamphetamine-induced locomotor activity 30 min post- pregabalin or saline pretreatment on Day 3 in 5-min bins over a 60-min period in females **(C)** and males **(D)** separately. Wild-types, but not *Hnrnph1* mutants,

bioRxiv preprint doi: https://doi.org/10.1101/2021.07.06.451358; this version posted November 28, 2022. The copyright holder for this preprint (which was not certified by peer review) is the author/funder, who has granted bioRxiv a license to display the preprint in perpetuity. It is made available under aCC-BY-NC-ND 4.0 International license.

showed a sex-dependent differential response to pregabalin pretreatment following methamphetamine [$F(11,1298)_{Treatment \times Sex \times Time} = 1.953$, $p = 0.030$], prompting separate analyses in females and males. Pregabalin pre-treatment decreased methamphetamine-induced locomotor activity in wild-type females relative to their saline counterparts while having no effect in wild-type males or in *Hnrnph1* mutants [$F(1,61)_{Genotype \times Treatment} = 4.536$, $p = 0.037$]. The result was significant from 15 min through 35 min post-methamphetamine injection [WT_SAL versus WT_pregabalin: t(396) = -2.938, -3.551, -3.408, -3.140, -3.061, *p.adj = 0.042, 0.005, 0.009, 0.022, 0.028 for time points marked with *, in consecutive order]. However, for males, there was no effect of pretreatment [$F(1,57)_{Treatment} = 0.656$, $p = 0.421$] and no genotype-dependent effect of pregabalin pretreatment [$F(1,57)_{Genotype \times Treatment} = 0.292$, $p = 0.591$] on methamphetamine-induced locomotor activity. Sample size of each group is indicated in the legend. Data are presented as the mean ± S.E.M.

Figure 16. Baseline locomotion on Days 1 and 2 to test for effect of pregabalin pretreatment on the acute locomotor effect of methamphetamine. Days 1 and 2 served as habituation days for mice to get accumulated to the testing apparatus where all mice received only saline pretreatment and a following bolus dose of saline. On Days 1 and 2, thirty min after pretreatment with saline, mice were injected again with saline (i.p.) and placed into testing apparatus for 1 h. On Day 3, mice were first pretreated with saline (i.p.) or pregabalin (i.p.) 30 min prior to being injected with 2 mg/kg methamphetamine (i.p.) or saline (i.p.) and placed into testing apparatus for 60 min followed by immediate sacrifice and removal of the striatum. WT_SAL = wild-types pretreated with saline; WT_Pregabalin = wild-types pretreated with pregabalin; MUT_SAL = *Hnrnph1* mutants pretreated with saline; MUT_Pregabalin = *Hnrnph1* mutants pre-treated with pregabalin. **(A):** Locomotor activity on Day 1 for 1 h in 5-min bins. Mice that would be treated with an acute dose of saline on Day 3 (left) showed no difference in locomotor activity in response to saline [$F(11,627)_{Genotype \times Treatment \times Time} = 0.0896$, $p = 0.544$]. Mice that would be treated with an acute dose of methamphetamine on Day 3 (right) showed slight difference in locomotor activity in response to saline [$F(11,616)_{Genotype \times Treatment \times Time} = 1.964$, $p = 0.029$]. Simple main effect of Treatment at each level of time was only detected in *Hnrnph1* mutants but not wild-types, with *Hnrnph1* mutants that would be pretreated with pregabalin showing higher locomotor activity relative to saline only at the 5 – 10 min bin [t(732) = 3.085, *p.adj = 0.025]. **(B):** Locomotor activity on Day 2 for 1 h in 5-min bins. Mice that would be treated with an acute dose of saline on Day 3 (left) showed no difference in locomotor activity in response to saline [$F(11,627)_{Genotype \times Treatment \times Time} = 0.822$, $p = 0.618$]. Mice that would be treated with an acute dose of

bioRxiv preprint doi: https://doi.org/10.1101/2021.07.06.451358; this version posted November 28, 2022. The copyright holder for this preprint (which was not certified by peer review) is the author/funder, who has granted bioRxiv a license to display the preprint in perpetuity. It is made available under aCC-BY-NC-ND 4.0 International license.

methamphetamine on Day 3 showed a Sex-specific effect in locomotion in response to saline [$F(11,1265)_{Treatment \times Sex \times Time} = 2.241$, $p = 0.011$]. When broken down into females (middle) and males (right) separately, only the males show differences in locomotor activity [$F(11,627)_{Genotype \times Treatment \times Time} = 1.884$, $p = 0.0039$] but no time-dependent differences after correcting for multiple comparisons. Sample size of each group is indicated in the legend. Data are presented as the mean ± S.E.M.

Figure 17. Pregabalin pretreatment increases proximal 3' UTR usage of *Cacna2d2* in wild-types but not in *Hnrnph1* mutants. Sixty min post-saline or methamphetamine injection (90 min post-saline or pregabalin pretreatment), mice from the locomotor study (Figure 16) were sacrificed and whole striatum for each mouse was dissected and harvested for RT-qPCR to detect differential usage 3'UTR of *Cacna2d2* **(A – D)** and Western blot to quantify CACNA2D2 protein quantification **(E – F)**. SAL = saline; MA = methamphetamine; PGB = pregabalin; WT = wild-types; H1 MUT = *Hnrnph1* mutants**. (A-B):** In examining the effect of pregabalin pretreatment (30 mg/kg, i.p.) followed by saline (i.p.) **(A)**, there was no difference in the usage of the proximal 3'UTR of *Cacna2d2* regardless of pregabalin pretreatment or genotype [$F(1,57)_{Genotype \times Treatment} = 0.005$, $p = 0.941$]. However, in examining the effect of pretreatment with pregabalin (30 mg/kg, i.p.) followed by methamphetamine (2 mg/kg, i.p.) **(B)**, wild-types but not *Hnrnph1* mutants pretreated with pregabalin relative to saline showed an increased usage in the proximal 3'UTR of *Cacna2d2* [$F(1,74)_{Genotype \times Treatment} = 4.4369$, $p = 0.04$]. In examining the effect of Treatment at each level of Genotype, a significant, simple main effect of Treatment was found in the wild-types [$F(1,78)_{Treatment} = 4.059$, $^{*}p = 0.047$] but not in the *Hnrnph1* mutants [$F(1,40)_{Treatment} = 1.062$, $p = 0.305$], with pair-wise comparison in the wild-type group revealing a pregabalin-dependent increase in usage of the proximal 3'UTR of *Cacna2d2* [$t(78) = 2.015$, $^{*}p = 0.047$]. **(C-D):** Negative results were observed for the distal 3'UTR of *Cacna2d2* after saline **(C)** [$F(1,57)_{Genotype \times Treatment} = 0.683$, $p = 0.412$] or methamphetamine **(D)** [$F(1,74)_{Genotype \times Treatment} = 1.498$, $p = 0.225$]. **(E-F):** The right striata from the same mice used in RT-qPCR analysis (**Figures 17A-D**) were collected for Western blot analysis to quantify CACNA2D2 protein expression. There was no difference in the level of CACNA2D2 protein in saline- or pregabalin-pretreated following saline **(E)** [$F(1,57)_{Genotype \times Treatment} = 2.737$, $p = 0.104$] or methamphetamine **(F)** [$F(1,78)_{Genotype \times Treatment} = 1.968$, $p = 0.165$]. No effect of Sex or interaction of Sex with other factors was detected for any of the measure reported. Data are presented as the mean ± S.E.M.

bioRxiv preprint doi: https://doi.org/10.1101/2021.07.06.451358; this version posted November 28, 2022. The copyright holder for this preprint (which was not certified by peer review) is the author/funder, who has granted bioRxiv a license to display the preprint in perpetuity. It is made available under aCC-BY-NC-ND 4.0 International license.

EXTENDED DATA

Figure 5-1. Data table containing pathway and GO enrichment results for hnRNP H RNA-binding targets in wild-types treated with saline.

Figure 6-1. Data table containing peaks for each condition.

Figure 7-1. Data table containing hnRNP H RNA binding targets showing main effect of Genotype, Treatment, and interaction of Genotype and Treatment.

Figure 7-2. Data table containing pathway and GO enrichment results for hnRNP H RNA-binding targets showing Genotype and Treatment interaction.

Figure 12-1. Data table containing differential expressed genes showing with Genotype and Treatment interaction.

Figure 12-2. Data table containing genes showing differential exon and intron usage with Genotype and Treatment interaction.

Figure 1

bioRxiv preprint doi: https://doi.org/10.1101/2021.07.06.451358; this version posted November 28, 2022. The copyright holder for this preprint (which was not certified by peer review) is the author/funder, who has granted bioRxiv a license to display the preprint in perpetuity. It is made available under aCC-BY-NC-ND 4.0 International license.

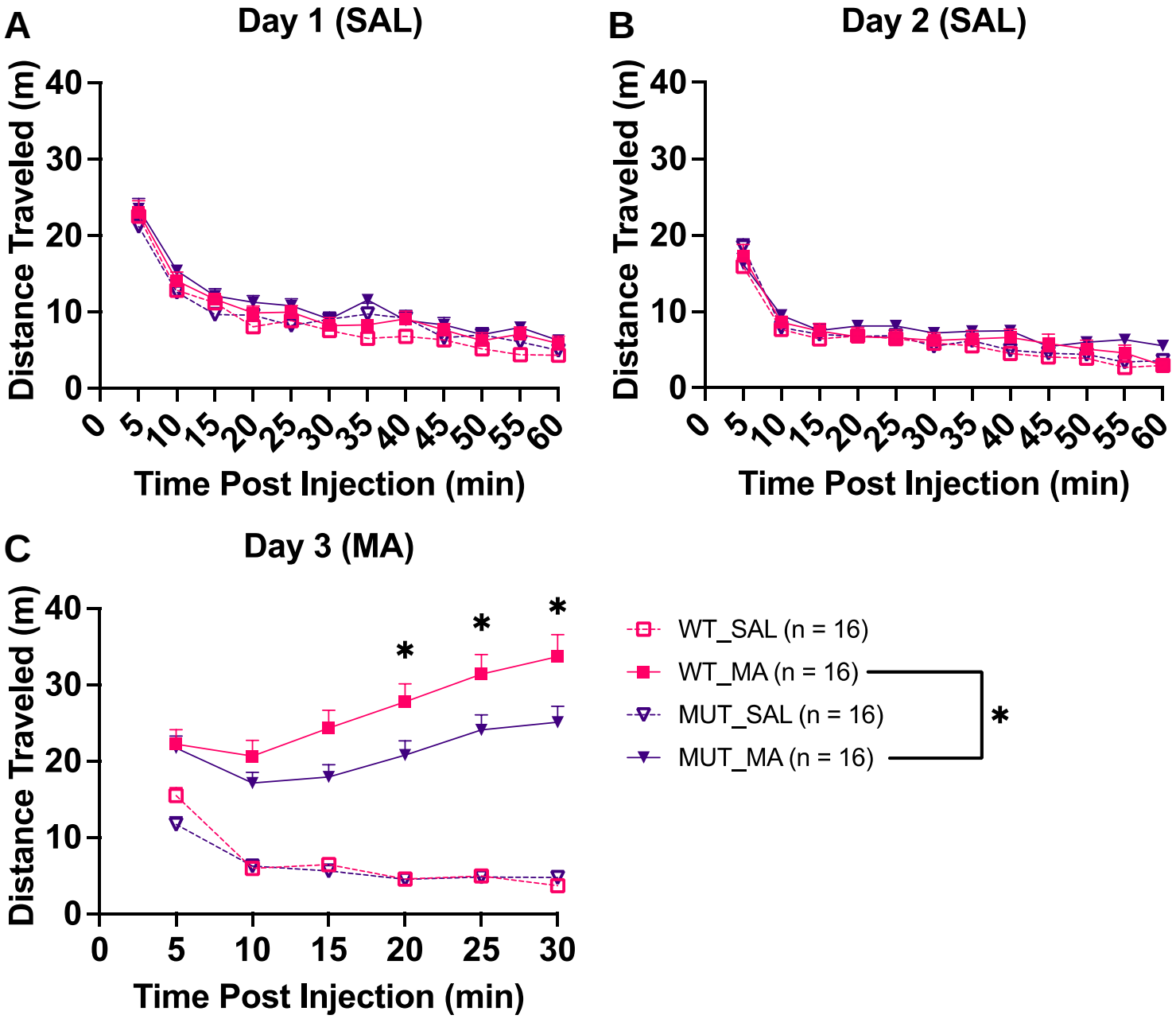

Figure 2

bioRxiv preprint doi: https://doi.org/10.1101/2021.07.06.451358; this version posted November 28, 2022. The copyright holder for this preprint (which was not certified by peer review) is the author/funder, who has granted bioRxiv a license to display the preprint in perpetuity. It is made available under aCC-BY-NC-ND 4.0 International license.

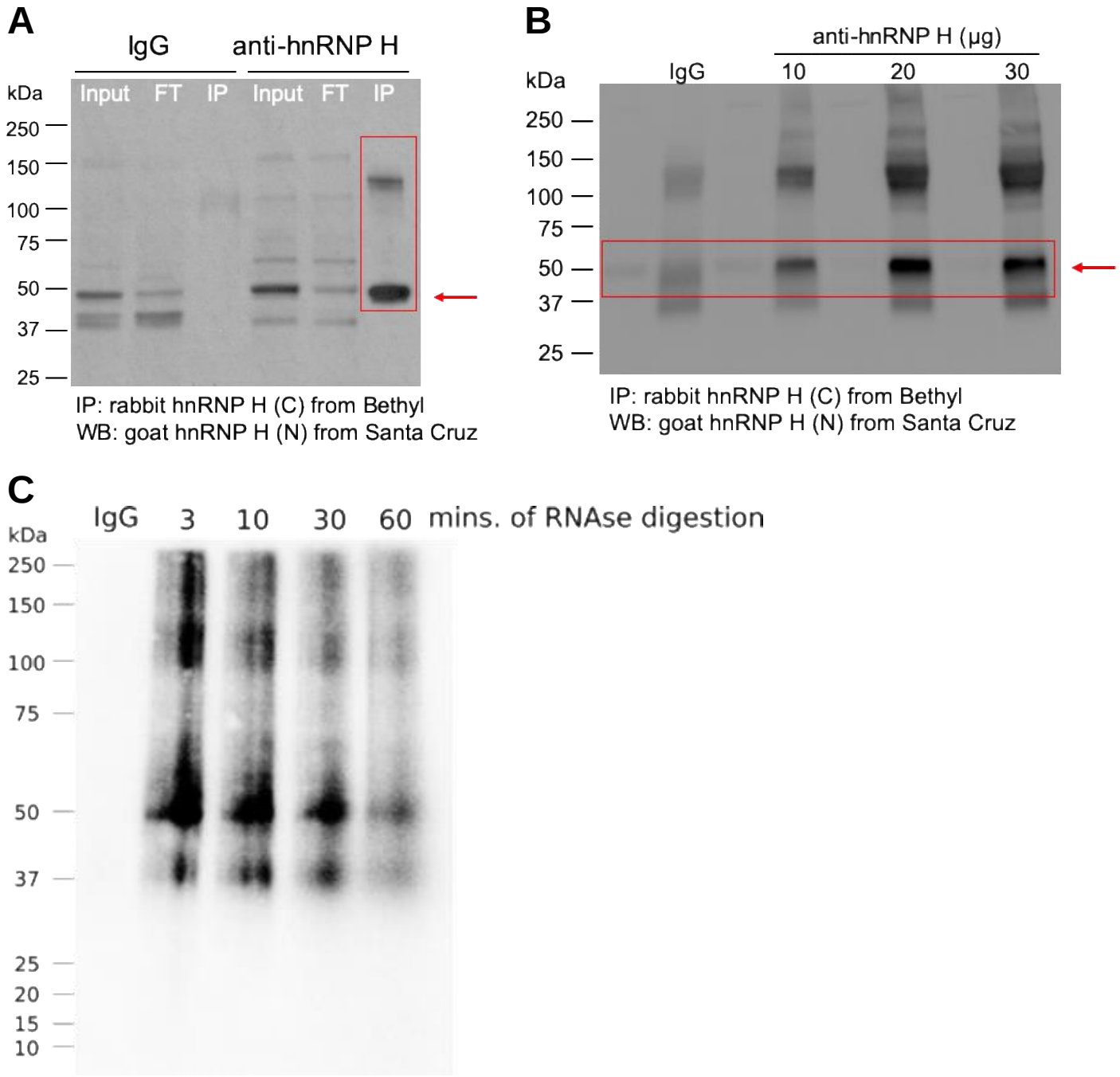

Figure 3

bioRxiv preprint doi: https://doi.org/10.1101/2021.07.06.451358; this version posted November 28, 2022. The copyright holder for this preprint (which was not certified by peer review) is the author/funder, who has granted bioRxiv a license to display the preprint in perpetuity. It is made available under aCC-BY-NC-ND 4.0 International license.

A

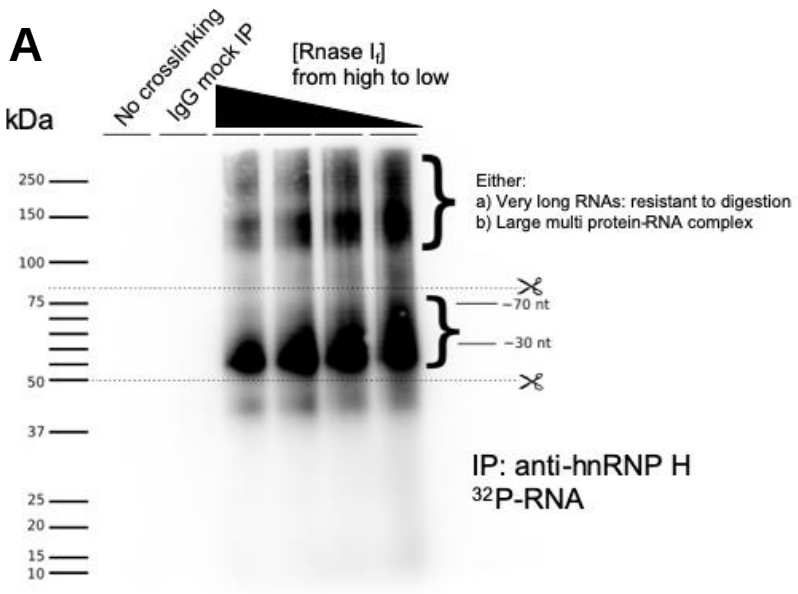

B

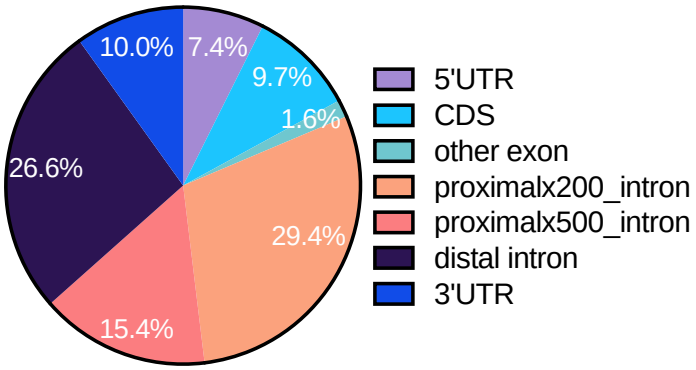

C

Rank	Motif	p value	% of targets
1		1E-129	14.21%
2		1E-108	5.78%
3		1E-102	20.44%
4		1E-101	46.28%
5		1E-71	3.00%

D **hnRNP H-associated targets with G-rich motif in wild-types treated with saline**

Top 10 Pathways by Enrichment Ratio (FDR > 0.05)

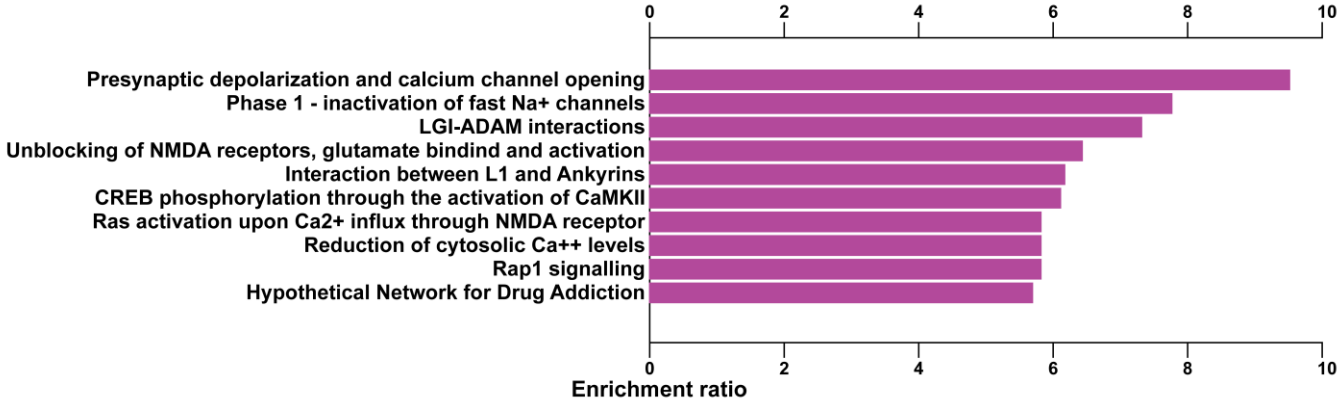

Figure 4

bioRxiv preprint doi: https://doi.org/10.1101/2021.07.06.451358; this version posted November 28, 2022. The copyright holder for this preprint (which was not certified by peer review) is the author/funder, who has granted bioRxiv a license to display the preprint in perpetuity. It is made available under aCC-BY-NC-ND 4.0 International license.

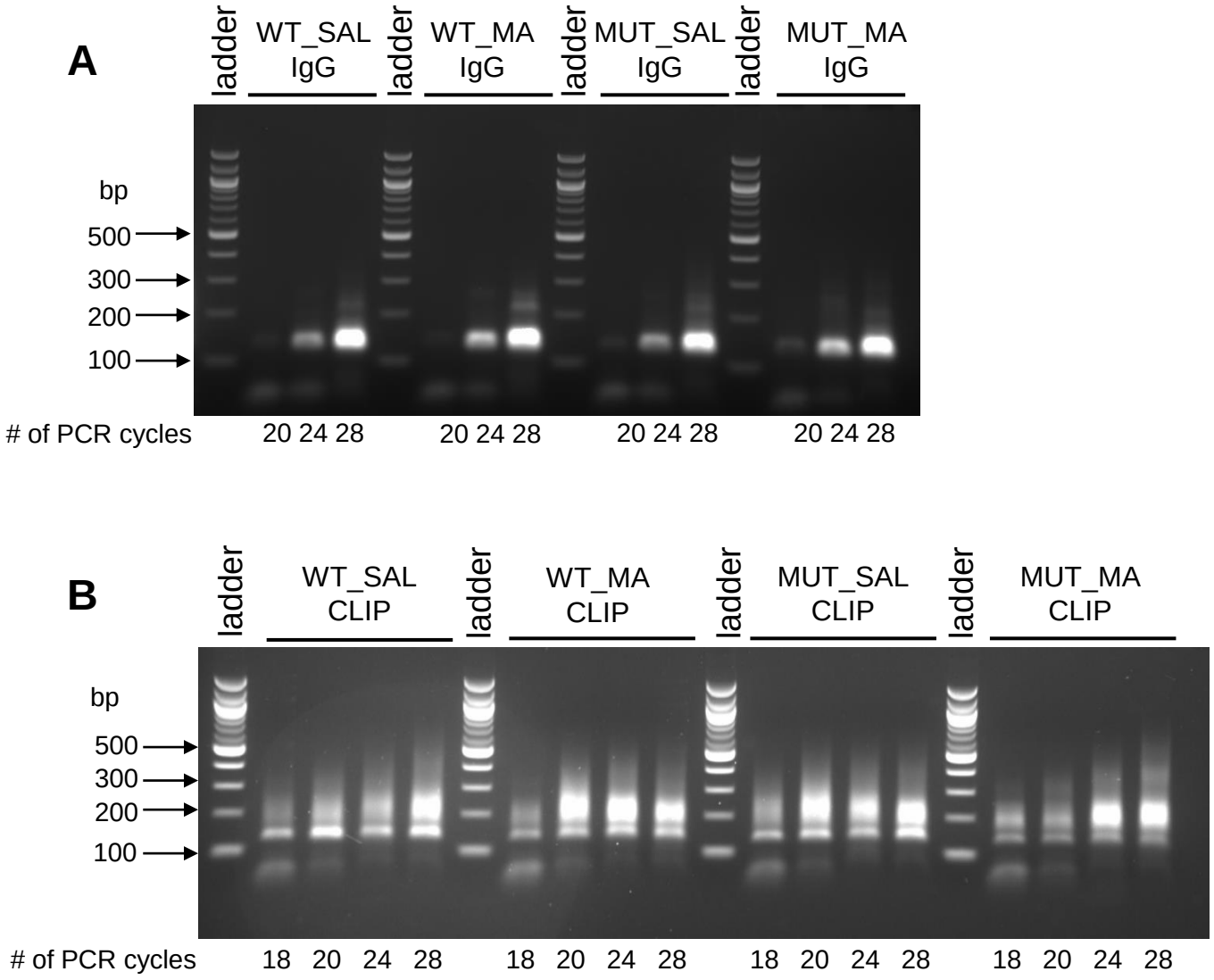

Figure 5

bioRxiv preprint doi: https://doi.org/10.1101/2021.07.06.451358; this version posted November 28, 2022. The copyright holder for this preprint (which was not certified by peer review) is the author/funder, who has granted bioRxiv a license to display the preprint in perpetuity. It is made available under aCC-BY-NC-ND 4.0 International license.

hnRNP H RNA-binding targets in wild-types treated with saline

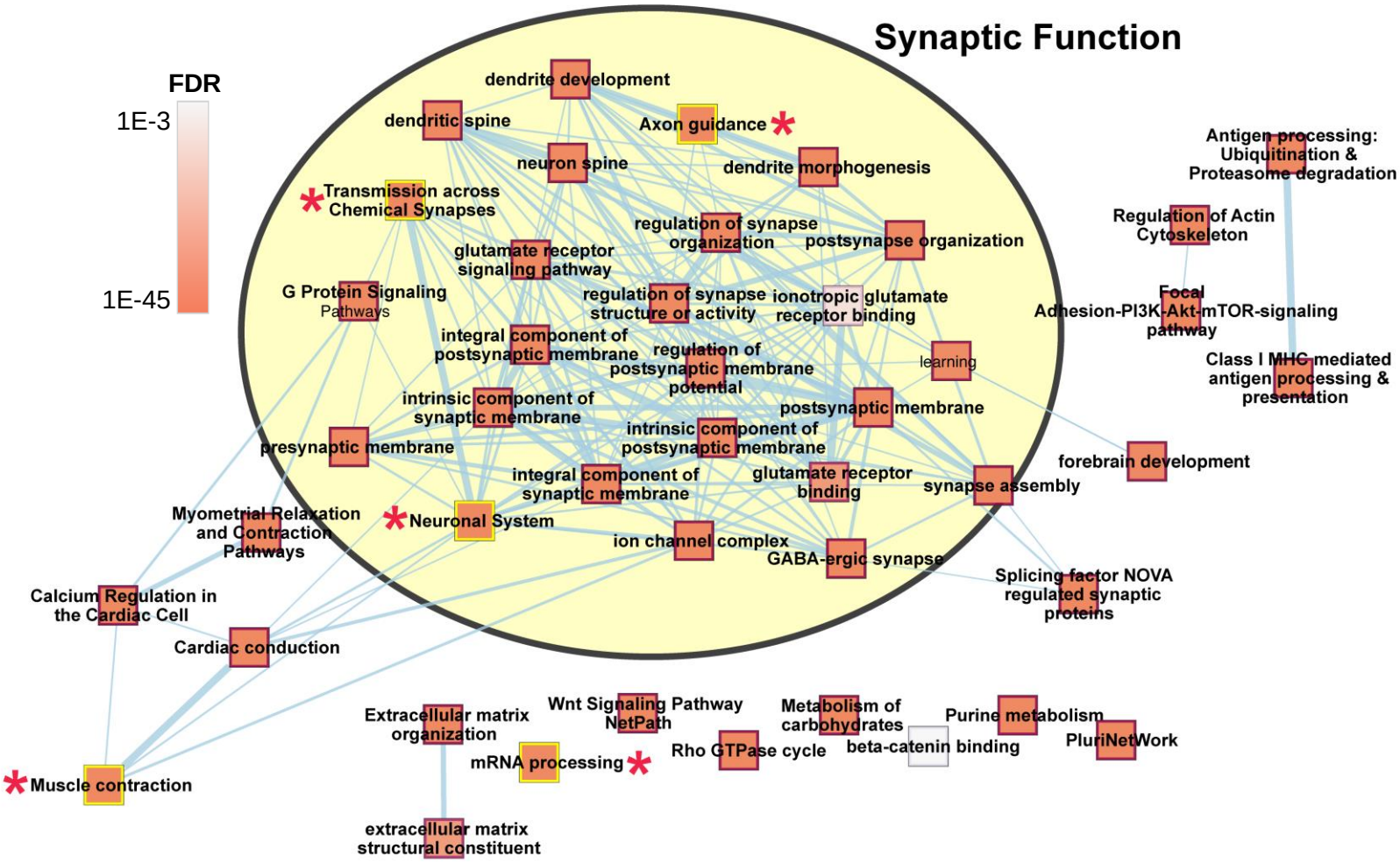

Figure 6

bioRxiv preprint doi: https://doi.org/10.1101/2021.07.06.451358; this version posted November 28, 2022. The copyright holder for this preprint (which was not certified by peer review) is the author/funder, who has granted bioRxiv a license to display the preprint in perpetuity. It is made available under aCC-BY-NC-ND 4.0 International license.

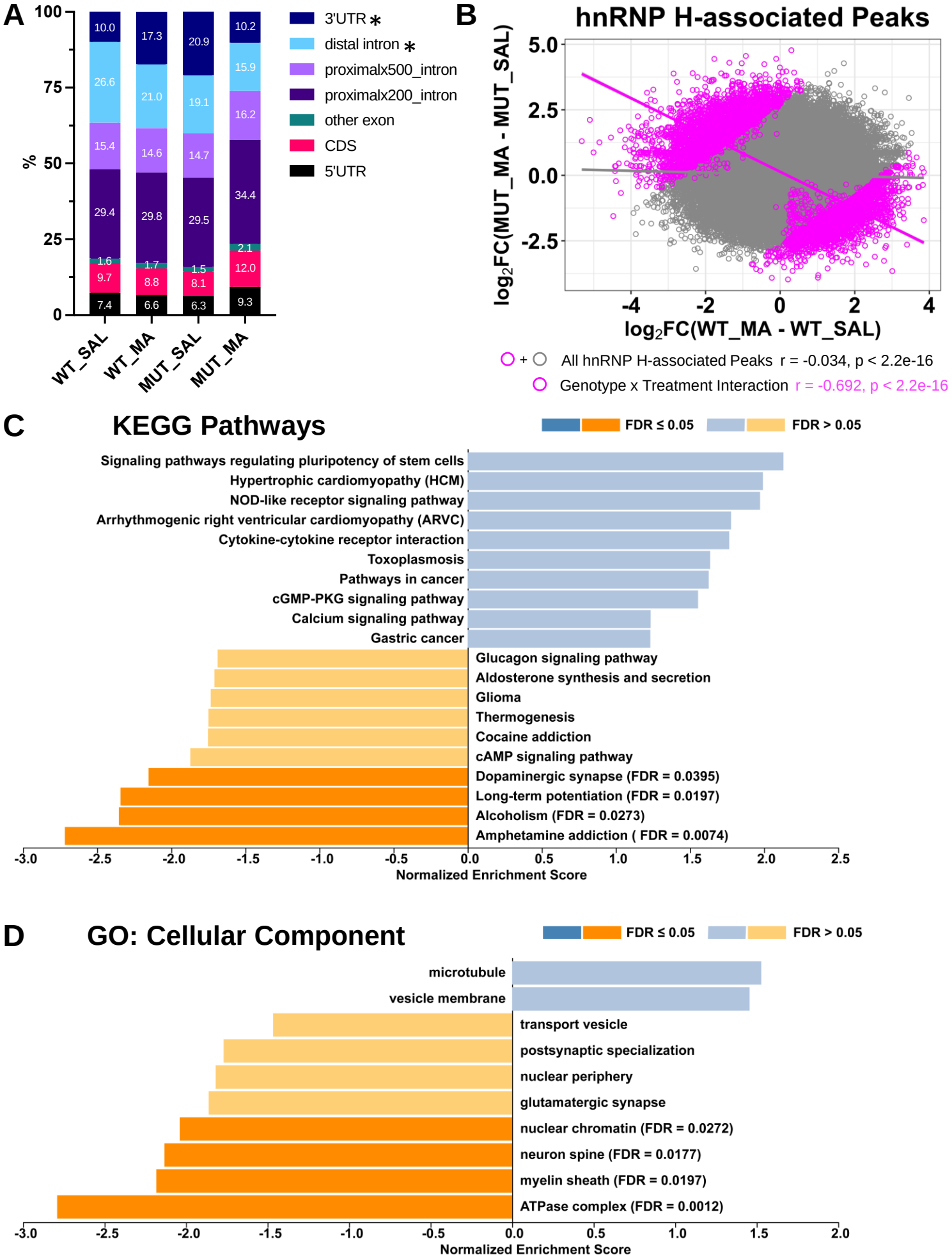

Figure 7

bioRxiv preprint doi: https://doi.org/10.1101/2021.07.06.451358; this version posted November 28, 2022. The copyright holder for this preprint (which was not certified by peer review) is the author/funder, who has granted bioRxiv a license to display the preprint in perpetuity. It is made available under aCC-BY-NC-ND 4.0 International license.

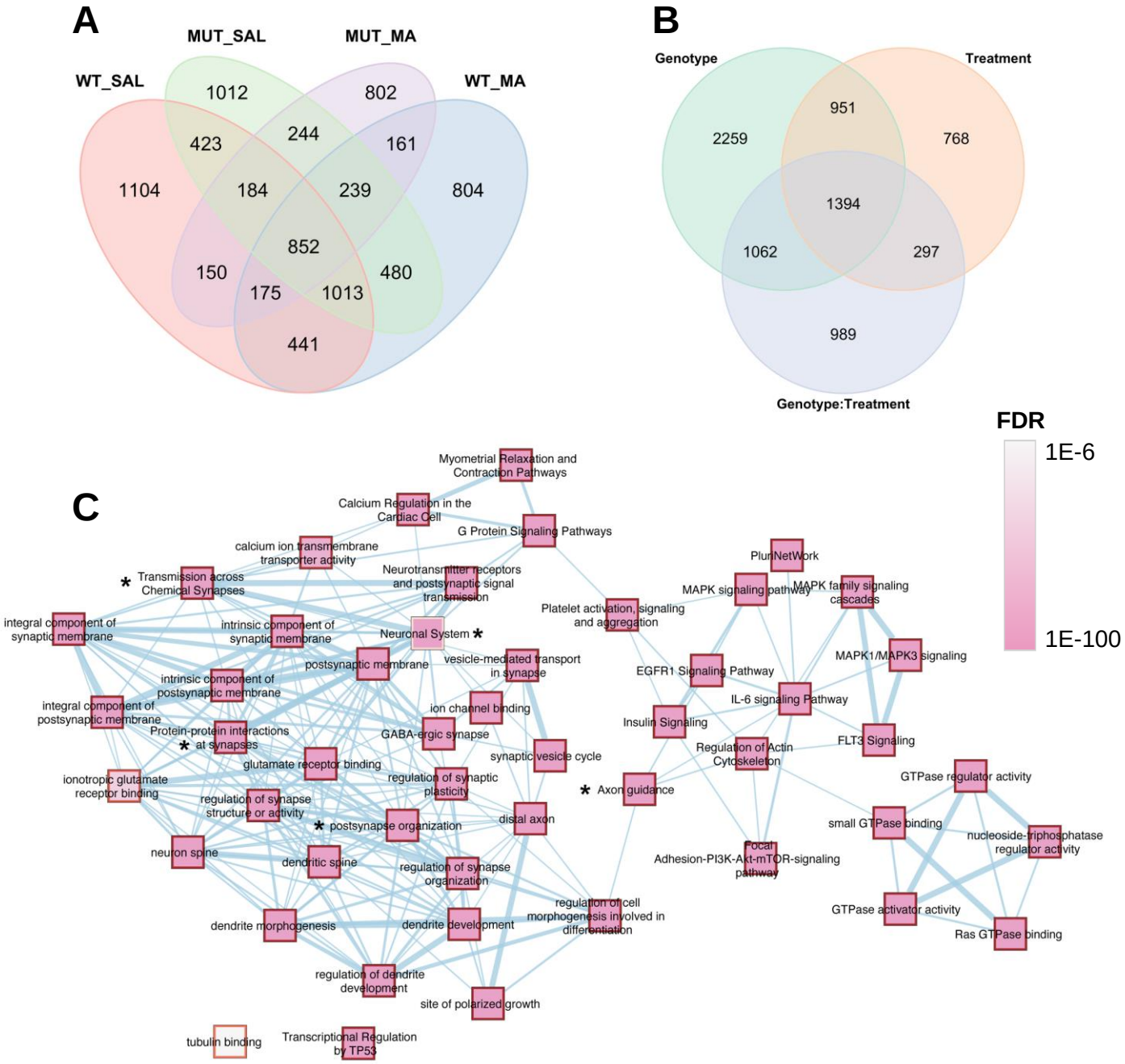

bioRxiv preprint doi: https://doi.org/10.1101/2021.07.06.451358; this version posted November 28, 2022. The copyright holder for this preprint (which was not certified by peer review) is the author/funder, who has granted bioRxiv a license to display the preprint in perpetuity. It is made available under aCC-BY-NC-ND 4.0 International license.

Figure 8

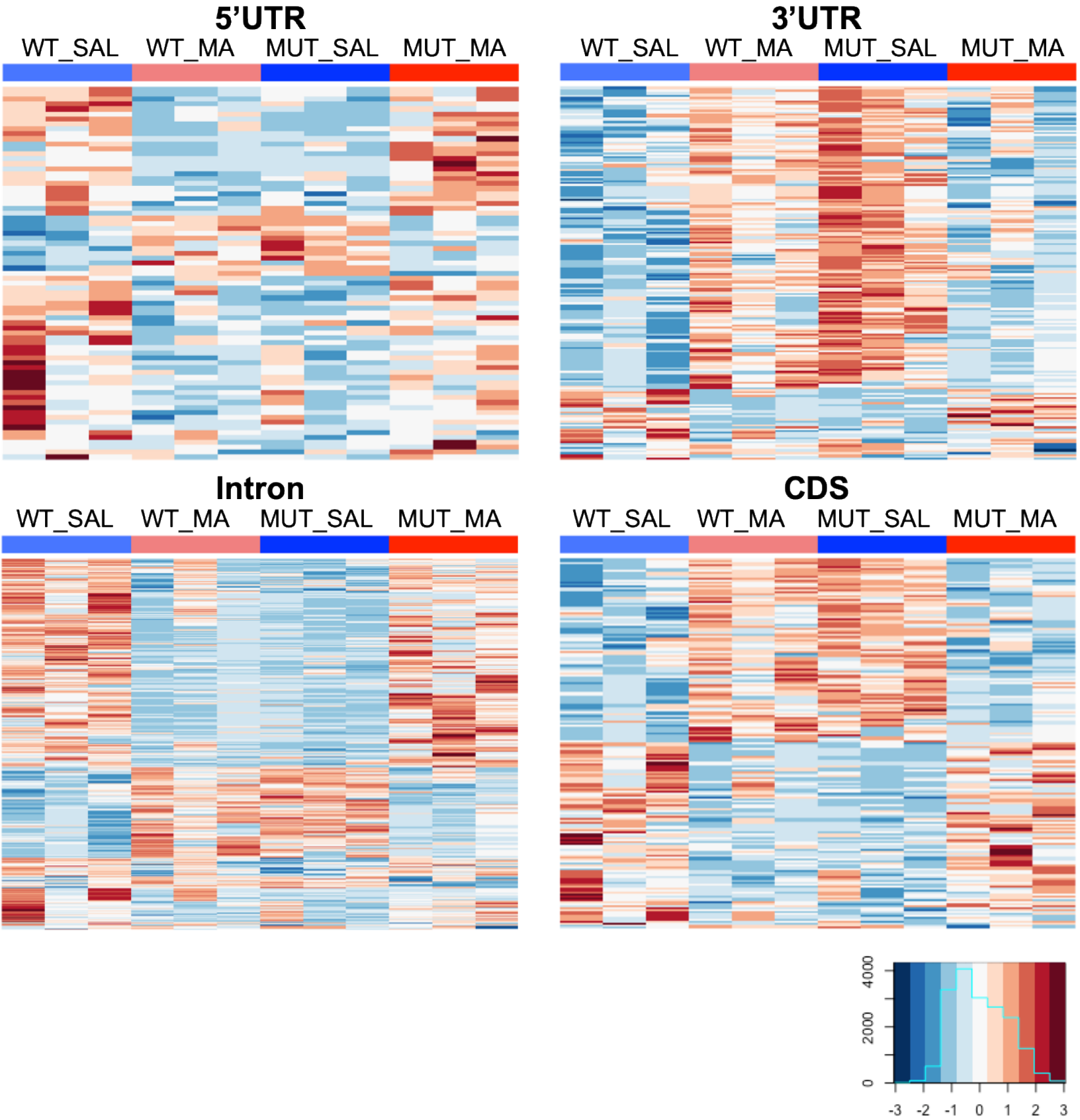

Figure 9

bioRxiv preprint doi: https://doi.org/10.1101/2021.07.06.451358; this version posted November 28, 2022. The copyright holder for this preprint (which was not certified by peer review) is the author/funder, who has granted bioRxiv a license to display the preprint in perpetuity. It is made available under aCC-BY-NC-ND 4.0 International license.

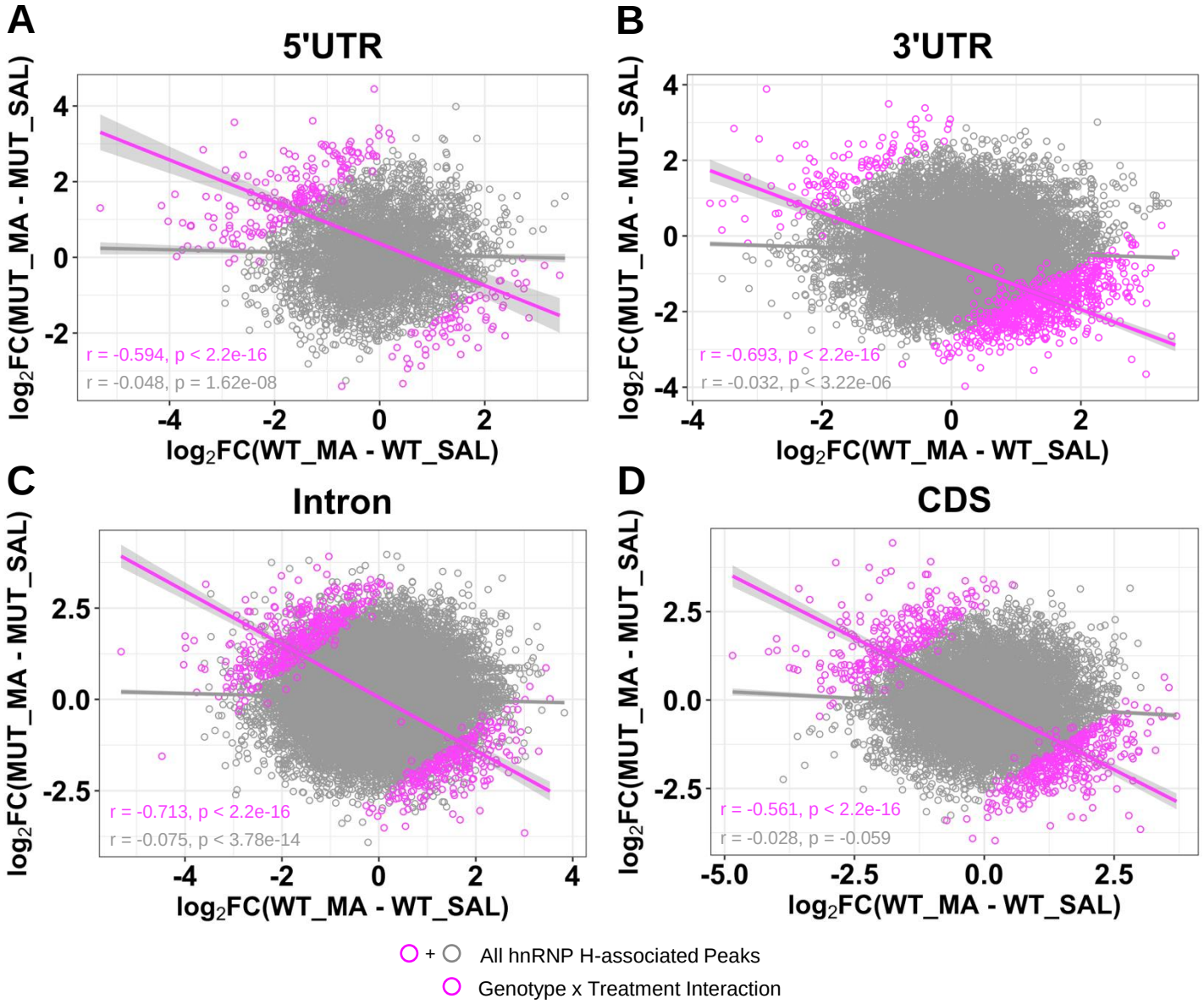

Figure 10

bioRxiv preprint doi: https://doi.org/10.1101/2021.07.06.451358; this version posted November 28, 2022. The copyright holder for this preprint (which was not certified by peer review) is the author/funder, who has granted bioRxiv a license to display the preprint in perpetuity. It is made available under aCC-BY-NC-ND 4.0 International license.

A "synaptic vesicle cycle" associated targets

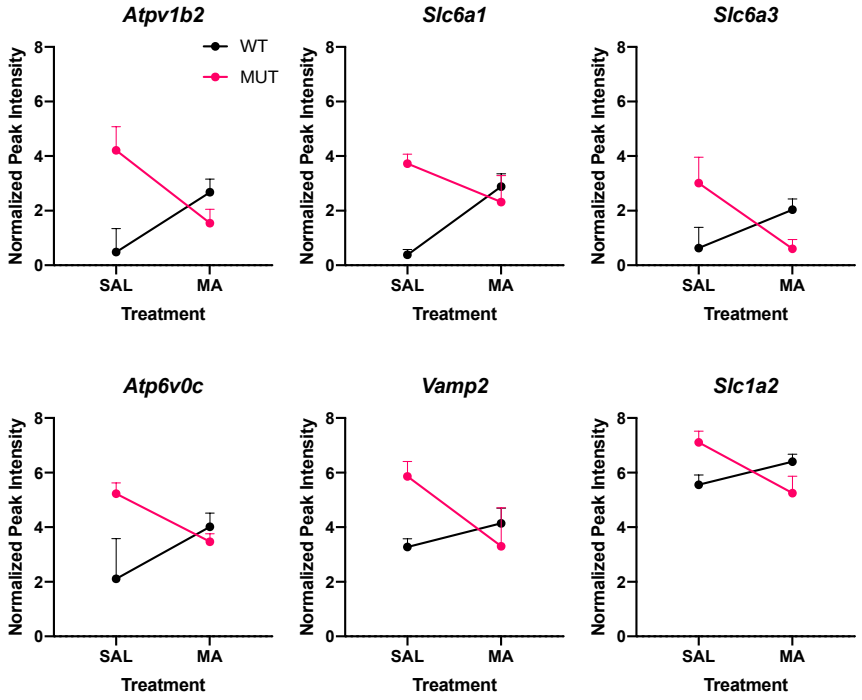

B "dopaminergic synapse" associated targets

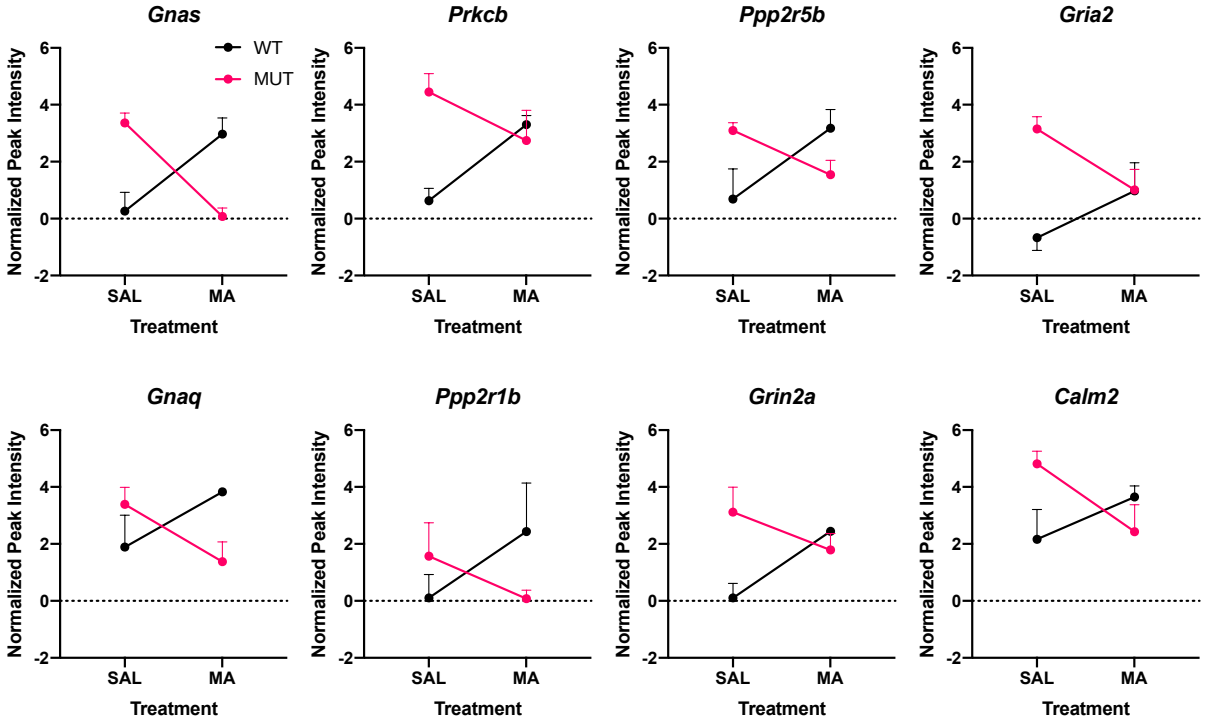

Figure 11

bioRxiv preprint doi: https://doi.org/10.1101/2021.07.06.451358; this version posted November 28, 2022. The copyright holder for this preprint (which was not certified by peer review) is the author/funder, who has granted bioRxiv a license to display the preprint in perpetuity. It is made available under aCC-BY-NC-ND 4.0 International license.

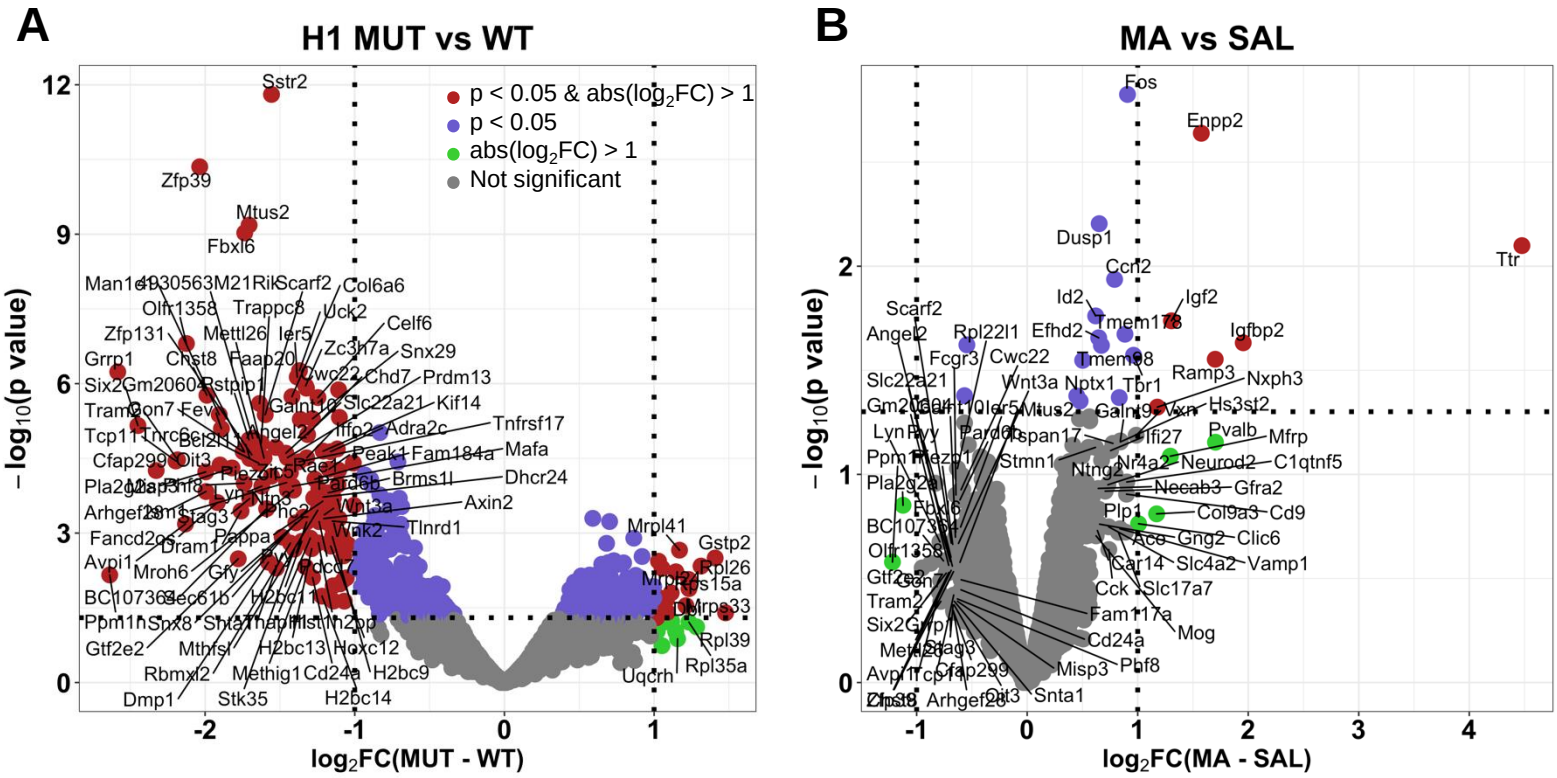

Figure 12

bioRxiv preprint doi: https://doi.org/10.1101/2021.07.06.451358; this version posted November 28, 2022. The copyright holder for this preprint (which was not certified by peer review) is the author/funder, who has granted bioRxiv a license to display the preprint in perpetuity. It is made available under aCC-BY-NC-ND 4.0 International license.

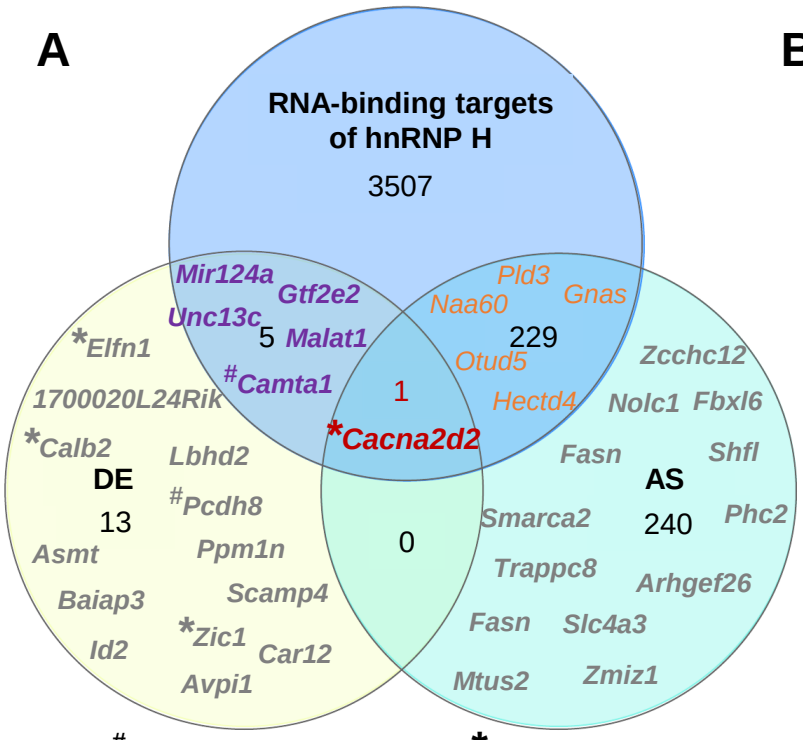

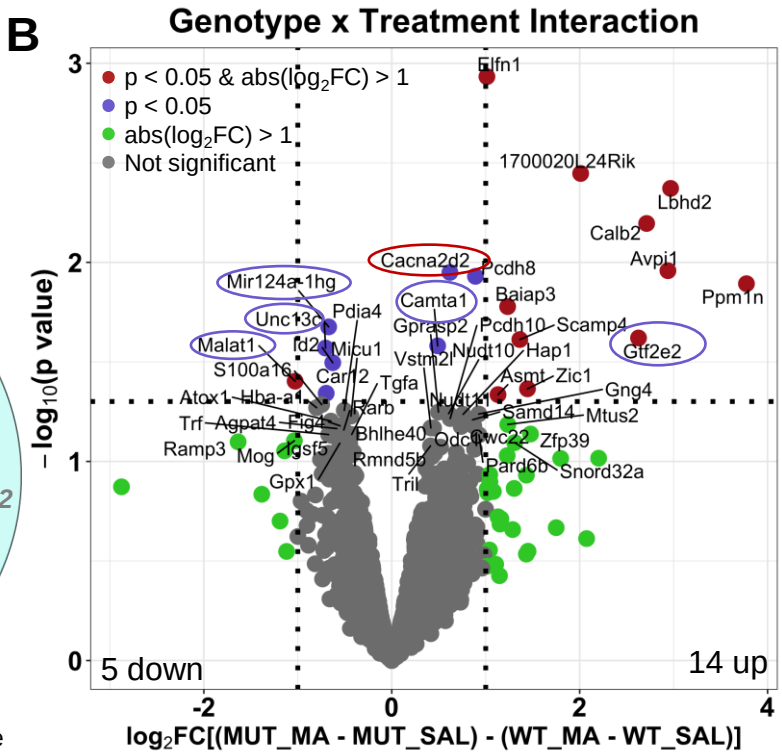

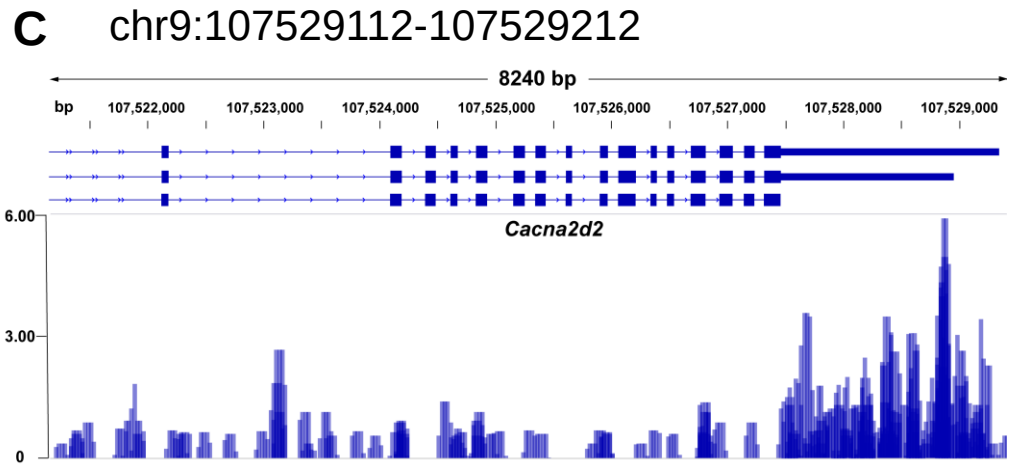

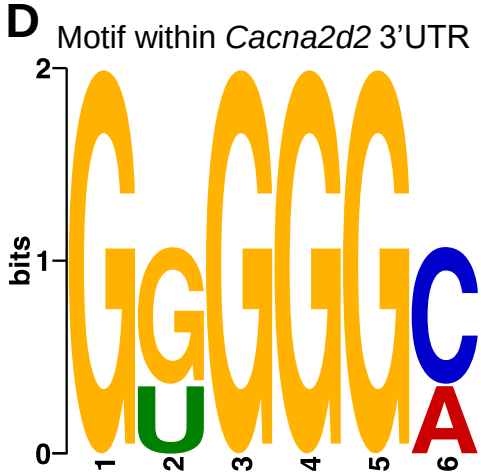

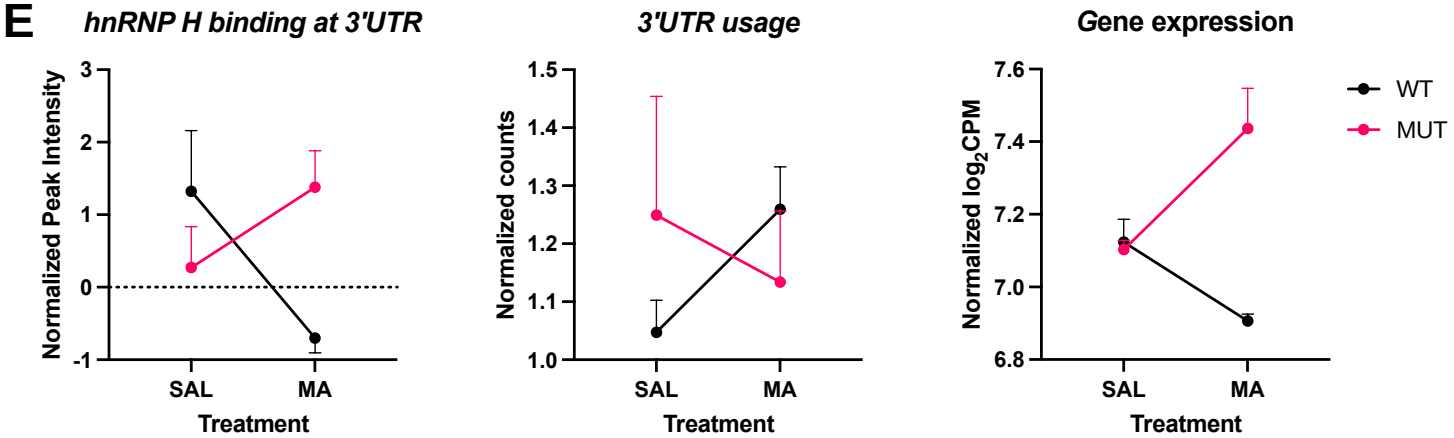

Figure 13

bioRxiv preprint doi: https://doi.org/10.1101/2021.07.06.451358; this version posted November 28, 2022. The copyright holder for this preprint (which was not certified by peer review) is the author/funder, who has granted bioRxiv a license to display the preprint in perpetuity. It is made available under aCC-BY-NC-ND 4.0 International license.

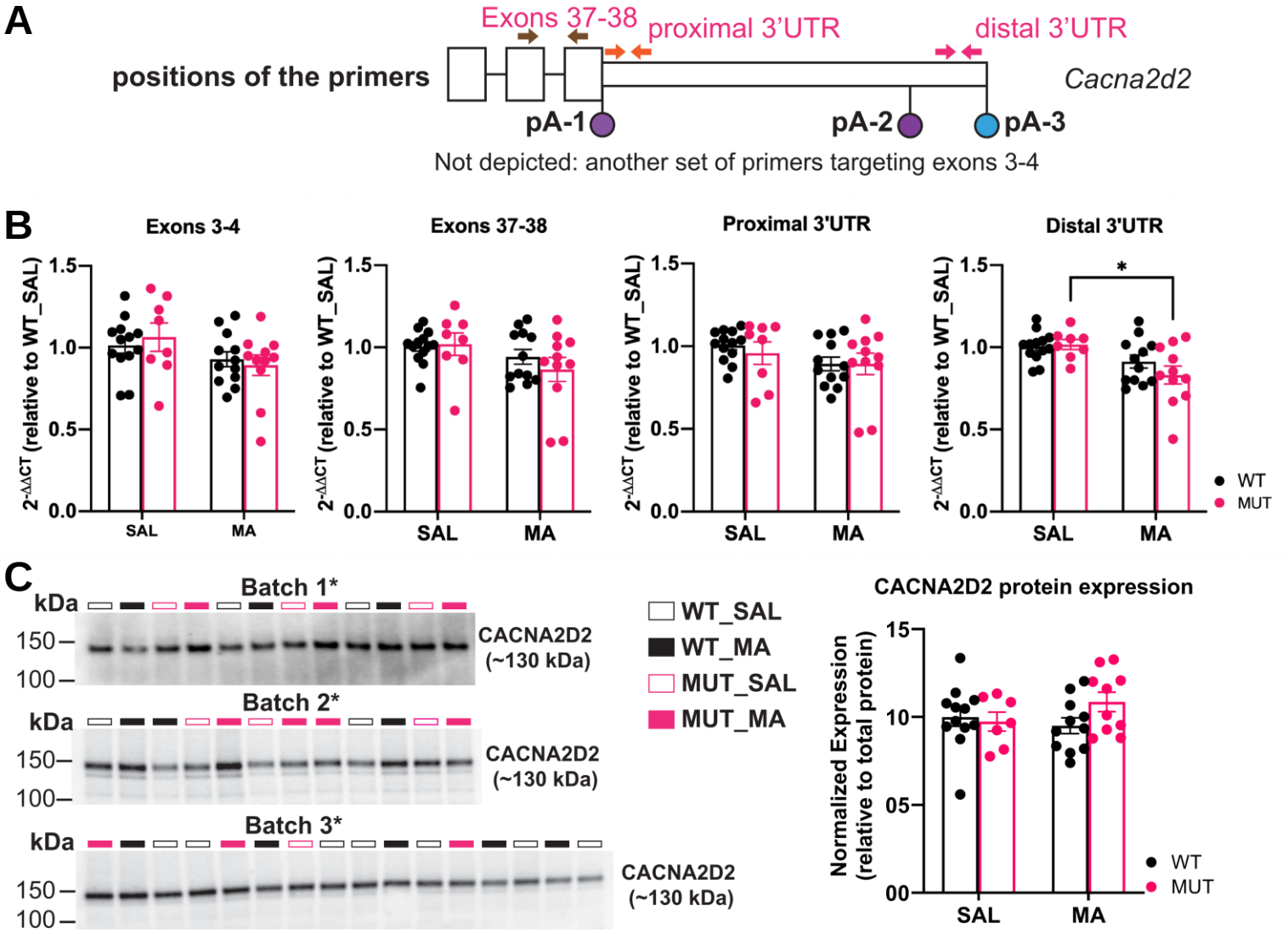

Figure 14

bioRxiv preprint doi: https://doi.org/10.1101/2021.07.06.451358; this version posted November 28, 2022. The copyright holder for this preprint (which has not certified by peer review) is the author/funder, who has granted bioRxiv a license to display the preprint in perpetuity. It is made available under aCC-BY-NC-ND 4.0 International license.

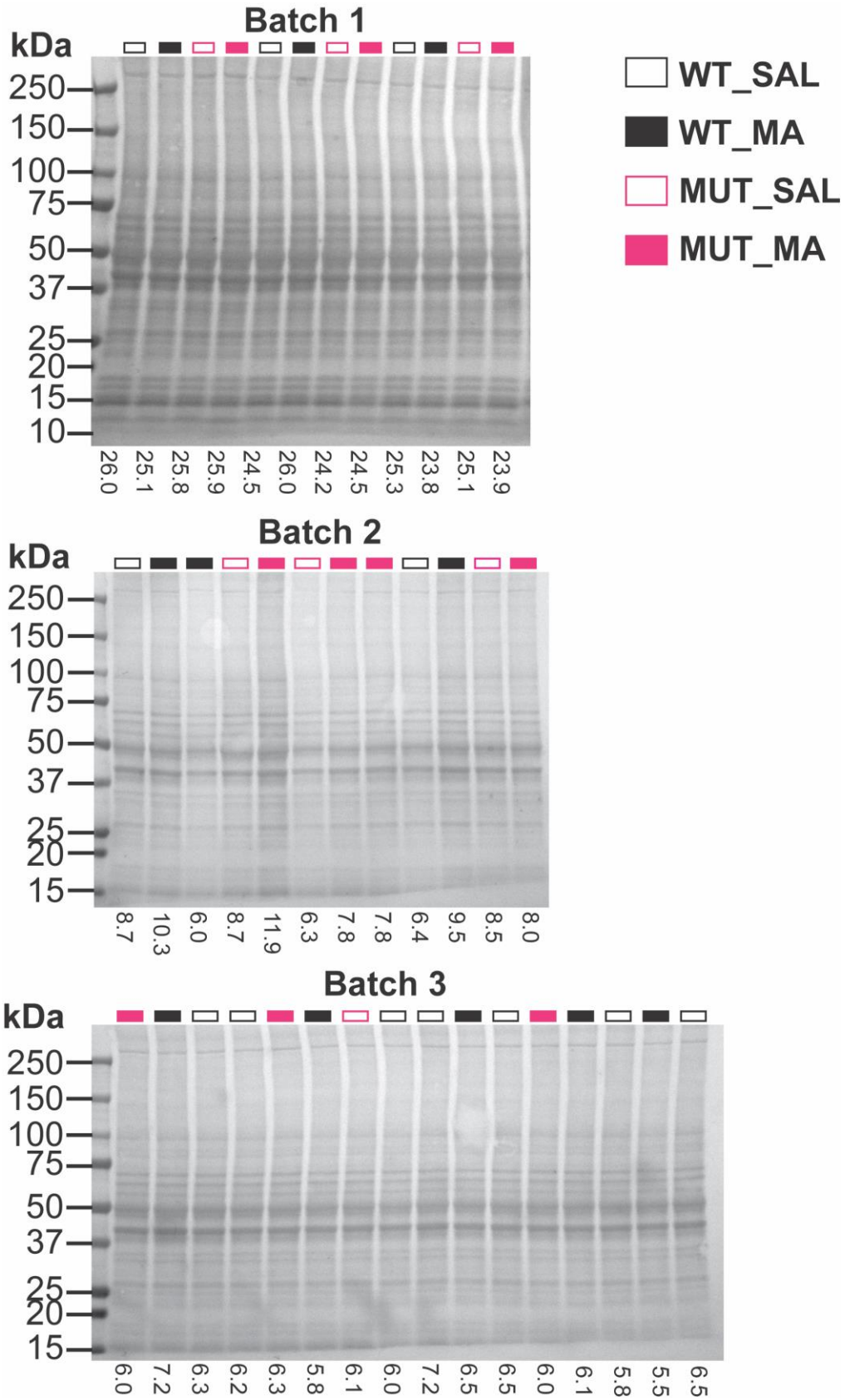

Figure 15

bioRxiv preprint doi: https://doi.org/10.1101/2021.07.06.451358; this version posted November 28, 2022. The copyright holder for this preprint (which was not certified by peer review) is the author/funder, who has granted bioRxiv a license to display the preprint in perpetuity. It is made available under aCC-BY-NC-ND 4.0 International license.

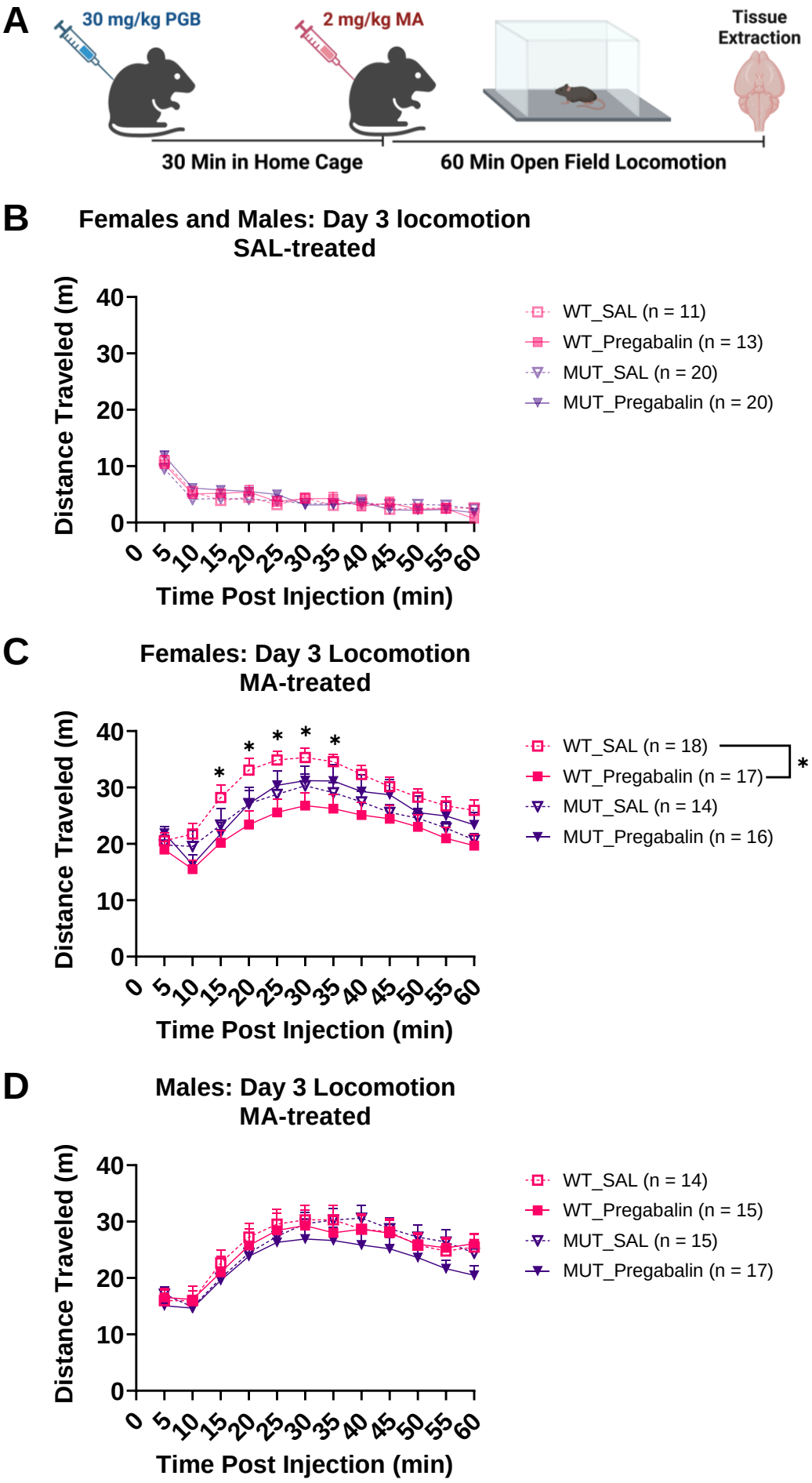

Figure 16

bioRxiv preprint doi: https://doi.org/10.1101/2021.07.06.451358; this version posted November 28, 2022. The copyright holder for this preprint (which was not certified by peer review) is the author/funder, who has granted bioRxiv a license to display the preprint in perpetuity. It is made available under aCC-BY-NC-ND 4.0 International license.

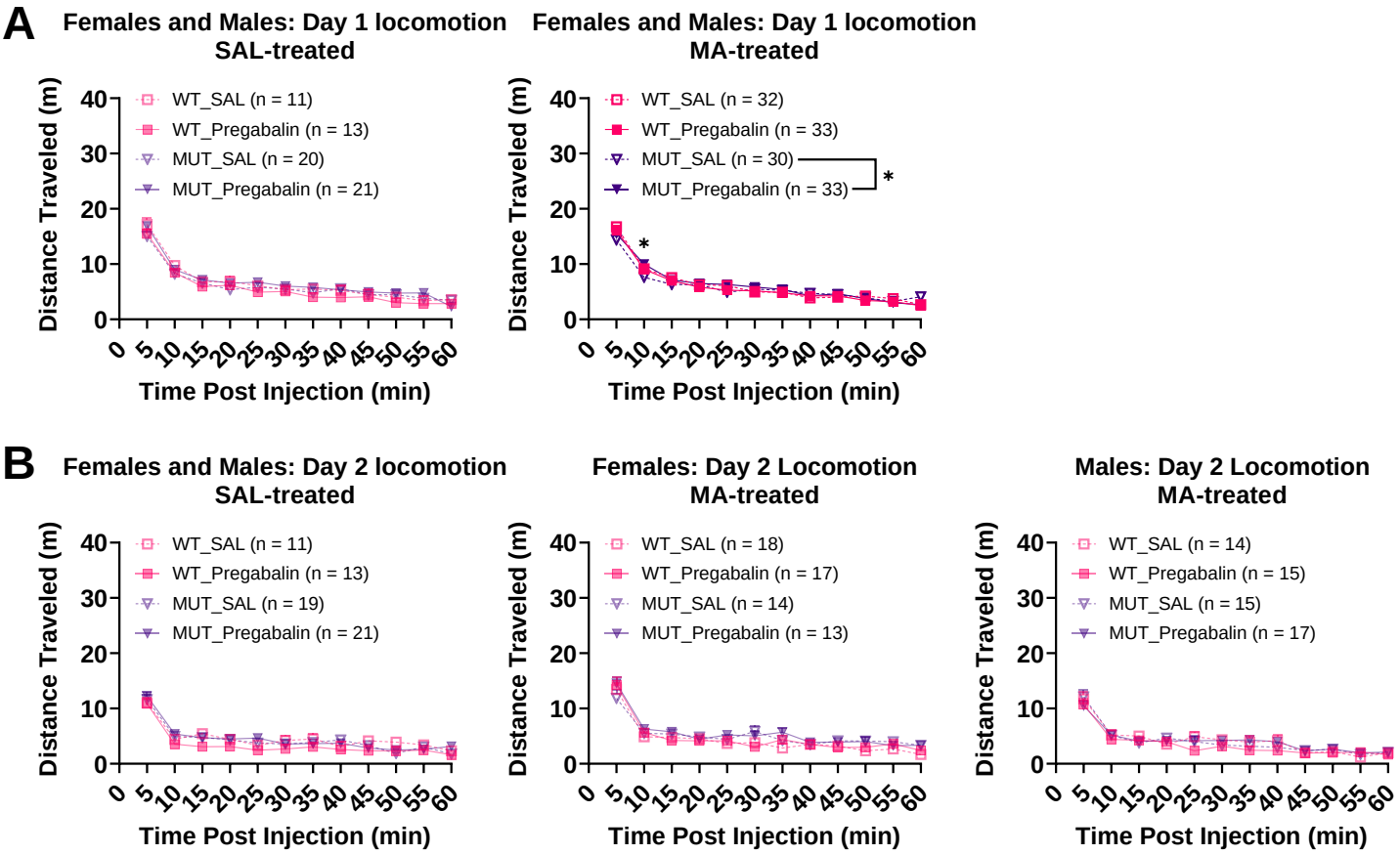

Figure 17

bioRxiv preprint doi: https://doi.org/10.1101/2021.07.06.451358; this version posted November 28, 2022. The copyright holder for this preprint (which was not certified by peer review) is the author/funder, who has granted bioRxiv a license to display the preprint in perpetuity. It is made available under aCC-BY-NC-ND 4.0 International license.

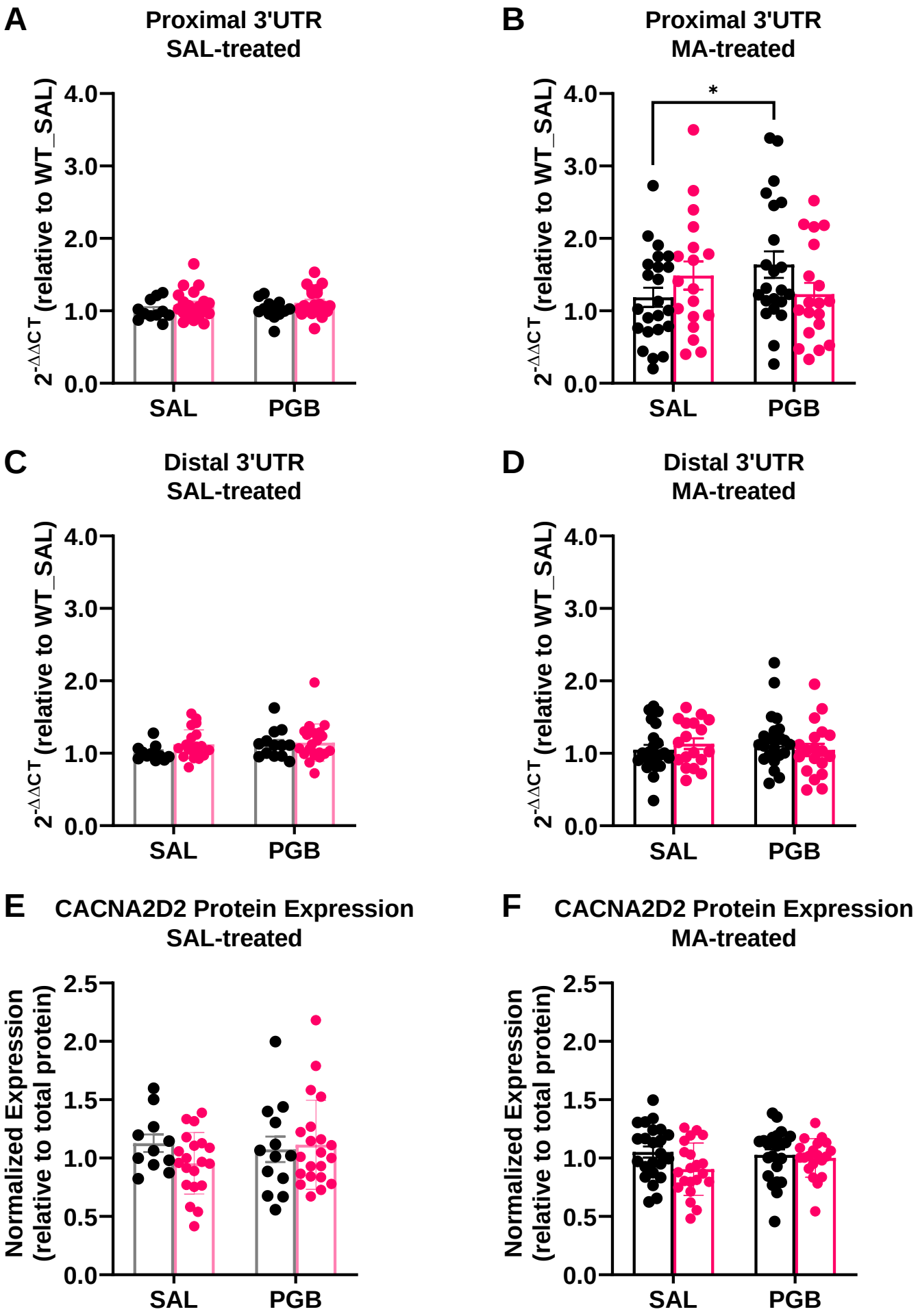

bioRxiv preprint doi: https://doi.org/10.1101/2021.07.06.451358; this version posted November 28, 2022. The copyright holder for this preprint (which was not certified by peer review) is the author/funder, who has granted bioRxiv a license to display the preprint in perpetuity. It is made available under aCC-BY-NC-ND 4.0 International license.

Table 1. Read Coverage in CLIP-seq and input RNA-seq samples.

Sample Name	Type	# of Mice	Genotype	Treatment	Replicate	Barcode Sequence	Read Counts
CLIP_WT_SAL_1	CLIP-seq	2 M + 2 F	WT	SAL	1	ACAGTG	16,446,905
CLIP_WT_SAL_2	CLIP-seq	2 M + 2 F	WT	SAL	2	GATCAG	12,440,933
CLIP_WT_SAL_3	CLIP-seq	2 M + 2 F	WT	SAL	3	AGTCAA	22,826,085
CLIP_WT_MA_1	CLIP-seq	2 M + 2 F	WT	MA	1	GCCAAT	24,419,809
CLIP_WT_MA_2	CLIP-seq	2 M + 2 F	WT	MA	2	TAGCTT	16,402,702
CLIP_WT_MA_3	CLIP-seq	2 M + 2 F	WT	MA	3	AGTTCC	13,376,067
CLIP_MUT_SAL_1	CLIP-seq	2 M + 2 F	MUT	SAL	1	CAGATC	25,759,157
CLIP_MUT_SAL_2	CLIP-seq	2 M + 2 F	MUT	SAL	2	GGCTAC	27,432,645
CLIP_MUT_SAL_3	CLIP-seq	2 M + 2 F	MUT	SAL	3	ATGTCA	25,812,360
CLIP_MUT_MA_1	CLIP-seq	2 M + 2 F	MUT	MA	1	ACTTGA	17,903,276
CLIP_MUT_MA_2	CLIP-seq	2 M + 2 F	MUT	MA	2	CTTGTA	16,116,861
CLIP_MUT_MA_3	CLIP-seq	2 M + 2 F	MUT	MA	3	CCGTCC	12,899,100
INPUT_WT_SAL_1	RNA-seq	2 M + 2 F	WT	SAL	1	GTTTCG	44,421,956
INPUT_WT_SAL_2	RNA-seq	2 M + 2 F	WT	SAL	2	ACTGAT	48,930,085
INPUT_WT_SAL_3	RNA-seq	2 M + 2 F	WT	SAL	3	CAACTA	53,470,359
INPUT_WT_MA_1	RNA-seq	2 M + 2 F	WT	MA	1	CGTACG	53,843,037
INPUT_WT_MA_2	RNA-seq	2 M + 2 F	WT	MA	2	ATGAGC	55,822,205
INPUT_WT_MA_3	RNA-seq	2 M + 2 F	WT	MA	3	CACGAT	44,088,258
INPUT_MUT_SAL_1	RNA-seq	2 M + 2 F	MUT	SAL	1	GAGTGG	43,697,136
INPUT_MUT_SAL_2	RNA-seq	2 M + 2 F	MUT	SAL	2	ATTCCT	45,817,909
INPUT_MUT_SAL_3	RNA-seq	2 M + 2 F	MUT	SAL	3	CACTCA	42,147,542
INPUT_MUT_MA_1	RNA-seq	2 M + 2 F	MUT	MA	1	GGTAGC	37,184,152
INPUT_MUT_MA_2	RNA-seq	2 M + 2 F	MUT	MA	2	CAAAAG	39,745,547
INPUT_MUT_MA_3	RNA-seq	2 M + 2 F	MUT	MA	3	CAGGCG	33,706,973

bioRxiv preprint doi: https://doi.org/10.1101/2021.07.06.451358; this version posted November 28, 2022. The copyright holder for this preprint (which was not certified by peer review) is the author/funder, who has granted bioRxiv a license to display the preprint in perpetuity. It is made available under aCC-BY-NC-ND 4.0 International license.

Table 2. hnRNP H motif by genomic region in saline-treated wildtypes. Related to Figure 1D. The top 3 Homer de novo motif results are shown for each genomic region type (5'UTR, CDS, intron and 3'UTR). The motif discovery was performed in Homer (Heinz et al., 2010).

Genomic Region Type	Motif	p value	% of Target
5'UTR		1e-20	5.57%
		1e-16	23.49%
		1e-14	10.87%
CDS		1e-122	18.76%
		1e-75	15.00%
		1e-70	18.36%
Intron		1e-47	12.19%
		1e-34	9.88%
		1e-34	7.75%
3'UTR		1e-54	15.74%
		1e-47	9.85%
		1e-42	30.08%

bioRxiv preprint doi: https://doi.org/10.1101/2021.07.06.451358; this version posted November 28, 2022. The copyright holder for this preprint (which was not certified by peer review) is the author/funder, who has granted bioRxiv a license to display the preprint in perpetuity. It is made available under aCC-BY-NC-ND 4.0 International license.

Table 3. Top 10 pathways enriched in hnRNP H-associated targets with G-rich motif in saline-treated wildtypes.

Pathway	Database	Adjusted p	RNA targets
Presynaptic depolarization and calcium channel opening	pathway_Reactome	9.52E-05	*Cacna1a, Cacnb4, Cacna1e, Cacng4, Cacna1b, Cacng2, Cacnb2*
Phase 1 - inactivation of fast Na+ channels	pathway_Reactome	0.0225	*Kcnd3, Kcnip3, Kcnip2, Kcnd2*
LGI-ADAM interactions	pathway_Reactome	6.95E-04	*Dlg4, Adam23, Stx1b, Lgi4, Cacng4, Cacng2, Adam22*
Unblocking of NMDA receptors, glutamate binding and activation	pathway_Reactome	1.85E-04	*Gria1, Dlg4, Dlg2, Grin2a, Gria3, Camk2d, Grin2b, Actn2, Camk2a*
Interaction between L1 and Ankyrins	pathway_Reactome	0.0186	*Sptbn4, Ank3, Ank2, Ank1, Sptb*
CREB phosphorylation through the activation of CaMKII	pathway_Reactome	2.86E-04	*Dlg4, Creb1, Dlg2, Grin2a, Calm1, Camk2d, Grin2b, Actn2, Camk2a*
Ras activation upon Ca2+ influx through NMDA receptor	pathway_Reactome	4.41E-04	*Rasgrf1, Dlg4, Dlg2, Grin2a, Calm1, Camk2d, Grin2b, Actn2, Camk2a*
Reduction of cytosolic Ca++ levels	pathway_Reactome	0.0096	*Atp2a2, Atp2b2, Slc8a2, Atp2b1, Calm1, Slc8a1*
Rap1 signaling	pathway_Reactome	0.0096	*Rap1gap, Ywhaz, Prkg1, Rasgrp2, Rap1gap2, Rasgrp1*
Hypothetical Network for Drug Addiction	pathway_Wikipathway	1.76E-05	*Cacna1a, Cacnb4, Cacna1e, Cacng4, Cacna1b, Cacng2, Cacnb2*

bioRxiv preprint doi: https://doi.org/10.1101/2021.07.06.451358; this version posted November 28, 2022. The copyright holder for this preprint (which was not certified by peer review) is the author/funder, who has granted bioRxiv a license to display the preprint in perpetuity. It is made available under aCC-BY-NC-ND 4.0 International license.

Table 4. hnRNP H binding sites on the 7 targets enriched for "presynaptic depolarization and calcium channel opening."

RNA-binding Target	Peak Position(s)	Genomic Region Type
Cacna1a	chr8: 84611302-84611402	Intron
Cacnb4	chr8: 52629320- 52629420 chr8: 52560620- 52560720 chr8: 52472520- 52472620	Intron Intron Intron
Cacna1e	chr1:154446931- 154447031	Intron
Cacng4	chr11:107794366- 107794466	5'UTR or CDS depending on the mRNA isoform
Cacna1b	chr2: 24608087- 24608187 chr2: 24606587-24606687	CDS or intron depending on the mRNA isoform CDS
Cacng2	chr15: 78045548 - 78045548 chr15: 78103948- 78104048	Intron Intron
*Cacnb2**	Chr2: 14762588- 14762688 Chr2:14685188- 14685288 Chr2: 14622788- 14622888	Intron Intron Intron

***only 3 out of 9 peaks lists**

bioRxiv preprint doi: https://doi.org/10.1101/2021.07.06.451358; this version posted November 28, 2022. The copyright holder for this preprint (which was not certified by peer review) is the author/funder, who has granted bioRxiv a license to display the preprint in perpetuity. It is made available under aCC-BY-NC-ND 4.0 International license.

Table 5. Chi-square tests comparing difference in proportion of hnRNP H associated binding regions. Related to Figure 2A. Given the binding events associated with hnRNP H detected in WT_SAL, the proportions of 3'UTR and intron targets in the other three conditions are significantly differently as depicted by the p values calculated in chi square test.

Subregion	Comparison to WT_SAL		
	WT_MA vs WT_SAL	MUT_SAL vs WT_SAL	MUT_MA vs WT_SAL
3'UTR	0.0008 (***)	< 0.0001 (****)	< 0.0001 (****)
distal intron	< 0.0001 (****)	< 0.0001 (****)	< 0.0001 (****)
proximalx500_intron	< 0.0001 (****)	< 0.0001 (****)	< 0.0001 (****)
proximax200_intron	< 0.0001 (****)	0.453	< 0.0001 (****)
other_exon	0.42	0.864	0.226
CDS	0.208	0.714	< 0.0001 (****)
5'UTR	0.237	0.88	0.0008 (***)

bioRxiv preprint doi: https://doi.org/10.1101/2021.07.06.451358; this version posted November 28, 2022. The copyright holder for this preprint (which was not certified by peer review) is the author/funder, who has granted bioRxiv a license to display the preprint in perpetuity. It is made available under aCC-BY-NC-ND 4.0 International license.

Table 6. KEGG pathways and GO cellular components enriched for hnRNP H-associated RNA targets with Genotype x Treatment interaction. Only those pathways or cellular components that are significantly enriched are shown.

(A): KEGG Pathway	
Gene Set	**RNA targets**
Amphetamine addiction	*Adcy5, Arc, Cacna1c, Calm2, Camk2a, Camk2b, Camk4, Creb3, Gnas, Gria1, Gria2, Grin2b, Ppp1cc, Ppp1ccb, Ppp1r1b, Ppp3ca, Ppp3r1*
Long-term potentiation	*Adcy1, Braf, Cacna1c, Calm2, Camk2a, Camk2b, Camk4, Ep300, Gnaq, Gria1, Gria2, Grin1, Grin2b, Grin2c, Grm1, Grm5, Hras, Map2k2, Ppp1cc, Ppp1ccb, Ppp3ca, Ppp3r1, Prkacb, Raf1, Rap1a*
Alcoholism	*Adcy5, Braf, Calm2, Camk4, Creb3, Gnas, Gnb1, Gng7, Grin2b, H3f3b, Hdac11, Hdac5, Hras, Ntrk2, Pkia, Ppp1cc, Ppp1ccb, Ppp1r1b*
Dopaminergic synapse	*Adcy5, Akt3, Cacna1a, Cacna1c, Calm2, Camk2a, Camk2b, Creb3, Gnaq, Gnas, Gnb1, Gng7, Gria1, Gria2, Grin2b, Gsk3b, Ppp1cc, Ppp1ccb, Ppp1r1b, Ppp2r1b, Ppp2r2a, Ppp2r5b, Ppp3ca*
(B): GO: Cellular Component	
Gene Set	**RNA targets**
ATPase complex	*Actl6b, Anp32e, Appl1, Arid1a, Arid1b, Atp1a3, Atp1b1, Atp1b2, Atp2a2, Bicra, Bicral, Brd8, Chd4, Chd5, Dpf1, Ep400, Gatad2b, Kat5, Mta1, Rbbp7, Ruvbl2, Smarca4, Smarcc2, Smarcd1, Srcap*
neuron spine	*Anks1b, Arc, Arhgap32, Arhgap33, Arrb1, Asic2, Atp2b1, Baiap2, Camk2a, Cdk5r1, Dgki, Dlg4, Dlgap3, Dnm1, Fus, Gria1, Grin2b, Grm5, Gsk3b, Hspa8, Itpka, Kcna4, Map1b, Myh10, Nrgn, Ntrk2, Pde4b, Ppp1cc, Ppp1r1b, Ppp1r9b, Ppp3ca, Pten, Rgs7bp, Sez6, Shisa7, Shisa9, Sipa1l1, Strn4, Syne1*
myelin sheath	*Aco2, Actg1, Aldoa, Atp1a3, Atp1b1, Atp5b, Atp5c1, Atp6v1a, Atp6v1b2, Car2, Cltc, Dlat, Dnm1, Eef1a1, Eef1a2, Eno1, Gjc2, Gjc3, Glul, Gnb1, Gsn, Gstm1, Hrh3, Hspa8, Hspa9, Mbp, Mog, Napb, Ncam1, Ndrg1, Nefm, Pdcd6ip, Pdia3, Pebp1, Pkm, Plp1, Pten, Rap1a, Slc25a3, Stxbp1, Syn2, Tppp, Tspan2, Vdac1, Ywhag*

bioRxiv preprint doi: https://doi.org/10.1101/2021.07.06.451358; this version posted November 28, 2022. The copyright holder for this preprint (which was not certified by peer review) is the author/funder, who has granted bioRxiv a license to display the preprint in perpetuity. It is made available under aCC-BY-NC-ND 4.0 International license.

nuclear chromatin	*Actl6b, Aldoa, Anp32e, Appl1, Arid1a, Arid1b, Bicra, Bicral, Brd4, Brd8, Cenpb, Chd4, Chd5, Clock, Cpsf6, Dpf1, Enc1, Ep400, Gatad2b, H1f0, H2afy, Jun, Kat2a, Kat5, Mef2d, Mta1, Nsmf, Polr2a, Ppp1r10, Rbbp7, Rcc1, Ruvbl2, Sfr1, Sin3b, Smad4, Smarca4, Smarcc2, Smarcd1, Srcap, Stat3, Suds3, Tbp, Tcf4, Trnp1, Zfp385a, Zfp57*

bioRxiv preprint doi: https://doi.org/10.1101/2021.07.06.451358; this version posted November 28, 2022. The copyright holder for this preprint (which was not certified by peer review) is the author/funder, who has granted bioRxiv a license to display the preprint in perpetuity. It is made available under aCC-BY-NC-ND 4.0 International license.

Table 7. KEGG Enrichment analysis of dynamic hnRNP H 3'UTR targets. The table shows those 3'UTR RNA targets responding to the interaction of Genotype and Treatment. The interaction is expressed as (MUT_{MA} – MUT_{SAL}) – (WT_{MA} – WT_{SAL}) with $p < 0.01$. WT_SAL = untreated saline wild-types; WT_MA = methamphetamine-treated wild-types; MUT_SAL = untreated saline *Hnrnph1* mutants; MUT_MA = methamphetamine-treated *Hnrnph1* mutants.

Pathway	Adjusted p	RNA targets
Long-term potentiation	1.36E-06	*Braf, Prkcb, Grm5, Ppp3r1, Hras, Gria2, Gnaq, Grin2a, Calm2*
Glutamatergic synapse	5.69E-06	*Gnas, Prkcb, Slc38a1, Grm5, Ppp3r1, Gria2, Gnaq, Grin2a, Slc1a3, Slc1a2*
Long-term depression	7.15E-05	*Gnas, Braf, Prkcb, Hras, Gria2, Gnaq, Ppp2r1b*
Salivary secretion	2.87E-04	*Gnas, Prkcb, Atp1b1, Atp1b2, Gnaq, Calm2, Vamp2*
Dopaminergic synapse	9.51E-04	*Gnas, Prkcb, Ppp2r5b, Gria2, Gnaq, Ppp2r1b, Grin2a, Calm2*
Aldosterone synthesis and secretion	9.51E-04	*Gnas, Prkcb, Pde2a, Atp1b1, Atp1b2, Gnaq, Calm2*
Amphetamine addiction	9.51E-04	*Gnas, Prkcb, Ppp3r1, Gria2, Grin2a, Calm2*
Gastric acid secretion	1.24E-03	*Gnas, Prkcb, Atp1b1, Atp1b2, Gnaq, Calm2*
Synaptic vesicle cycle	1.31E-03	*Atp6v1b2, Slc6a1, Slc1a3, Atp6v0c, Vamp2, Slc1a2*
Cocaine addiction	1.31E-03	*Gnas, Rgs9, Gria2, Cdk5r1,Grin2a*

bioRxiv preprint doi: https://doi.org/10.1101/2021.07.06.451358; this version posted November 28, 2022. The copyright holder for this preprint (which was not certified by peer review) is the author/funder, who has granted bioRxiv a license to display the preprint in perpetuity. It is made available under aCC-BY-NC-ND 4.0 International license.

Table 8. KEGG Enrichment analysis of dynamic hnRNP H intronic targets. The table shows those intronic RNA targets responding to the interaction of Genotype and Treatment. The interaction is expressed as (MUT_{MA} – MUT_{SAL}) – (WT_{MA} – WT_{SAL}) with $p < 0.01$. WT_SAL = untreated saline wild-types; WT_MA = methamphetamine-treated wild-types; MUT_SAL = untreated saline *Hnrnph1* mutants; MUT_MA = methamphetamine-treated *Hnrnph1* mutants.

Pathway	Adjusted p	RNA targets
Oxytocin signaling pathway	1.31E-11	*Prkag2, Itpr1, Prkcb, Rock1, Cacnb2, Plcb1, Adcy5, Cacng2, Ryr2, Ppp1cb, Ppp3ca, Kcnj4, Camk1d, Ppp3r1, Cacna2d4, Cacna2d3, Cacna1d, Ppp1r12c, Camk4, Elk1, Camk2a, Map2k2, Cacna1c, Cacnb4, Gnas, Cacng8, Prkag1, Ppp3cb, Cacnb1, Hras, Rock2, Adcy6, Calm2, Plcb4*
Long-term potentiation	6.66E-09	*Itpr1, Prkcb, Gria1, Grin2b, Plcb1, Grin2a, Ppp1cb, Ppp3ca, Ppp3r1, Camk4, Camk2a, Map2k2, Cacna1c, Grin2d, Gria2, Ppp3cb, Hras, Calm2, Plcb4*
Glutamatergic synapse	7.93E-09	*Itpr1, Prkcb, Gria1, Grin2b, Plcb1, Adcy5, Grm4, Grin2a, Slc1a3, Ppp3ca, Gng7, Dlgap1, Ppp3r1, Grik5, Cacna1d, Cacna1c, Grin2d, Gria2, Gnas, Ppp3cb, Adcy6, Cacna1a, Slc38a3, Plcb4, Slc1a1*
Dopaminergic synapse	1.70E-08	*Itpr1, Prkcb, Gria1, Ppp1r1b, Grin2b, Plcb1, Mapk10, Adcy5, Grin2a, Ppp1cb, Ppp3ca, Gng7, Ppp2cb, Kif5c, Cacna1d, Mapk14, Camk2a, Cacna1c, Gria2, Gnas, Scn1a, Ppp3cb, Cacna1a, Calm2, Ppp2r2d, Plcb4, Ppp2r1b*
Adrenergic signaling in cardiomyocytes	3.34E-08	*Atp2b2, Cacnb2, Plcb1, Adcy5, Cacng2, Scn7a, Slc8a1, Ryr2, Ppp1cb, Cacna2d4, Cacna2d3, Ppp2cb, Cacna1d, Mapk14, Scn4b, Camk2a, Cacna1c, Atp1a2, Cacnb4, Gnas, Cacng8, Cacnb1, Adcy6, Calm2, Ppp2r2d, Plcb4, Atp1b2, Ppp2r1b*
Amphetamine addiction	5.46E-08	*Prkcb, Gria1, Ppp1r1b, Grin2b, Adcy5, Grin2a, Ppp1cb, Ppp3ca, Ppp3r1, Cacna1d, Camk4, Camk2a, Cacna1c, Grin2d, Gria2, Gnas, Ppp3cb, Calm2*

bioRxiv preprint doi: https://doi.org/10.1101/2021.07.06.451358; this version posted November 28, 2022. The copyright holder for this preprint (which was not certified by peer review) is the author/funder, who has granted bioRxiv a license to display the preprint in perpetuity. It is made available under aCC-BY-NC-ND 4.0 International license.

Circadian entrainment	1.88E-07	*Itpr1, Prkcb, Gria1, Grin2b, Plcb1, Nos1ap, Adcy5, Ryr2, Grin2a, Gng7, Cacna1h, Cacna1d, Camk2a, Cacna1c, Grin2d, Gria2, Gnas, Per1, Adcy6, Calm2, Plcb4*
cGMP-PKG signaling pathway	6.19E-07	*Itpr1, Atp2b2, Rock1, Prkce, Pde2a, Plcb1, Slc8a3, Adcy5, Mef2d, Slc8a1, Ppp1cb, Ppp3ca, Ppp3r1, Slc8a2, Cacna1d, Insr, Gna13, Map2k2, Cacna1c, Atp1a2, Mef2b, Ednra, Ppp3cb, Rock2, Adcy6, Calm2, Plcb4, Atp1b2*
Arrhythmogenic right ventricular cardiomyopathy (ARVC)	7.64E-07	*Cacnb2, Sgcd, Cacng2, Slc8a1, Ryr2, Cacna2d4, Ctnna2, Cacna2d3, Cacna1d, Dag1, Cacna1c, Cacnb4, Itgb8, Cacng8, Cacnb1, Gja1, Itga9*
Calcium signaling pathway	1.29E-06	*Itpr1, Prkcb, Atp2b2, Plcb1, Pde1a, Slc8a3, Htr2c, Slc8a1, Ryr2, Grin2a, Ppp3ca, Ppp3r1, Slc8a2, Cacna1h, Cacna1d, Camk4, Camk2a, Cacna1c, Chrna7, Grin2d, Ednra, Gnas, Ppp3cb, Cacna1a, Calm2, Itpka, Plcb4, Pde1b, Ptk2b*

bioRxiv preprint doi: https://doi.org/10.1101/2021.07.06.451358; this version posted November 28, 2022. The copyright holder for this preprint (which was not certified by peer review) is the author/funder, who has granted bioRxiv a license to display the preprint in perpetuity. It is made available under aCC-BY-NC-ND 4.0 International license.

Table 9. Differential expressed genes overlapping with hnRNP H targets with Genotype by Treatment interaction. Related to Figure 4A.

Gene	Expression		Peak Intensity		Peak Location	
	logFC	p value	logFC	p value	Coordinate	Type
Cacna2d2	0.619	0.011	3.078	0.032	chr9:107529112-107529212	3'UTR or intron
Mir124a-1hg	-0.672	0.021	-4.020	0.004	chr14:64592731-64592831	Other exon
			-3.306	0.019	chr14:64592631-64592731	Other exon
			-3.062	0.030	chr14:64593631-64593731	Other exon
Gtf2e2	2.627	0.024	3.737	0.008	chr8:33774733-33774833	Intron
			3.102	0.035	chr8:33759333-33759433	Intron
Camta1	0.488	0.026	4.781	2.985E-04	chr4:151134622-151134722	Intron
			3.223	0.022	chr4:151107922-151108022	Intron
			-2.994	0.033	chr4:151717622-151717722	Intron
			-2.997	0.036	chr4:151060922-151061022	3UTR
			2.830	0.041	chr4:151510022-151510122	Intron
Unc13c	-0.705	0.027	3.343	0.018	chr9:73765622-73765722	Intron
			2.858	0.037	chr9:73509222-73509322	Intron
*Malat1**	-1.029	0.040	-2.381	2.155E-04	ch19:5801590-5801690	Intron
			-2.296	2.603E-04	chr19:5798090-5798190	Other exon
			-1.872	7.208E-04	chr19:5797290-5797390	Intron or other exon
			-1.774	8.040E-04	chr19:5797390-5797490	Intron or other exon
			-2.093	0.001	chr19:5797990-5798090	Other exon

*5 out of 48 peaks shown